



Norwegian University of  
Science and Technology

# Application of RADAR SAR for Indoor Visual Inspection

**Snorre Jablonski**

Master of Science in Cybernetics and Robotics

Submission date: June 2018

Supervisor: Tor Arne Johansen, ITK

Co-supervisor: Kristian Klausen, ITK

Norwegian University of Science and Technology  
Department of Engineering Cybernetics





## MSC THESIS DESCRIPTION SHEET

**Name:** Snorre Jablonski  
**Department:** Engineering Cybernetics  
**Thesis title:** Application of RADAR SAR for Indoor Visual Inspection

### Thesis Description:

A system for automatic and safe inspection of tanks and other infrastructure with Unmanned Aerial Vehicles (UAVs) is under investigation at the department. Critical to the system is methods for collision avoidance and detection of obstacles, such as wires, pipes and walls.

The system is a part of an ongoing commercialization process (Scout Drone Inspection AS) in cooperation with NTNU TTO, and the student will sign a "Standardavtale" with NTNU TTO.

This project aims to investigate algorithms for classification of data coming from one or several light-weight ultra-wide-band (UWB) radars on the UAV.

The following items should be considered:

1. Conduct a literature review on usage of Radar on drones, and the different types of Radars available (UWB, pulsed, impulse, etc)
2. Conduct a literature review on the use of Synthetic Aperture Radar (SAR), and search for possible available implementations/libraries.
3. Discuss how Radars and SAR can aid in drone operations through local navigation.
4. Using data from the radars, implement and test a suitable SAR generation algorithm in Python.
5. Compare and discuss issues regarding run-times, computational costs for real time processing, accuracy and repeatability.
6. Using test-data provided, generate a SAR image of a mildly cluttered environment *including hard-to-see elements such as wires*, and discuss results. Also provide means to reference accuracy of data.
7. Conclude findings in a report. Include Matlab/Python/C-code as digital appendices together with a user-guide.

**Start date:** 2018-01-08  
**Due date:** 2018-06-04

**Thesis performed at:** Department of Engineering Cybernetics, NTNU  
**Supervisor:** Professor Thor Arne Johansen, Dept. of Eng. Cybernetics, NTNU  
**Co-Supervisor:** Dr. Kristian Klausen, Dept. of Eng. Cybernetics, NTNU



NORWEGIAN UNIVERSITY OF SCIENCE AND TECHNOLOGY

## *Abstract*

Faculty of Information Technology and Electrical Engineering  
Department of Engineering Cybernetics

Master Thesis

### **Application of RADAR SAR for Indoor Visual Inspection**

by Snorre JABLONSKI

Utilizing Unmanned Aerial Vehicles (UAVs) for the purpose of indoor visual inspection poses great possibilities within many industries regarding cost reduction and efficiency. The development of mapping techniques and collision avoidance systems for UAVs is in the wind, but there are many challenges that remains to be solved. One of the big challenges is that of creating reliable and accurate imagery of local environments by the use of small robust low cost sensors. Radio Detection and Ranging, also known as Radar, is a promising contender within this domain. Because there are limited test results of Radar on small sized UAVs, it remains to be seen if Radar proves as promising as the literature might suggest.

During the course of this thesis, the fundamentals of Radar technology along with a review of different types of Radars will be assessed with emphasis on UAV applications before moving on to the principles of Synthetic Aperture Radar (SAR). Challenges and possibilities concerning collision avoidance by the use of SAR on small-sized UAVs will also be discussed. Furthermore, signal processing theory, techniques and different classifications of SAR algorithms will be presented. These sections will be built upon the research presented in my project thesis [1]. The thesis will move on to present a Python implementation of a simple SAR algorithm. The algorithm will be tested on different data sets acquired by a light-weight Ultra-Wide Band (UWB) Radar mounted on a multirotor UAV. Using the acquired test-data, several SAR images of different environments, ranging from simple environments with easy-to-see objects to mildly cluttered environments including hard-to-see elements such as wires. The test results, concluding SAR as a feasible method for collision avoidance purposes, will be presented in an orderly manner. The results, combined with the literature presented in this thesis will be thoroughly reviewed in a closing discussion while addressing the possibilities of future research prospects within the same domain.



## Sammendrag

Bruk av droner for inspeksjon av lukkede miljøer kan åpne mange nye muligheter for industrien når det kommer til kostnadsreduksjon og effektivitet. Utviklingen av teknikker for kartlegging og anti-kollisjon-systemer for droner er et populært tema, men det er fortsatt mange utfordringer og problemer som mangler fullstendige løsninger. En av de store utfordringene gjelder muligheten for presis og pålitelig avbildning av lukkede områder ved bruk av små robuste billige sensorer/instrumenter. Innenfor dette feltet er Radar omtalt i litteraturen som en lovende kandidat, men det er fortsatt mangel på testing av Radar på små droner.

I denne masteroppgaven vil de grunnleggende konseptene bak radarteknologi bli presentert med litteratur og informasjon om forskjellige typer radarsystemer, med hovedvekt på ideen om bruk av Radar på droner. Deretter vil spesifikke deler av konseptet Syntetisk Aperture Radar (SAR) bli forklart til beste evne. Utfordringer og muligheter for anti-kollisjon ved bruk av SAR på små droner vil bli presentert og diskutert etterfulgt av signalbehandlingsteori, signalbehandlingsteknikker, og forskjellige SAR-algoritmer. Disse seksjonene vil være inspirert og delvis bygget på noe av teorien og forskningen som ble presentert i prosjektoppgaven min fra i fjor [1]. Oppgaven vil gå videre å presentere en implementasjon av en enkel SAR-algoritme i Python. Algoritmen vil bli testet på datasett hentet fra en lettvektig Ultra-Wide-Band (UWB) Radar festet på en multirotor-drone. Ved hjelp av algoritmer og testdata vil det bli generert og presentert SAR-bilder av forskjellige objekter, med alt fra store objekter som er enkle å se, til mindre objekter som er vanskeligere å oppdage. Resultatene fra testingen, som konkluderer at SAR er en lovende metode for anti-kollisjon-systemer, vil bli presentert på ryddigst mulig vis og sammenlignet med resultater fra forskningen presentert tidligere i oppgaven. Hele oppgaven avsluttes med en omfattende diskusjon rundt arbeidet, etterfulgt av ideer til potensielle temaer for videre forskning innenfor samme domene.



## Preface

The work done in this thesis was carried out during the course of the spring semester of 2018 (January to June) at the Department of Engineering Cybernetics at the Norwegian University of Science and Technology. The work accounts for a full semester of 30 study points. I would first and foremost thank my supervisor Tor Arne Johansen and co-supervisors Kristian Klausen and Morten Fyhn Amundsen for their assistance. The master thesis is built upon the previous work done during my project assignment during the autumn semester of 2017 (August-December). Some of the literature is directly taken from my project assignment, but as I often considered it to lack some relevant information, I have made slight modifications and added extra information where I found it to be necessary. Literature and research presented have been cited to the best of my ability, and viewed to be coming from reliable sources to my better judgment. When explaining the specificities of the software and hardware used in this thesis, it is important to mention that all hardware (UAV, Radar, test objects) presented was provided by NTNU and Scout Drone Inspection AS. The code concerning the SAR algorithm presented in the appendix was written by me, though the libraries for extraction of Radar data was written by Kristian Klausen and Morten Fyhn Amundsen. All tests performed in this thesis was done by the help of Kristian Klausen and Morten Fyhn Amundsen. Test data and my discussion on the results acquired in this thesis has been reviewed by Kristian Klausen and Tor Arne Johansen. I would like to thank Kristian and Morten for assistance on Radar data logging, UAV operation and providing means for accurate positioning data during all tests. Beginning my project I was fairly new to the concepts of Radar imaging, Synthetic Aperture Radar algorithms and signal processing, and I have really appreciated all the help given to me by several meetings with "Radar expert" Egil Eide at NTNU. In that regard I also want to thank Kristian Klausen for attending those meetings and discussing the more complex concepts of Radar imaging with me thus helping me to formulate my own understanding on those concepts.



## *Acknowledgements*

First, I would like to extend a big thanks to my girlfriend Inga Haukaas, who has, with former experience from writing her master thesis, guided me away from some of the common pitfalls when writing a thesis. Not to mention the moral support received.

I would also like to thank David Billdal, my fellow student with whom I've discussed some of the literature and research presented in this thesis.

I want to thank Egil Eide as well, for helping me with understanding some of the aspects concerning Radar and synthetic aperture Radar algorithms.

At last I would also like to thank Tor Arne Johansen and Kristian Klausen for their guidance and help with practicalities as well as their support during the course of the entire semester.



# Contents

<b>Abstract</b>	<b>iii</b>
<b>Sammendrag</b>	<b>v</b>
<b>Preface</b>	<b>vii</b>
<b>Acknowledgements</b>	<b>ix</b>
<b>List of Figures</b>	<b>xiii</b>
<b>List of Tables</b>	<b>xv</b>
<b>List of Abbreviations</b>	<b>xvii</b>
<b>List of Abbreviations</b>	<b>xvii</b>
<b>1 Introduction</b>	<b>1</b>
1.1 Motivation for this thesis . . . . .	1
1.2 Scope of this thesis . . . . .	1
1.3 A Historical Perspective . . . . .	2
1.4 Thesis Outline . . . . .	3
1.5 Nomenclature . . . . .	4
<b>2 Synthetic Aperture Radar (SAR)</b>	<b>5</b>
2.1 Radar Systems . . . . .	5
2.2 The Radar Equation . . . . .	9
2.3 Different types of Radars . . . . .	13
2.3.1 Pulsed Radar . . . . .	13
2.3.2 Continuous Wave Radar . . . . .	14
2.4 Radar for Collision Avoidance . . . . .	18
2.5 The Principles of Synthetic Aperture Radar (SAR) . . . . .	19
2.5.1 Different types of SAR Acquisition Modes . . . . .	20
2.5.2 SAR Resolution . . . . .	22
2.6 Study: Synthetic Aperture Radar Imaging Using a Small Consumer Drone . . . . .	24
2.7 SAR & Radar to Aid in Local Navigation . . . . .	25
2.8 Existing Challenges . . . . .	26
2.9 Summary . . . . .	29

<b>3</b>	<b>SAR Signal Processing &amp; Algorithms</b>	<b>31</b>
3.1	Radar Scattering	31
3.2	The Pulse Compression Technique	34
3.2.1	Matched Filter	37
3.3	Essential Tools for Frequency Domain Algorithms	38
3.3.1	Fast Fourier Transform	39
3.3.2	Interpolation	40
3.4	SAR Algorithms & Image formation	41
3.4.1	Migration Algorithms	41
3.4.2	Range Migration (FK-migration)	42
3.4.3	Kirchhoff Migration	43
3.4.4	Diffraction Stack Migration	43
3.4.5	Simple Summation Algorithm	44
3.5	Comparison regarding UWB Short-Range Imaging	44
3.6	Discussion	46
3.7	Summary	47
<b>4</b>	<b>Software &amp; Hardware</b>	<b>51</b>
4.1	Software	51
4.2	Hardware	52
4.3	Implementation Steps	55
4.4	Discussion	56
4.5	Summary	57
<b>5</b>	<b>Testing &amp; Results</b>	<b>59</b>
5.1	Test Setup	59
5.2	Test Results for Simple Summation Algorithm	61
5.2.1	SAR test: Metallic Plate	62
5.2.2	SAR test: Metallic Plate 45 degrees	64
5.2.3	SAR test: Metallic Square Pole	66
5.2.4	SAR test: Metallic Square Pole 45 degrees	69
5.2.5	SAR test: Circular Metallic Pole	72
5.2.6	SAR test: Circular Plastic Pole	74
5.2.7	SAR test: Metallic Wire	76
5.3	Comparison with Results from Other Studies	78
5.4	Discussion	79
5.5	Summary	80
<b>6</b>	<b>Conclusion</b>	<b>81</b>
6.1	Closing Discussion	81
6.2	Further Research Prospects	82
<b>A</b>	<b>Simple Summation Algorithm Python Code</b>	<b>85</b>

# List of Figures

2.1	Block diagram of the dynamics between transmitter and receiver . . .	5
2.2	Antenna Lobes - taken from Wikipedia . . . . .	7
2.3	Diagram of an antennas surrounded by its three field regions - (www.giangrandi.ch - field regions around an antenna) . . . . .	8
2.4	Back-scatter from different shapes - taken from [14]) . . . . .	11
2.5	Back-scatter from cylinder and a plane - taken from [14]) . . . . .	12
2.6	Illustration of the Radar shadow - taken from [15] . . . . .	12
2.7	A 4 inch resolution image from Sandia National Laboratories - taken from [16] . . . . .	13
2.8	CW vs Pulsed Radar during transmission . . . . .	15
2.9	UWB Radar transmission power spectrum - taken from [19] . . . . .	17
2.10	Synthetic Aperture Synthesis - taken from [25]) . . . . .	20
2.11	SAR Stripmap mode . . . . .	21
2.12	SAR Spotlight mode . . . . .	21
2.13	SAR Scan mode . . . . .	22
2.14	SAR Geometry - taken from [29] (Accessed: 18.12.2017) . . . . .	23
2.15	Range profiles [11] . . . . .	24
2.16	Imaging of four trihedrals [11] . . . . .	25
3.1	Illustration of the pulse compression technique . . . . .	35
3.2	Linear FM CHIRP signal . . . . .	36
3.3	FFT process for a signal with N=16 samples . . . . .	39
3.4	Data distribution before (○) and after (●) interpolation . . . . .	40
3.5	Block diagram illustrating the main steps of an RMA algorithm . . . . .	42
3.6	Generation of hyperbolic reflection [55] . . . . .	44
3.7	Scheme: Point-like target [12] . . . . .	45
3.8	Performance for point-like target: Figure 3.7 [12] . . . . .	46
4.1	UAV used during tests . . . . .	52
4.2	Novelda XeThru X4 Circuit Overview [65] . . . . .	54
4.3	The Radar module mounted on the UAV . . . . .	55
5.1	UAV flight . . . . .	60
5.2	Test objects from the UAV's position . . . . .	61
5.3	Generated SAR image of the metallic plate . . . . .	63
5.4	Magnitudes for the metallic plate summed up at all distances . . . . .	63
5.5	Manually flown UAV path for the metallic plate (Metallic plate center in red) . . . . .	64
5.6	Generated SAR image of the metallic plate at 45 degrees . . . . .	65

5.7	Amplitudes for the metallic plate at 45 degrees summed up at all distances . . . . .	65
5.8	Manually flown UAV path for the metallic plate (red circle) at 45 degrees . . . . .	66
5.9	Generated SAR image of the metallic square pole . . . . .	67
5.10	Amplitudes for the metallic square pole summed up at all distances . . . . .	68
5.11	1 second snapshot of the amplitudes summed up for when the UAV flies in front of the metallic square pole . . . . .	68
5.12	Manually flown UAV path for the metallic square pole shown as a red circle . . . . .	69
5.13	Metallic square pole at 45 degrees . . . . .	70
5.14	Generated SAR image of the metallic square pole at 45 degrees . . . . .	70
5.15	Amplitudes for the metallic square pole at 45 degrees summed up at all distances . . . . .	71
5.16	Manually flown UAV path for the metallic square pole (red circle) at 45 degrees . . . . .	72
5.17	Generated SAR image of the circular metallic pole . . . . .	73
5.18	Magnitudes for the circular metallic pole summed up at all distances . . . . .	73
5.19	Manually flown UAV path for the circular metallic pole (red circle) . . . . .	74
5.20	Generated SAR image of the circular plastic pole . . . . .	75
5.21	Amplitudes for the circular plastic pole summed up at all distances . . . . .	75
5.22	Manually flown UAV path for the circular plastic pole shown as a red circle . . . . .	76
5.23	Generated SAR image of the metallic wire . . . . .	77
5.24	Amplitudes for the metallic wire summed up at all distances . . . . .	77
5.25	Manually flown UAV path for the metallic wire (approximately at the red circle) . . . . .	78

# List of Tables

2.1	Example of Pulsed Radar System Performance . . . . .	14
2.2	Comparison of CW Radar Systems [4] . . . . .	17
4.1	NTNU research UAV with XeThru X4 UWB System on Chip Radar . . .	53
4.2	Radar Bands and Usage (similar to table 1.1 in [7]) . . . . .	55
4.3	DJI Phantom with PulsON 410 UWB Smart Sensor [66] [67] . . . . .	57



# List of Abbreviations

<b>UAV</b>	<b>Unmanned Aerial Vehicle</b>
<b>SAR</b>	<b>Synthetic Aperture Radar</b>
<b>RF</b>	<b>Radio Frequency</b>
<b>SNR</b>	<b>Signal to Noise Ratio</b>
<b>RCS</b>	<b>Radar Cross Section</b>
<b>UWB</b>	<b>Ultra Wide-Band</b>
<b>CW</b>	<b>Continuous Wave</b>
<b>PRF</b>	<b>Pulse Repetition Frequency</b>
<b>IPP</b>	<b>Inter-Pulse Period</b>
<b>IF</b>	<b>Intermediate Frequency</b>
<b>AC</b>	<b>Alternating Current</b>
<b>DC</b>	<b>Direct Current</b>
<b>FM</b>	<b>Frequency Modulated</b>
<b>FMCW</b>	<b>Frequency Modulated Continuous Wave</b>
<b>SFCW</b>	<b>Stepped Frequency Continuous Wave</b>
<b>FSK CW</b>	<b>Frequency Shift Keyed Continuous Wave</b>
<b>GPS</b>	<b>Global Positioning System</b>
<b>SoC</b>	<b>System on Chip</b>
<b>CHIRP</b>	<b>Compressed High Intensity Radar Pulse</b>
<b>DFT</b>	<b>Discrete Fourier Transform</b>
<b>FFT</b>	<b>Fast Fourier Transform</b>
<b>RMA</b>	<b>Range Migration Algorithm</b>
<b>ERM</b>	<b>Exploding Reflector Model</b>
<b>IDE</b>	<b>Integrated Development Environment</b>
<b>VCS</b>	<b>Version Control System</b>



## Chapter 1

# Introduction

### 1.1 Motivation for this thesis

Today, developed technology focuses a lot on autonomy by the use of surface and aerial based vehicles to aid in every aspect of the modern world. Autonomous systems are supposed to be more predictable, more efficient, and safer than human beings. For example, within the car industry there is a lot of incentive to go towards less human interaction and more autonomy as there are still thousands of people dying, and several million people sustaining injuries from car accidents every year [2]. When it comes to aerial vehicles the statistics are different and the airspace is a lot more regulated regarding traffic. But the airspace is getting more and more crowded. With a blooming consumer drone market, as well as drone taxi services being tested in major cities like Dubai, the need for safe navigation is crucial [3]. To ensure safe navigation, a highly functioning and robust anti-collision/collision avoidance system is needed. Within a collision avoidance system there can be found many different types of sensors. The common denominator for all parts of a collision avoidance system is that they should be able to give some information about the system's environment, whether it is by the use of thermal energy, sound waves, electromagnetic waves, or other means. Within the use of electromagnetic waves there are many types of techniques that can be used for detecting and gathering information about specific environments. This thesis will explore the use of electromagnetic waves, more specifically radio waves, as a means to acquire relevant information about a specific area using an Unmanned Aerial Vehicle (UAV). Even more specifically, the use of Synthetic Aperture Radar (SAR), a Radar imaging technique, which will be introduced in the following chapters.

There has not been done a lot of testing of SAR on small UAVs and it will be interesting to see what kind of results a small UAV can produce by the use of SAR. And of course, if it may aid in safer and more accurate navigation for the UAV.

### 1.2 Scope of this thesis

This thesis aims to test the feasibility of using SAR on a small-sized multirotor UAV. Radar technology has been used for a long time and as the technology improves, its usability increases. Using Radar on multirotor UAVs for the purpose of navigational aid is a subject yet to be thoroughly researched. First, to capture the

obvious question; "why Radar?", it is important to note the following.

Radar-based sensors possess a number of specific advantages comparing them to other types of sensors such as laser rangefinders, computer vision/focal plane arrays, acoustic sensors, etc... [4] As opposed to optical sensors, Radars are not dependant on lighting conditions, and neither affected by smoke, fog, dust and other factors that typically affect optical wavelengths. Continuing the argumentation, Radars usually have better directionality and range characteristics compared to acoustic systems and Radar systems can also be used on-board UAVs with high levels of acoustic noise and still be able to detect other aircraft with little to no acoustic noise emissions. This is something that increases in importance as the number of UAVs driven by electric propulsion increases. At present, as far as I know, there exists no other non-cooperative sensor type that possess all these capabilities [5].

### 1.3 A Historical Perspective

During the 1940s, the United States Army was searching for and trying to develop an aerial reconnaissance system that could see through clouds and not having any dependencies on the hours of daylight. SAR was developed in the 1950s solely as a solution to the 1940s need for a 24-hour remote aerial surveillance system with no limitations when it came to weather. Radar possesses the ability to penetrate clouds and for, and is not dependant on the wavelengths of visible light, and so it became the logical choice for the US Army. The main challenge was how to be able to achieve a fine enough resolution for the system to become useful. With existing knowledge about Radar it was estimated that the Radar antenna would have had to be about the size of a football field in order to achieve fine enough resolution, and that would be an antenna too large for any reconnaissance aircraft to carry. [6]

Carl Wiley, known to have invented SAR [7], suggested in 1951 a principle that each object has its own significant Doppler shift because each object in the Radar beam has a slightly different speed relative to the antenna. Therefore one could analyze the frequency of the Radar reflections which in turn would make it possible to construct a detailed image. With this technique, a Radar antenna of one meter could be able to acquire an image which otherwise would have required a much larger antenna. About one year after Wiley invented SAR, researchers at the University of Illinois independently developed the same concept, as well as developing beam sharpening and auto-focus concepts. The following year, the plans were laid out for creating a practical SAR under a project named "Project Wolverine" at the University of Michigan. Since SAR requires a lot of processing it was at that time pushing the limits of analog processors. This is where one of the pioneers of holography, Emmett Leith came in with the idea of using optical processing of the data. The method ended up working, and in 1957, airborne SAR was yielding astonishing results. [8]

In 1974, the National Oceanic and Atmospheric Administration and engineers from Jet Propulsion Laboratories started investigating the possibilities for oceanic observations using a SAR mounted on a satellite. The wavelengths of SAR gives it the ability to detect small surface roughness changes, which makes it ideal for monitoring surface wave patterns and currents in the ocean. SAR is so sensitive to surface roughness changes that it can measure displacement accuracy to within several millimeters. In 1978, the satellite Seasat was launched - the first ever civilian application of SAR [9]. Seasat was a very successful application which provided scientists with a new powerful tool when studying the earth. Prior to Seasat, civilian image acquisition of the earth was taken by Landsat cameras dependant on visible light and with poor resolution in tens of meters. [6] Even though Seasat only operated a couple of months before it was disabled by a massive short circuit in its power system, SAR was now proven to be a very useful imaging tool.

SAR has in modern times become one of the most valuable and useful tools for remote sensing of our planet and its environment. At distances of tens of kilometers SAR can obtain centimeter resolution [10], which gives it great advantages for observation of for example, sea ice. SAR is also used to measure glacier variations, collecting wind pattern data, rainfall and erosion, vegetation structures, disaster management and identification of potential storm surges, landslide areas and drought prediction. Forests play a great role when talking about local and global climate. The health of forests is closely linked with the health of the soil, to the quality of the watershed and since forests often cover vast areas that are inaccessible, airborne and satellite SAR are great tools for a detailed study of such areas. SAR can be used to map forests, which in turn can be used to predict, and even monitor forest fires.

SAR has for a long time been an expensive imaging tool mounted on large aircraft. In the last years low-cost SAR systems have been developed and mounted on smaller devices for use in other applications. Short-range imaging and mapping of nearby surroundings are among the things SAR have been tested on in recent years [11], [12].

## 1.4 Thesis Outline

This thesis is built upon the literature and research presented in my project thesis. Thereby, some of the sections in the first three chapters contain parts of what has already been presented in my project thesis. As some of these parts are mixed with added literature and altered with different formulations they will not be mentioned explicitly.

- **Chapter 1:** An introduction to the motivation behind this thesis as well as the scope and purpose of the thesis, followed by a historical perspective on SAR and how this master thesis will be presented.

- **Chapter 2:** Radar technology and SAR fundamentals are explained with a review and discussion on how Radar can be used in local navigation and collision avoidance with emphasis on the use of small multirotor UAVs.
- **Chapter 3:** SAR signal processing is explained to the best of my abilities and understanding and several algorithms are presented to show some differences in SAR signal processing.
- **Chapter 4:** A summary of the software and hardware that was used followed by my the implementation steps of a simple SAR algorithm that can run on Radar data generated by a UAV at the NTNU Motion Capture Lab.
- **Chapter 5:** Test setup and results for drone data processing is presented and discussed.
- **Chapter 6:** Using SAR as part of an anti-collision system on consumer-sized multirotor drones is discussed along side the findings in this master thesis. Following is a self-evaluation of the findings in this thesis ending in a discussion around further research prospects.

## 1.5 Nomenclature

- **Multirotor (drone/UAV):** An unmanned rotorcraft/aerial vehicle relying on symmetrically positioned rotors in order to fly.
- **Small-sized UAV/drone/multirotor** An unmanned rotorcraft/aerial vehicle with a maximum take-off weight of 10 kg.
- **Radar:** A system that uses radio waves to collect information on its surroundings.
- **Target:** An object on which a Radar wants to gather information about (distance, speed, heading, size, etc)
- **UWB (Ultra-wide band):** A Radar system that uses a large spectrum, either through very short pulses, or frequency hopping is considered to be ultra-wide band.
- **SAR system/device:** When talking about a SAR system I will be referring to a Radar system running a SAR algorithm.

## Chapter 2

# Synthetic Aperture Radar (SAR)

Before covering the concept of Synthetic Aperture Radar one must first capture the fundamentals of Radio Detection and Ranging, also known as Radar. This chapter is built upon literature on the basic concepts of Radar and SAR alongside research and thoughts on how Radar and SAR can aid in local navigation and what challenges to be considered. Finishing with a short summary of the key elements to be taken away from this chapter.

### 2.1 Radar Systems

Figure 2.1 shows a basic block diagram of the important subsystems found in a Radar. I will now continue by examining the basic parts of a Radar.

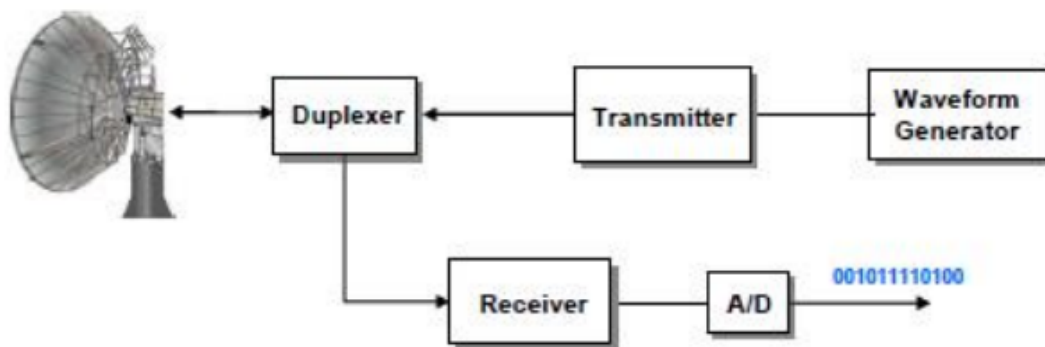


FIGURE 2.1: Block diagram of the dynamics between transmitter and receiver

#### Transmitter

Radio transmitting is usually accomplished in two stages. First, the waveform generator produces a low power waveform signal and up converts it to radio frequency (RF). Secondly the transmitter amplifies the signal which is then radiated into space by the antenna. The waveform is made suitable for the particular job the Radar is to perform. Most Radars use a short pulse waveform so that a single antenna can be used on a time-shared basis for both transmitting and receiving.

### Receiver

The function of the receiver is to amplify the weak echoes from the antenna system sufficiently. As noise is the ultimate limitation on a Radars ability to make a reliable detection and to extract information about the target, it is extremely important that the receiver produces the minimum amount of noise possible. Receivers used in Radars are able to detect weak signals and augmenting their amplitudes by factors of 20 to 30 million, even more. It is important that the receiver is able to reject interfering signals so that the relevant information can be optimally detected.

Figure 2.1 shows the basic transmit- and receive-dynamics of a Radar system. When a single antenna is used to both transmit and receive signals, as in some Radar systems, an electronic switch is used. The electronic switch, also called a *duplexer* allows for bi-directional communication over a single path. For the Radar it transfers the antenna connection from the receiver to the transmitter during the transmitted pulse and back to the receiver during the echo pulse.

### Antenna

The Radar antenna is the device that propagates the transmitted energy into space and then collects the echo energy on receive. There exists mainly two/three types of antenna systems in Radars. Primarily there is the *monostatic*, antenna system where the same antenna is used for transmitting and receiving. There are also Radar systems which uses separate antennas for transmitting and receiving, so called *bi-static* or *multi-static* antenna systems. In this thesis, the theory will assume monostatic antenna configuration if not specified.

But to understand the fundamentals of Synthetic Aperture Radar in the next chapter it is important to go into a bit more detail on the essentials of Antenna theory.

The *Antenna Radiation Pattern* is a distribution plot of the radiated signal power from the antenna to everywhere around it. Looking at this plot you will achieve a visual understanding of the area coverage by the antenna. And while analyzing the antenna radiation pattern of a directional antenna, a big portion of the radiated power is distributed in the desired direction, also referred to as the mainlobe. But because of the attributes of electromagnetic radiation it is impossible to build an antenna that radiates coherently equal in all directions. Therefore you end up with many smaller beams in other directions known as sidelobes, shown in figure 2.2. *Antenna Beamwidth* is the angular measurement of the mainlobe which determines the area the antenna covers during transmission.

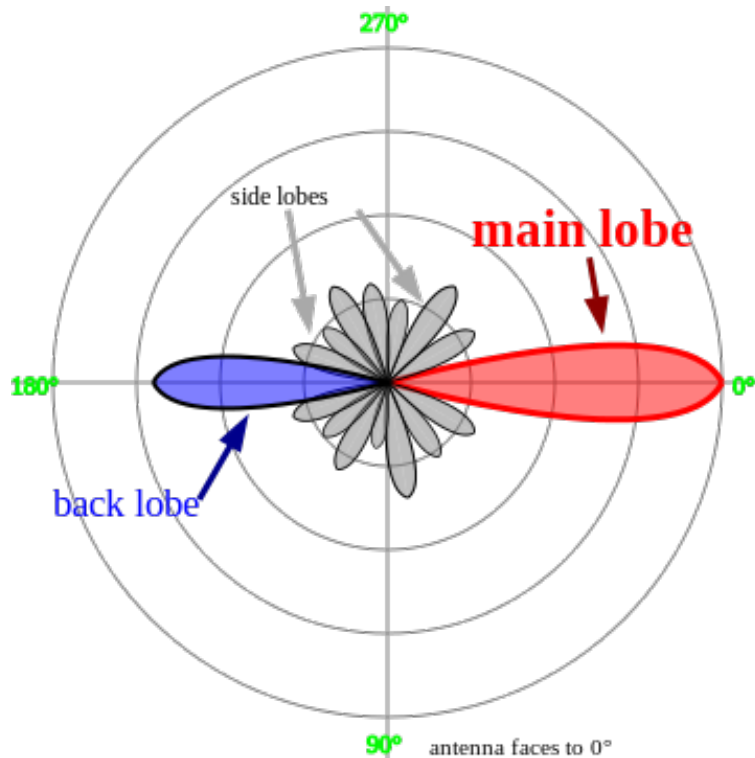


FIGURE 2.2: Antenna Lobes - taken from Wikipedia

*Directivity* is a fundamental antenna parameter. It is a measure on the antenna's radiation pattern, on how directional it is. An antenna that radiates coherently equal in all directions would have zero directionality and the directivity of that antenna would be 0 dB (or 1). The directivity of an antenna combined with the antenna efficiency (the percentage of the physical aperture area which actually captures radio frequency energy) gives the antenna gain. With a higher gain, the transmitted energy will become more powerful, hence the received power will be stronger which yields a better signal to noise ratio (SNR).

An antenna with a high frequency current generates a high frequency electromagnetic field around it. The structure of this field depends on the antenna shape and it is usually very complex in detail. The closer to the antenna you are the harder it is to visualize and analyze the structure of the electric and magnetic fields without involving complex numerical calculations. But as we move further away from the antenna, the field ends up looking more and more like spherical waves. In fact, the greater the distance, the better the resemblance with spherical waves. And calculations with spherical waves can usually be done with simple equations. So, to classify, the surrounding space of an antenna is subdivided into three *Field Regions*: the *reactive near-field region*, the *radiating near-field (Fresnel) region*, and the *far-field (Fraunhofer) region*. The reason for these classifications of the field structure, is to know which mathematical simplifications can be applied, though there is no abrupt change in the field configuration, hence no precise boundaries between them [13].

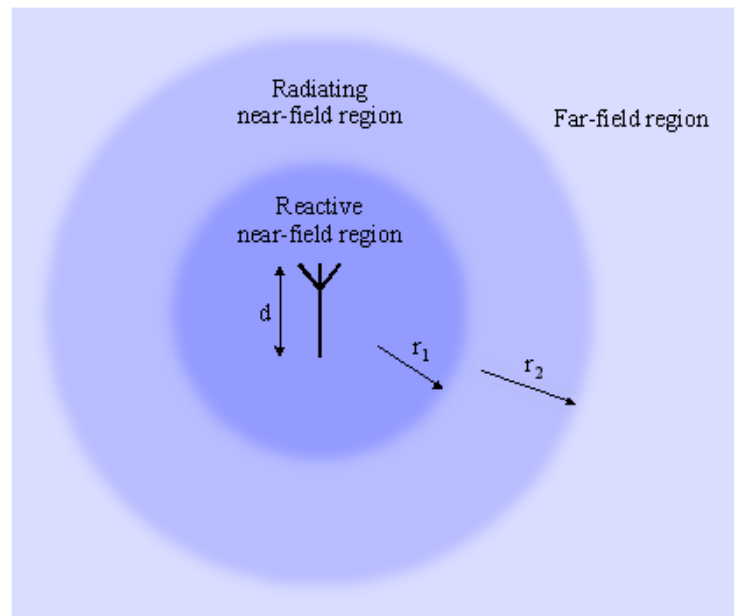


FIGURE 2.3: Diagram of an antennas surrounded by its three field regions - ([www.giangrandi.ch](http://www.giangrandi.ch) - field regions around an antenna)

1. The *reactive near-field region* is the closest region to the antenna. To determine the structure of this field would require a lot of calculus, or specific numerical methods. You can imagine this field as a volume the antenna needs to "prepare" the field that will actually radiate. In this region, the magnetic and electric fields are out of phase.
2. Next in line is the *radiating near-field (Fresnel) region* where the electric and magnetic fields are in phase, though the angular field distribution still depends on the distance to the antenna. This means that almost the entire region radiates. Even though this field is further away than the reactive field it is still too close to the antenna to ignore its shape. It would still require a lot of calculus to determine the complex field structure.
3. The *far-field (Fraunhofer) region* surrounds the reactive and radiating near-field regions described above. As this field extends to infinity it represents the vast majority of space the wave travels. The angular field distribution does no longer depend on the distance to the antenna and can be approximated with spherical wave-fronts. The entire field radiates. All along this thesis, when SAR radiation properties are discussed, it is always done in terms of the far field. Range of this field for an antenna with diameter  $d$  and wavelength  $\lambda$  is,  $R > \frac{2d^2}{\lambda}$ .

**Antenna Resolution** defines the antenna's ability to distinguish one object from another. When talking about the quality of resolution with respect to SAR, the preferred terms are *fine* and *coarse*. Fine resolution simply implies that the antenna

is able to differentiate between two objects that are not far from each other. There are two types of resolutions to consider, *Range Resolution* (the resolution of the direction parallel to the direction of the mainlobe) and *Azimuth Resolution* (the resolution of the direction perpendicular to the mainlobe direction).

- Range resolution depends strongly on the pulse width, shorter pulse gives a finer resolution. Though, in practical Radar systems, longer pulse is preferred because of power efficiency (this also goes for SAR). Fine resolution would in this case require a greater bandwidth as the longer pulse will eventually be compressed for finer resolution. Therefore, greater bandwidth equals better compression which, in turn, yields finer resolution, this will be brought up in more detail in chapter 3.
- Azimuth resolution depends on the length of the antenna. Considering a phased array antenna the azimuth resolution gets finer the longer the antenna is. The reason for considering a phased array antenna is that it works in a similar way to SAR. The phased array antenna uses the diffraction property of electromagnetic waves to radiate the signal. It consists of several radiating elements, each with a phase shifter which dictates the direction of propagation. More radiating elements would give a more powerful (because of constructive interference) and sharper (because of destructive interference) radiation. Though this is considered true for a real aperture antenna, SAR works in a slightly different way, which will be discussed later in this chapter.

## 2.2 The Radar Equation

Having deep knowledge of electromagnetic wave propagation is not necessarily needed to work with Radar systems. Usually a rudimentary understanding of the Radar equation (2.1) is enough. There exists many different versions of the Radar equation, but the one discussed in this section is taken from the Radar Handbook, written by Merrill I. Skolnik [7]. The Radar equation represents the physical dependencies of the transmit power, that is the wave propagation until the signal is received upon return.

$$P_r = \frac{P_t G_t G_r \lambda^2 \sigma F^4}{(4\pi)^3 R^4} \quad (2.1)$$

where

- $P_r$  and  $P_t$  is received and transmitted power respectively
- $G_r$  and  $G_t$  is the receiver and transmitter antenna gain respectively
- $\lambda$  is the transmitted wavelength
- $\sigma$  is the Radar cross section (RCS), also called the scattering coefficient

- $F$  is the pattern propagation factor
- $R$  is the distance from the Radar to the target

First of all,  $R$  makes the assumption that the transmitter and the receiver are located at the same spot. The key points to take away from the Radar equation is that the signal strength decreases inversely by the fourth power of the distance between the Radar and the target. This is caused by so called free-space path loss, which is the electromagnetic energy spreading equally as the distance from the antenna increases. To exemplify, an object two meters from the antenna will be perceived sixteen times weaker than an object one meter away. This means that the transmitted signal must be powerful at the same time as the receiver must be sensitive.  $F$ , the pattern propagation factor, which is a term regarding several effects, among others the loss caused by propagation in air versus vacuum, or by multi-path propagation also needs to be taken into consideration. There are two other major factors concerning the Radar equation, the antenna gain which was mentioned in the previous section, and the Radar cross section  $\sigma$  which will be discussed next.

The Radar Cross Section (RCS) is the measure of a specific target's ability to reflect a Radar signal in the direction of the Radar receiver. A target's RCS can be seen as a comparison between the power of the reflected signal from a target and the reflected signal from a perfectly smooth sphere of a cross sectional area of  $1 \text{ m}^2$ . RCS is best visualized as the product of:

- The *projected cross section*: Depends on the physical geometry of the target
- The *reflectivity*: The percent of intercepted power scattered (reradiated) by the target
- And the *directivity*: The ratio of the power scattered back in the direction of the Radar to the power that would have been back-scattered had the scattering been uniform in all directions.

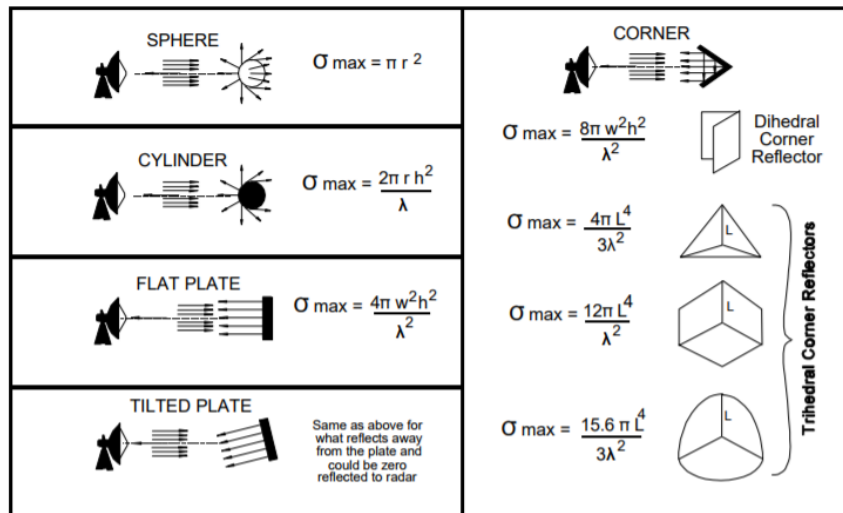


FIGURE 2.4: Back-scatter from different shapes - taken from [14])

The RCS is complicated to compute precisely by hand and thus it is often determined experimentally or by computer simulations. Considering figure 2.4 different shapes have very different RCS, which will greatly affect the way in which they are "seen" by a Radar. When assuming the relative size of the RCS there are always three factors to consider:

1. **Size:** For example, stealth planes are constructed in such a way that the RCS matches that of a small bird, while in reality the plane is several hundred times the size of the bird
2. **Shape:** A factor that is better described by figure 2.5 where one can see the different scattering on a plane-shaped structure and a circular structure.
3. **Material:** The general rule of thumb is that the more electrically conductive the material is, the more reflective it will be. That is why targets made out of metal are more visible to a Radar than targets made of non-conductive materials such as plastic or glass fiber. Smart utilization of shape and material makes it possible for the designer to choose an appropriate RCS.

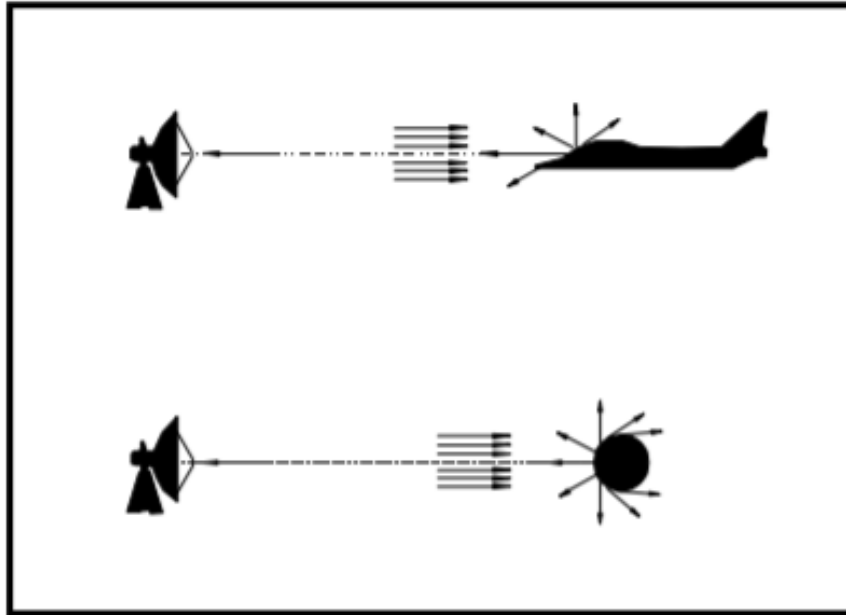


FIGURE 2.5: Back-scatter from cylinder and a plane - taken from [14])

Even though the RCS is a big factor on how easy it would be to detect or generate an image of an object there is another factor that also comes in. The Radar shadow. The Radar shadow is the area which is not illuminated because of obstructions in route or curvature of the earth (Radar horizon). For airborne Radar illuminating the earth surface it could be caused by a mountain, see figure 2.6. For smaller objects the Radar shadow might give some indication on the shape of the object, see figure 2.7.

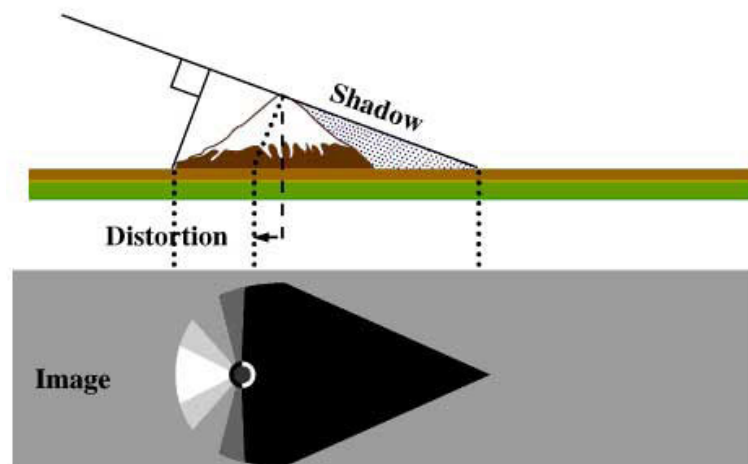


FIGURE 2.6: Illustration of the Radar shadow - taken from [15]



FIGURE 2.7: A 4 inch resolution image from Sandia National Laboratories - taken from [16]

## 2.3 Different types of Radars

Radar systems are normally divided into two broad categories depending on the nature of their transmitted energy [4]: Pulsed, and Continuous Wave (CW).

### 2.3.1 Pulsed Radar

In a pulsed Radar architecture, the transmitter generates Radio Frequency (RF) pulses of a specified duration and transmits this energy towards the region/target under observation. These pulses are then reflected off a target (if present) and part of the energy returns to the receive antenna. The range to the target can then be found by equation (2.2):

$$R = \frac{cT}{2} \quad (2.2)$$

$R$ , which is the range is defined in terms of  $c$ , the speed of light, and  $T$ , the elapsed time between the transmitted pulse and the reception of that same pulse.  $T$  is set by what is known as the Pulse Repetition Frequency (PRF) - the rate at which the RF pulses are transmitted. In a pulsed Radar architecture it is critical that the PRF stays constant, if this is not followed, range ambiguities will occur. Naturally, the PRF has a direct impact on the maximum distinguishable range of the system, also known as the unambiguous range,  $R_{unamb}$ , which can be described as follows:

$$R = \frac{c}{2(PRF)} \quad (2.3)$$

As pulsed Radar systems switch on and off between transmitting and receiving, they are typically limited to a minimum detectable range. The receive circuitry of

the Radar is switched off during the transmission of RF pulses, since close range reflections, i.e. high energy reflections would saturate and worst case scenario, destroy the highly sensitive receiver electronics. The lower bound on the minimum detectable range is described by the following equation:

$$R_{min} = \frac{c(T_{tx} + T_{config})}{2} \quad (2.4)$$

In this equation,  $T_{tx}$  represents the duration of the transmit pulse, and  $T_{config}$  is the time needed to enable the receiver. Hence, for moderate pulse widths, the minimum achievable range is easily in the region of tens of meters. The range resolution of pulsed Radars,  $\Delta R_{min}$  is described by the following equation (given that advanced techniques like, intra-pulse modulation, pulse compression, etc... are absent):

$$\Delta R_{min} = \frac{cT_{tx}}{2} \quad (2.5)$$

Given the equations above and using the parameters of a theoretical Radar system as in [4] with a minimum  $T_{tx}$  of 500 ns, a  $T_{config}$  of 11 ns, and a PRF of 20kHz, the system will possess the following properties:

Parameters	Value (meters)
Unambiguous Range	7494.8
Range Resolution	79.6
Minimum Range	74.9

TABLE 2.1: Example of Pulsed Radar System Performance

Considering the parameters minimum range, and range resolution, there are a large number of targets with dimensions significantly smaller than those presented in table 2.1. Thus, designing a pulsed Radar system with acceptably small minimum range and resolution characteristics is an expensive task. This is mostly due to the high power requirements during the short pulses as well as the precise and fast timing requirements of such a system.

### 2.3.2 Continuous Wave Radar

Continuous Wave (CW) Radars on the other hand operate in a way that they continuously illuminate the target area with RF waves. As a difference to pulsed Radar systems, CW Radars normally operates on a much lower power levels, up to three magnitudes lower power for similar range performance [17]. Since CW Radar is not able to use pulse timing to calculate the range to illuminated targets it uses some form of frequency modulation to determine the range. Furthermore, CW Radars eliminates the strict timing requirements a pulsed Radar system has and this allows them simpler circuitry. Another advantage of CW Radars is that they have no theoretical limit on minimum range because of the continuous illumination of targets and they are also capable of providing arbitrary range resolutions.

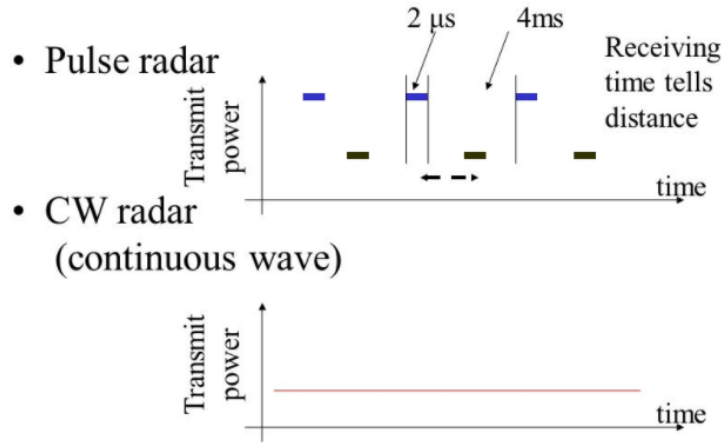


FIGURE 2.8: CW vs Pulsed Radar during transmission

Figure 2.8 captures the main difference between CW and pulsed Radars considering signal transmission.

The most basic, and probably most common CW Radar configuration is the Doppler Radar. The Doppler Radar transmits a continuous signal towards the area of interest and if an object is present a portion of that energy is reflected back to the receiver. When a target is moving radially relative to the Radar system, the carrier frequency of the reflected wave is shifted slightly, which is called the Doppler frequency shift. Upon reception of the reflected signal the Doppler Radar performs a down-conversion (multiplying in the frequency domain) to produce the desired frequency, also known as the "Beat Frequency" or "Intermediate Frequency" (IF) and is described as follows:

$$F_{beat} = F_{tx} - F_{rx} \quad (2.6)$$

$F_{tx}$  and  $F_{rx}$  are the frequencies of the transmitted and received signal, respectively. While  $F_{tx}$  is determined by the radial velocity  $v$  of the target object relative to the Doppler Radar system,  $F_{rx}$  is usually determined by the following equation (assuming that the receive and transmit antennas are located at the same spot):

$$F_{rx} = F_{tx} \frac{1 + \frac{v}{c}}{1 - \frac{v}{c}} \quad (2.7)$$

For most terrestrial applications this equation is simplified by the fact that  $v \ll c$ , and  $F_{beat}$  can be written as:

$$F_{beat} \approx F_{tx} \frac{2v}{c} \quad (2.8)$$

Unmodulated CW Radars does not have the ability to calculate range between its Radar antenna and a target. Continuing, unmodulated CW Radars are not capable of detecting stationary targets because  $F_{beat}$  results in a Direct Current (DC)

signal which is lost because of the Alternating Current (AC) coupling between the RF front end and the amplifier stages. Adding to the fact that most CW Radar front ends usually produce a DC signal even if there is no target present, because of the leakage between the receiver and transmitter. Though there exists many methods for measuring range in CW Radars, they are normally divided into two main categories:

1. Frequency Modulated Continuous Wave (FMCW) and
2. Stepped Frequency Continuous Wave (SFCW) - of which Frequency Shift Keyed Continuous Wave (FSK CW) is a narrow-band subset.

FMCW Radars operate by modulating the transmit frequency, normally in a triangular fashion. Considering the speed of light being constant,  $F_{tx}$  will be offset from  $F_{rx}$  by an amount that is proportional to the range. Thus, the equation defining the range between the Radar antenna and a target object becomes:

$$R = \frac{2cTF_{beat}}{BW} \quad (2.9)$$

In this equation,  $T$  represents the period of the frequency modulation, and  $BW$  is the bandwidth. As opposed to unmodulated CW Radars, FMCW Radars possess the ability to detect both the presence and range of stationary targets. However, background clutter from walls, or different types of terrain will also become present in the output data. FSKCW Radars try to solve parts of this issue by changing the linear, triangular modulation of FMCW Radars with a square wave modulation of the transmit frequency.  $F_{beat}$  is thereby sampled synchronously with the modulation. Considering the transmit frequency modulation as well as the synchronous sampling of the received signal, we end up with two unmodulated CW Radar channels separated by a few MHz ( $BW$ ):  $IF_a$  and  $IF_b$ . Equation (2.8) shows that for all moving targets,  $F_{beat}$  will be marginally different for  $IF_a$  and  $IF_b$ . This specific marginal difference will also appear if it is used for velocimetry purposes, but it is important for ranging as it manifests itself as a phase shift in the time domain [4]. Using the phase difference between  $IF_a$  and  $IF_b$  one can determine the range to a target by the following equation ( $\phi_n$  is the phase shift of  $IF_n$ ) [18]:

$$R = \frac{c(\phi_A - \phi_B)}{4\pi BW} \quad (2.10)$$

FSK CW Radars possess the same abilities as different CW Radar types, namely: no theoretical limit on minimum range combined with a fine range resolution. It also offers the same advantages as unmodulated CW Radars, among an excellent ground clutter rejection and low total transmit power requirements. Though there is a limit on the maximum practical range - not considering any limits on transmit power and receiver sensitivity. The maximum range limit is defined by the range corresponding to a  $180^\circ$  phase shift. Similar to pulsed Radar systems, this range is known as the unambiguous range and is described by the following equation [18]:

$$R_{unamb} = \frac{c}{2BW} \quad (2.11)$$

Table 2.2 compares the parameters of the different types of CW Radars that have been presented:

Parameters	Doppler	FMCW	FSKCW
Range Measurement	-	Yes	Yes
Velocity - Range Ambiguity	-	Yes	No
# of Receiver Channels	1	1	2
Bandwidth Requirements	Single Frequency	500MHz	5MHz
Modulation Type	-	Triangular or Sawtooth	Square

TABLE 2.2: Comparison of CW Radar Systems [4]

Another type of Radar system worth mentioning within the domain of pulsed Radars is the Ultra Wide-Band (UWB) Radar that transmits signals across a much wider frequency than conventional Radar systems and are normally difficult to detect because of the transmitted signals having a very light power spectrum as illustrated in figure 2.9. Usually, UWB signal generation is done by transmitting pulses with very short durations (less than 1 nanosecond).

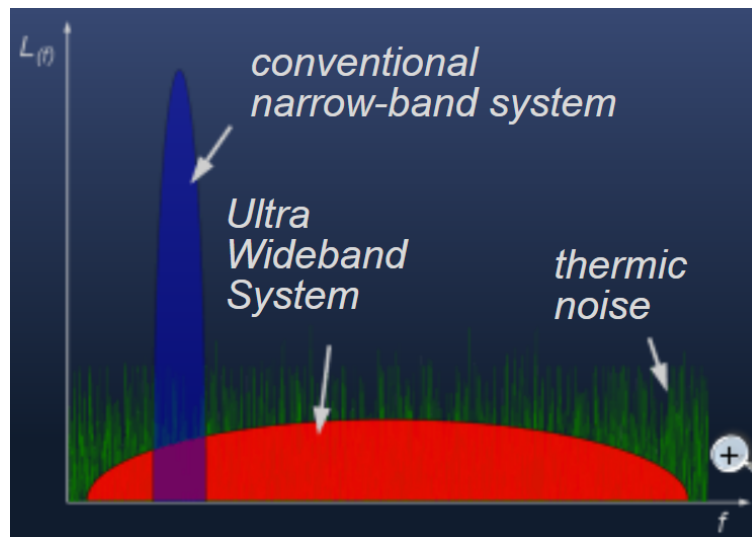


FIGURE 2.9: UWB Radar transmission power spectrum - taken from [19]

The frequency spectrum of a very narrow-width pulse approaches that of white noise as the pulse becomes more narrow. These very short pulses require the use of a wider receiver band-width than conventional radar systems. The size of the spectrum occupied by a UWB Radar signal, i.e. the band-width of the transmitted UWB signal, is at least 25% of the center frequency. Therefore, a UWB signal centered at for example 4 GHz, would have a minimum band-width of 1 GHz, though often the absolute band-width is greater than 1 GHz.

An example of a typical UWB Radar is the pulsed noise Radar which is transmitting at a center frequency of 24 GHz, thus its band-width is 8 GHz. It

transmits single pulses with a duration of a few nanoseconds and its pulse power is 4 mW. Because of its low pulse power it is not possible to detect if the Radar is transmitting or not since its transmitted pulses do not differ from environmental noise.

Referring to the earlier discussed CW Doppler Radar it is worth mentioning that there exists pulsed Radar systems built upon the technique of determining the velocity by the use of Doppler. Originally Doppler Radars utilized CW, and measured the Doppler shift of reflected waves, though having the disadvantage of not being able to detect the range to the target. As mentioned earlier, this disadvantage was solved by the use of Radar wave modulation, such as the FMCW, or by pulsing the Radar wave on and off. Namely a Pulse-Doppler Radar system.

## 2.4 Radar for Collision Avoidance

Starting with the automotive industry, Radar has been used for many applications and is greatly adopted into all new cars. Primarily, Radars serve as the main system for adaptive cruise control wherein the Radar provides information to the vehicle's computers for the purpose of maintaining a specific distance between the host vehicle and the vehicle in front. The automotive Radar systems are usually connected to the brakes so that the vehicle can be stopped without driver intervention [20]. Radar systems are also used for more than acquiring information about line of sight range.

There are a number of researchers that have dedicated a lot of time to demonstrate the versatility of Radar in autonomous ground vehicles, among them is Viikari et. al. [21]. They developed a 24GHz automotive Radar with the ability to identify road conditions (icy, sand, dirty, gravel, etc...) by measuring the polarization of the back-scattered energy. Bartch et. al. [22], shows the development and applicability of micro Doppler modulation target profiles in pedestrians as well as the differentiation of slowly moving pedestrians from other static targets. In addition to the expansion of Radar sensor capability, the ever growing demands and constraints of the automotive industry, with a strong emphasis on cost effectiveness, Radar systems have seen innovation when it comes to packaging arrangements as well as antenna designs [23].

A natural step in the use of Radar is naturally to apply them on airborne systems like UAVs. This is an area that has also been thoroughly researched by educational institutions and commercial groups. Richley et. al. [24] describe the development of a miniature UWB Radar for micro air vehicles. In the research they show the applicability of Radar technology on small UAVs less than 15cm in any dimension. Using a UWB Radar is of great advantage here as it substantially decreases the power requirements and mass of the Radar sensor, in this study, 0.8 watts peak and 42.5 grams.

Viquerat et. al. [24] demonstrate the viability of a miniature Doppler Radar working as a collision avoidance sensor. During their work they produced a lightweight (304 grams) continuous wave Doppler sensor consisting of 4 transmit-receive modules arranged in a quadrant pattern. The reason for the quadrant pattern is that it would allow them to implement what is described in their work as a "Reactive Collision Avoidance Algorithm" where the host vehicle simply steers away from the quadrants with the highest returned signal energy.

Fully operational systems, however, are not widely discussed in the literature. Though since UAVs are transitioning more and more to civilian applications the incentives of creating a fully operational collision avoidance system grows. From follow-me-UAVs that must be able to navigate through different terrain, like forests, mountains, etc, to inspection UAVs on industrial facilities that has to be able to navigate without fully depending on accurate GPS measurements. These needs, combined with the possibilities created by miniaturizing Radar systems pose many opportunities for UAV operations through local navigation.

## 2.5 The Principles of Synthetic Aperture Radar (SAR)

Figure 2.10 from [25] illustrates the basic principles of a typical space-based, stripmap, monostatic SAR. Testing conducted in chapter 5 will also be with a monostatic radar antenna configuration and stripmap SAR. The dots along the velocity vector in figure 2.10 are to be considered as points where the antenna transmits a pulse. Each transmitted pulse travels the distance to the target area where the objects at that location are illuminated, and the back-scatter is then collected by the same antenna. The principle of SAR is feasible because the Radar pulse travels to and from the target area at the speed of light, which is significantly faster than that of the aircraft. Which, in turn, makes the movement of the aircraft from transmitting the pulse to receiving the pulse negligible [26]. By collecting and saving the phase histories of the returned pulses at each position the SAR signal image processing system then performs weighting, shifting and summing to focus on each target (resolution element) in turn. SAR is able to achieve a high signal processing gain because of coherent (in-phase) summation of the range-correlated responses of the Radar [25]. In many cases, there will be thousands of pulses summed up for each resolution cell which gives a great increase to the target signal as opposed to what would come from a single pulse - for the SEASAT SAR this benefit is at approximately 4000.

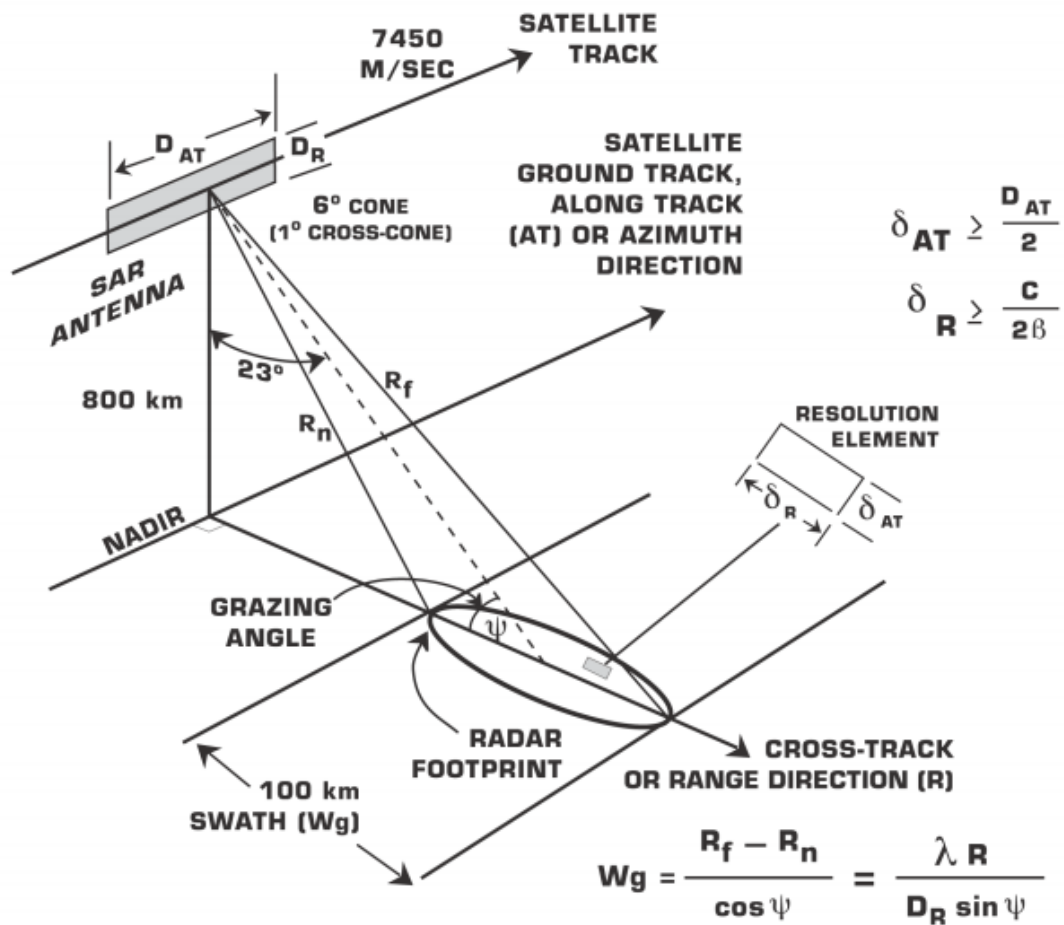


FIGURE 2.10: Synthetic Aperture Synthesis - taken from [25])

### 2.5.1 Different types of SAR Acquisition Modes

Depending on the configuration of the Radar system, SAR can acquire data in three different modes; *stripmap*, *scan*, and *spotlight*. All figures in this section are taken from [19].

1. The SAR **Stripmap mode** assumes a fixed pointing direction of the Radar antenna broadside to the platform track and the illumination footprint covers a strip on the ground as the platform moves. A stripmap is basically an image formed in width by the swath of the SAR and follows the length contour of the flight line of the platform itself. Figure 2.11 illustrates the principle of stripmap SAR in a simple way.

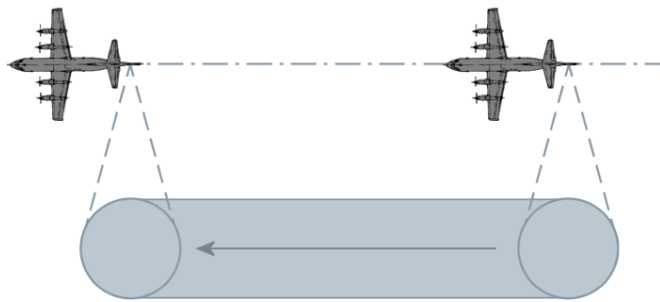


FIGURE 2.11: SAR Stripmap mode

2. SAR **Spotlight mode** achieves high-resolution imaging by directing the Radar beam to keep the target within the beam for a longer period of time and thus form a longer synthetic aperture. By doing this, Spotlight SAR is capable of extending the high-resolution SAR imaging capability significantly. The Spotlight mode usually comes at the expense of spatial coverage, as surrounding areas within a given accessibility swath of the SAR will not be illuminated as the Radar beam is covering the particular targeted area. Figure 2.12 illustrates the principle.

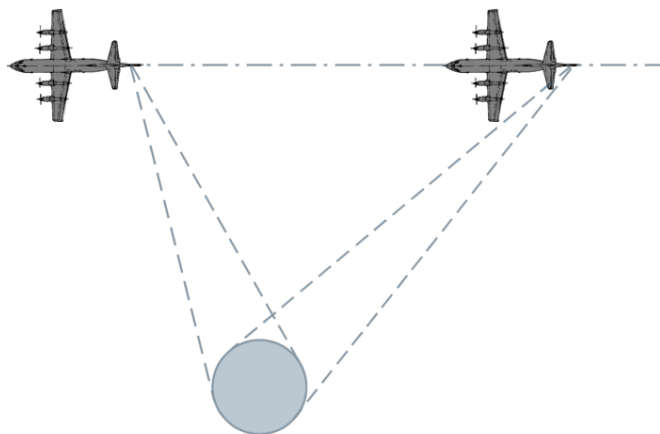


FIGURE 2.12: SAR Spotlight mode

3. While operating in SAR **Scan mode** the antenna beam is periodically stepped in range to neighbor swaths which are called sub-swaths. This results in an increased overall dimension of range swath for each target. While in SAR Scan mode the range swath increases at the expense of the azimuth resolution. Figure 2.13 illustrates the principle of SAR Scan mode.

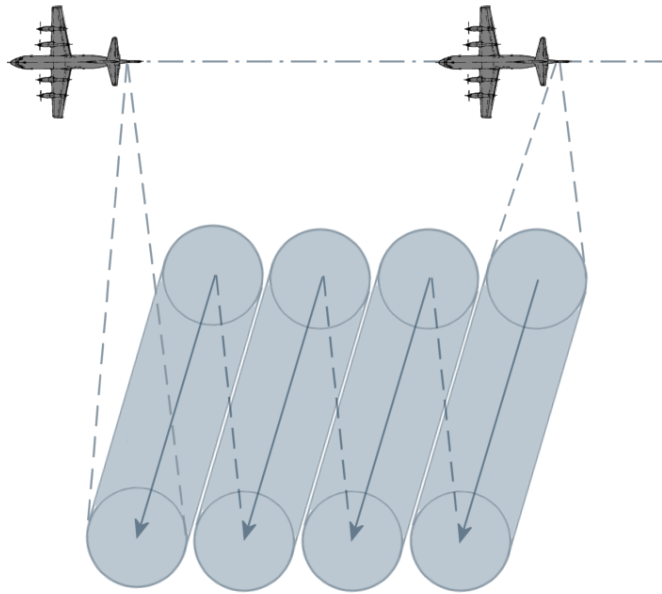


FIGURE 2.13: SAR Scan mode

### 2.5.2 SAR Resolution

When discussing two-dimensional SAR imaging, resolution is divided into two components (Fine resolution in imagery means you are able to detect smaller objects and differ between objects close to each other):

1. **Range resolution** is the resolution concerning the direction perpendicular to the flight path of the aircraft. It is defined as the minimum range separation between two objects traveling at the same speed before the Radar can detect two distinct reflections. The round-trip propagation delay is given by this equation (the same equation as 2.2):

$$\tau = \frac{2R}{c} \quad (2.12)$$

Here  $c$ , is the propagation velocity (speed of light) while  $R$  is the distance. A pulse of duration  $\tau$ , corresponds to a range increment and is given as:

$$\Delta R = \frac{c\tau}{2} \quad (2.13)$$

And as we see the pulse duration  $\tau$  is a very important parameter regarding range resolution. The logical solution would just be to decrease the pulse duration as to obtain finer resolution, but it comes with a cost. Decreasing pulse duration also means decreasing average transmitted power per time instance and this will weaken the signal to noise ratio (SNR), so the system has to make sure that every pulse is sent with a high peak power. As small-sized multirotor UAVs have limited power supply there has to be a

technique so that pulses can be sent with a high frequency, but yet with a high enough peak power. This will be brought up in chapter 4 section 1, "The Pulse Compression Technique".

- When talking about the direction parallel to the flight path of the aircraft where two targets can be distinctly separated it concerns the **azimuth** or **cross-range** resolution. Both azimuth, and range direction is shown in figure 2.14. SAR holds an exclusive property when it comes to azimuth resolution as opposed to generic Radar systems where the resolution is dependant on the range as well as the size of the antenna. For generic Radar systems a larger physical antenna improves resolution, though increased range causes for coarser resolution in azimuth. SAR simply uses the fact that each scatterer gives out a reflection with distinct Doppler shifts because of the motion of the platform. This knowledge is then utilized to distinguish between objects in azimuth. Since the SAR is then relying on recognizing the Doppler shifts, antenna length is shortened. Though as mentioned, shorter antenna length decreases SNR as well as signal ambiguities [27]. Ultimately the resolution in azimuth equals half the length of the antenna, therefore [27]:

$$\rho_a = \frac{L_a}{2} \quad (2.14)$$

So SAR often uses a shorter antenna attached to the platform to get better azimuth resolution as well as being able to operate on a wide range. When the platform moves in azimuth, it can theoretically cover an infinite length in azimuth, and after the end of flight, the collected data is processed and an image is created with enhanced azimuth resolution [28] (depending on the processing algorithm).

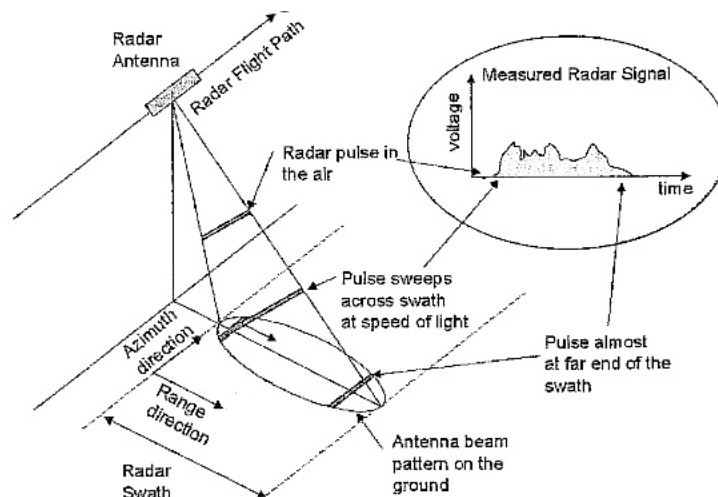
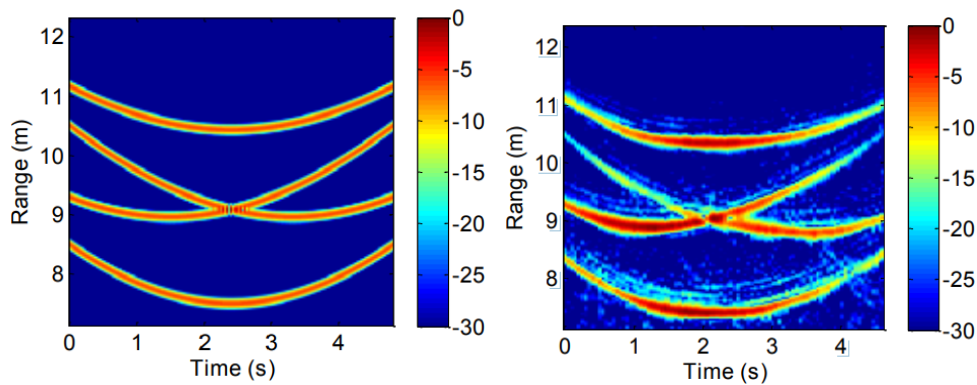


FIGURE 2.14: SAR Geometry - taken from [29] (Accessed: 18.12.2017)

## 2.6 Study: Synthetic Aperture Radar Imaging Using a Small Consumer Drone

A study was conducted in 2015, called "Synthetic Aperture Radar Imaging Using a Small Consumer Drone" [11]. This study demonstrated the capabilities of a low-cost SAR imaging system consisting of a UWB Radar, antennas and a single-board computer mounted on a small multirotor (the entire Radar system weighing less than 300 grams). Motion compensation was carried out using a prominent scatterer algorithm and a SAR image of four trihedrals, as well as imaging of a human and a car are presented in this study.



(A) Simulated range profiles based on (B) Measured range profiles vs. flight a point-scatterer model and constant time from 4 trihedrals on the ground velocity flight. collected from the drone-SAR

FIGURE 2.15: Range profiles [11]

For calibration and testing there was placed four trihedrals (16 cm per side) on the ground in a rhombus formation with 3m diagonals. The drone is then flown in a straight line (approximately 2 m above ground level) and the closest approach,  $R_{min}$  of approximately 7.5 m. Range profiles are collected over a distance of approximately 8 m or  $60^\circ$  of angular swath [11]. Figure 2.15 displays the measured range profiles vs. flight time. As the study expects, the tracks exhibit significant range migration because of the wide angle collection.

To be able to form an image from the acquired data, translation motion compensation is carried out by aligning to a prominent point-scatterer [30]. And next the study performs a rotation motion compensation to focus the scatterers located away from the rotation center and goes on to produce the SAR image shown in figure 2.16.

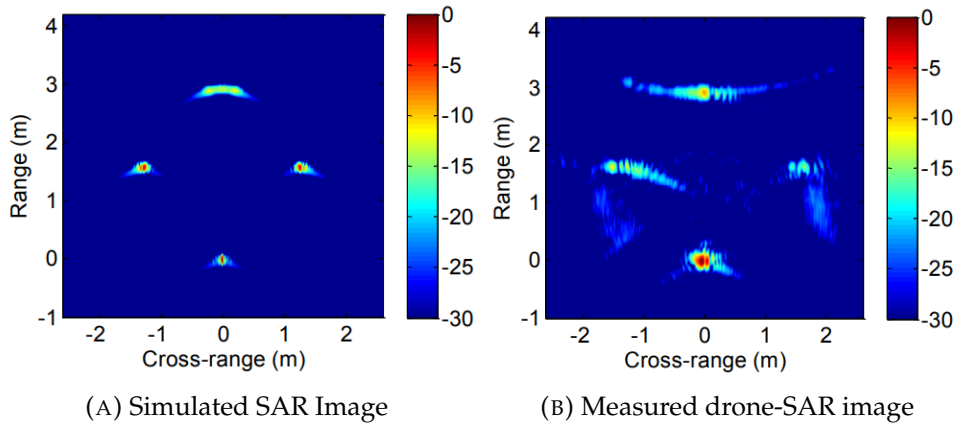


FIGURE 2.16: Imaging of four trihedrals [11]

The study concludes that it has demonstrated a low-cost, drone-based SAR imaging system and that the entire system fits on a small consumer drone that can be controlled through a Wi-Fi connection. And with this setup, four trihedrals was imaged using drone-collected measurements and a motion compensation algorithm. Pros are mentioned to be the low-cost and portability of the system, while cons regard the need of prominent scatterer (absence of navigation data) and drone flight instability.

We can see from figure 2.16b that the drone-SAR image exhibits some azimuth smearing. The SAR image was also generated with the drone placed on a rail and smoothly moved along the measurement path, where the image was of slightly higher quality. It is worth noting that this was conducted in an outdoor environment, whereas an indoor environment would most likely have created a different result. Indoors the electromagnetic waves would have reflected off of all surfaces and the SAR algorithm would have had to deal with much more incoming signals and been able to filter out irrelevant information. It is hard to say whether it is the SAR algorithm or the hardware quality that affects the imaging quality. But one thing is certain, the system must be tested more thoroughly and in other environments, before drawing any conclusions on its applicability in regard to collision avoidance or navigational aid.

## 2.7 SAR & Radar to Aid in Local Navigation

The use of Radars and SAR to aid in UAV operations through local navigation is an area with a lot of possibilities, some of them to be discussed in this thesis. Compared to a camera, a Radar is not dependant on lighting conditions to be able to sense its environment. Thus for a small-sized UAV this opens up many possibilities on what kind of environments the UAV will be able to operate in. As GPS signals offer limited aid in closed environments such as underground, in closed tubes, inside industrial facilities where signals are significantly weakened, Radar can come in very useful to be able to detect obstacles surrounding the UAV.

The use of target identification can be a great advantage to many types of UAV operations. For example the use of classifying what kind of objects that are surrounding the UAV, and if the objects are either static, or moving at certain velocities. The use of Radar in this domain is not new. This is functionality that has been present in larger vehicles and installations, especially in modern military aircraft. R.J Wellman, and J.L Silvius of the U.S Army Research Laboratory published the technical report ARL-TR-1637 [31] in 1998 showing how a 92GHz Doppler Radar system that can be used to characterize the spectral shifts generated by a full-scale helicopter, in this case a Mil Mi-24 HindD. In their research they measured the diameters and angular rates of the different rotating structures on the helicopter including the following: the main and tail rotor blades and hub components, the Auxiliary Power Unit (APU), oil coolers, and engine compressors and free turbines. The Doppler shift that these components generate is further associated with the tip velocity of the rotating structures and experimental validation proved their model quite accurate [4].

Local navigation refers to navigating a local area, for example an industrial facility. Earlier in this chapter the Radar Cross Section (RCS) was addressed. The RCS is partially determined by an objects ability to reflect electromagnetic signals, and the reflecting properties of an object is largely determined by its material. It is then only natural that some environments will have many objects with a high reflectivity. Consider an industrial facility with large and small pipes and tubes as well as different machinery that needs inspection. Lets say most of the objects within this facility are made of metal with high reflectivity. This can cause problems for a Radar system trying to interpret all incoming signals especially if those incoming signals may have been reflected off of several objects before reaching the receiver. If a small-sized UAV was to navigate such an environment and at the same time have the ability to inspect and possibly map parts of it, the UAV would need a very reliable Radar system with reliable signal processing.

## 2.8 Existing Challenges

There exists many different challenges regarding the use of Radar systems on UAVs for the purpose of collision avoidance. The first one worth mentioning is naturally the physical constraints of a UAV compared to the physical volume of many Radar systems. Many of the existing Radar systems available are far too large for widespread UAV implementation. Continuing there is the fact that most airborne Radar systems currently implemented on UAVs are designed to be used in air-to-ground modes either for mapping or target detection and/or tracking purposes. An example of a system like that can be found in ImSAR's NanoSAR line of Synthetic Aperture Radars [4][32]. A consequence of those systems being dedicated to air-to-ground operations is that it becomes less effective when used in air-to-air operations. They become less effective because air-to-air Radars in most cases must incorporate ground clutter rejection features that are not often implemented in dedicated air-to-ground Radars.

Another domain where challenges arise is concerning power consumption. Many airborne Radar systems possess high power demands to operate, often hundreds of Watts of electrical power. On small UAVs there are strict limitations on power consumption, and thus many Radar systems can not be integrated with the UAV platform. On the bright side, there exists small Radar systems with low electrical power consumption. The X4 UWB System on Chip (SoC) Radar used by the UAV during testing in this thesis is a good example. The specifications of the Radar system and the UAV platform to be used in this thesis will be presented in chapter 4.

When talking about power consumption there are several parts of a UAV that is run by electrical power. A fully operational collision avoidance system has certain demands when it comes to processing capabilities, for example when collecting Radar data for SAR image processing. A SAR is a two-dimensional imaging sensor system (azimuth and range), which means that a SAR has to be able to collect data in the azimuth direction as well as the range direction. These data must then be combined and processed into an unambiguous image (an image with only one solution). Figure 2.10 tries to illustrate and help visualize the two-dimensional ambiguity relationships that are crucial to all SAR applications. As described earlier, the azimuth resolution of a focused SAR is given by one half of the azimuth Radar antenna length, and this resolution is independent of the Radar frequency and range (to a certain extent). With this in mind it would seem natural that given a small antenna length one could obtain very fine azimuth resolution. This is correct, though the ambiguity conditions place certain limits on this fact. Being able to achieve fine azimuth resolution brings up a requirement for the Radar. It has to send a pulse each time the Radar platform translates half of the azimuth antenna length. This forces a lower bound on the Pulse Repetition Frequency (PRF). The relationship given by [33]:

$$\frac{2 * \text{Velocity of Radar}}{\text{Antenna Length}} < \text{PRF} \quad (2.15)$$

This relationship can also be described by:

$$\frac{\text{Velocity of Radar}}{\text{Azimuth Resolution}} = \frac{V}{\delta_{AT}} < \text{PRF} \quad (2.16)$$

Therefore, if the azimuth antenna length is diminished with the goal of improving azimuth resolution, the Radar has to be able to pulse faster. This results in less time between pulses, a smaller Inter-Pulse Period (IPP - the reciprocal of PRF). This gives, in turn, less time to collect data between pulses in the azimuth or range direction. Unfortunately, there can be only one pulse for a given Radar frequency in the target zone at each time instant. If this is not followed, range ambiguity occurs, thereby negating two-dimensional imaging [25]. From this we have an upper bound of the PRF which is a function based on the swath width ( $S = R_f - R_n$ ) in slant range direction as shown in figure 2.10/2.14 and the real pulse duration, T, giving the upper bound as:

$$\text{PRF} = \frac{1}{2T + 2(R_f - R_n)/c} \quad (2.17)$$

Increasing the swath width and/or incident angles creates a need for more spacing between pulses which leads to a collision between the wish for increased coverage and the desire for improved azimuth spatial resolution. In examples where the pulse duration,  $T$ , is much smaller than the swath width time, the general rule for the single look case is [34]:

$$\frac{V}{\delta_{AT}} < \text{PRF} < \frac{c}{2 * \text{Swath Width}} \implies \frac{2 * \text{Swath Width}}{\delta_{AT}} < \frac{c}{V} \quad (2.18)$$

In reality there are naturally more complex considerations to make when talking about transmit and receive event timing and coordination. For space-based applications, there will often be a multitude of pulses in transit at the same time. Therefore it is required to have temporal interlacing of returns with the transmitted pulses to avoid eclipsing the reflected signals. For SAR with interlaced pulses of a particular polarization designed to produce polarization specific, and unique target signatures, it is required to have even more intricate transmit and receive sequences to prevent ambiguous performance. So the theory may be simplified, but in practice, SAR often gets a lot more complicated than anticipated.

Another factor that can cause serious performance issues for Radar systems is *clutter*. Clutter is a uniform term concerning unwanted echoes for electronic systems, particularly Radar systems. Such echoes are normally returned from some kind of surface, precipitation, animal/insect, or atmospheric turbulence. What some may consider to be clutter, others may consider to be a target, it mainly depends on the area of interest. Weather is not clutter in a weather detecting Radar. There are mainly three types of clutter to consider:

1. **Surface clutter:** Unwanted echoes from the ground or sea are typical surface clutter. Echoes from geographical landmasses are normally stationary, though trees moving in the wind may introduce a Doppler shift to the Radar data.
2. **Volume clutter:** Weather or chaff are typical volume clutter. In outside environments, weather is considered to be a significant problem as the clutter derived from weather often has a high Doppler content.
3. **Point clutter:** Animals, buildings and structures not related to nature are typical point clutter. Flying animals like birds, and insects produce clutter that can be very hard to remove because the characteristics are very similar to that of an aircraft.

During this thesis and the testing that is conducted in chapter 5, the issue of surface clutter is the most important to address. Surface clutter depends solely on the nature of the specific surface. Its polarization, its roughness, the angle the Radar beam makes with the surface (the grazing angle), and the frequency.

Considering a multi-rotor UAV platform, we know that the ability to sustain stable flight compared to a satellite or larger aircraft carrying SAR will always be much more challenging. Detailed data on where the UAV position, heading, and velocity can be difficult to always keep track of as all those variables are more vulnerable to change than those of a larger aircraft. Because of UAVs more limited capacity to carry equipment there will always be a compromise between the weight of the SAR system and the quality of the images it can produce. Processing, imaging and sensory equipment all have restrictions when it comes to quality and physical size. It is an inevitable challenge of priorities.

## 2.9 Summary

A Radar system is a system that uses radio waves to determine the range to, and velocity of target objects. By the use of its antenna a Radar system transmits and receives radio frequency (RF) signals. There are many different options concerning antenna and transmit/receive configuration. When talking about the antenna radiation, the fundamental parameter *directivity* is important to mention. An antenna radiating coherently equal in all directions has zero directivity. The antennas directivity combined with the percentage of the physical aperture area which actually captures RF energy, the antenna efficiency, together make the antenna gain. Higher gain equals more powerful energy transmission, hence stronger received power, which in turn yields a better signal to noise ratio (SNR).

Furthermore, it is important to note the difference between the two main categories Radar systems are divided into. Continuous Wave (CW) and Pulsed Radar systems. Within those two categories there are several types of designs like Doppler, unmodulated or frequency modulated CW Radars and UWB pulsed Radars.

A Synthetic Aperture Radar (SAR), is a coherent Radar system that uses the motion of the Radar antenna over a target region to simulate a large antenna or aperture electronically and is able to provide finer spatial resolution than conventional beam-scanning Radars. SAR has also been tested on smaller aircraft like small-sized multi-rotor UAVs to verify the ability to sense the environment surrounding the UAV. Regarding collision avoidance systems for small-sized UAVs using Radar technology there are many considerations that have to be taken into account. The possibilities are almost endless in terms of use in local navigation, but considering small-sized UAV limitations like physical capabilities, power consumption, and processing power there are still plenty of challenges to be solved.



## Chapter 3

# SAR Signal Processing & Algorithms

Historically, image formation has been accomplished by analog means. During the course of the last decades, however, the advancements and availability within the domain of high-speed digital computers have enabled new possibilities within the field called computed imaging or digital imaging. Computed imaging refers to the synthesis or computation of imagery using data collected from an object, a material, or a scene. Application areas include medicine, biology, material science, surveillance, navigation, and astronomy. Digital imaging includes computer tomography (CT), magnetic resonance imaging (MRI), ultrasound and acoustic imaging, x-ray crystallography, radio astronomy, and synthetic aperture Radar (SAR) [35].

Signal processing of Synthetic Aperture Radar is a two-dimensional image processing operation. There is a fundamental difference between conventional optical image processing and Radar/SAR image processing. Radar/SAR uses the distance between its sensor and the objects to produce an image, while optical image generation systems, such as optical telescopes or cameras use the angular differences of the signals incident upon the sensor to create an image. The optical image does not show depth in the same way that an image produces by Radar/SAR does. In this chapter, theory and techniques relevant to SAR signal processing will be reviewed. Algorithms feasible for short-range SAR imaging are presented along with a comparison study on three algorithms.

### 3.1 Radar Scattering

Almost all Radar imaging systems are based upon the use of the start-stop approximation [36], where the sensor and scattering object (target) are presumed to be stationary during the time interval which the Radar pulse hits the target. The following discussion on Radar scattering will only consider the imaging of targets with zero velocity.

When talking about scalar waves we consider a scenario where the region existing between the Radar sensors and the scattering objects consists of a homogeneous, loss-less, non-dispersive atmosphere. In such a scenario, Maxwell's

equations can be used [37] to obtain an inhomogeneous wave equation for the electric field  $\epsilon$ .

$$\nabla^2 \epsilon(t, x) - \frac{1}{c^2} \frac{\partial^2 \epsilon(t, x)}{\partial t^2} = s(t, x) \quad (3.1)$$

And a similar equation for the magnetic field  $\beta$  [16]. In (3.1),  $c$  is the propagation speed of the wave in the described scenario, which for most remote sensing situations, is a good enough approximation to the propagation speed in the atmosphere. The term  $S$  is considered a source term that can involve both the electric field  $\epsilon$  and the magnetic field  $\beta$ . This source term is further discussed below, but for simplicity we rewrite equation (3.1) to consider only on Cartesian component:

$$\left( \nabla^2 - \frac{1}{c^2} \frac{\partial^2}{\partial t^2} \right) \epsilon(t, x) = s(t, x) \quad (3.2)$$

Here we have assumed atmospheric propagation between the source and the target.

A useful and one of the fundamental solutions [38] of the wave equation is a generalized function [39][38], satisfying:

$$\left( \nabla^2 - \frac{1}{c^2} \frac{\partial^2}{\partial t^2} \right) g(t, x) = -\delta(t)\delta(x) \quad (3.3)$$

A solution to (3.3) can be written as:

$$g(t, x) = \frac{\delta(t - |x|/c)}{4\pi|x|} = \int \frac{e^{-i\omega(t - |x|/c)}}{8\pi^2|x|} d\omega \quad (3.4)$$

In the second equality,  $\delta(t) = \frac{1}{2\pi} \int \exp(-i\omega t) d\omega$ . The function  $g(t, x)$  can be interpreted physically as the field at  $(t, x)$  because of a source at the origin  $x = 0$  at the time  $t = 0$ . This is often called the outgoing fundamental solution, also known as Green's function [40]. The Green's function makes it possible to solve the constant speed wave equation with any type of source term. Particularly, the outgoing solution of:

$$\left( \nabla^2 - \frac{1}{c^2} \frac{\partial^2}{\partial t^2} \right) u(t, x) = s(t, x) \quad (3.5)$$

is

$$u(t, x) = - \int g(t - t', x - y) s(t', y) dt' dy \quad (3.6)$$

In the frequency domain, the equations corresponding to (3.3) and (3.4) are:

$$(\nabla^2 + k^2)G = -\delta \quad (3.7)$$

and

$$G(\omega, x) = \frac{e^{ik|x|}}{4\pi|x|} \quad (3.8)$$

Where the wave number  $k$  is given by;  $k = \frac{\omega}{c}$ .

In common Radar problems, the source  $s$  is the sum of two distinct terms:  $s = s^{in} + s^{sc}$ , where  $s^{in}$  models the transmitting antenna and  $s^{sc}$  models the scattering object (target). The solution  $\epsilon$ , which is written as  $\epsilon^{tot}$ , gets cut into two different parts:  $\epsilon^{tot} = \epsilon^{in} + \epsilon^{sc}$ . In the simplified scalar model,  $\epsilon^{in}$  satisfies the wave equation for the already known source  $s^{in}$  and we call this part the *incident field*, given that it is incident upon the targets. The latter part of  $\epsilon^{tot}$  is due to target scattering and is naturally called the *scattered field*. One method of finding the scattered field is to simply solve (3.2) directly, using numerical time-domain techniques. Though, for several purposes, it can be very convenient to reformulate the scattering problem in terms of an integral equation [16].

Regarding scattering problems, the source term  $s^{sc}$  usually represents the target's response to an incident field. This particular part of the source function will naturally depend on the geometric and material properties of the target as well as on the form and strength of the incident field. Analytically,  $s^{sc}$  is pretty complicated to describe, and typically it will not have the same direction as  $s^{in}$ . For this thesis' purposes there is no need to provide a detailed analysis of certain target's response as the focus is more on the understanding of the underlying principles behind Radar imaging. Consequently, for stationary objects consisting of linear materials, the scalar model  $s^{sc}$  as the time-domain convolution can be written as:

$$s^{sc}(t, x) = - \int v(t - t', x) \epsilon^{tot}(t', x) dt' \quad (3.9)$$

This equation is also known as the *Lippmann-Schwinger integral equation*. The term  $v(t, x)$  is named the reflectivity function. In the full vector case,  $v$  would be a matrix operating on the full vector  $\epsilon^{tot}$ . Though in this case, the single matrix element, corresponding to the component considered in equation (3.2) is the only one to be used. Equations (3.6) and (3.8) can be used to express  $\epsilon^{sc}$  in terms of the *Lippmann-Schwinger integral equation* [41]:

$$\epsilon^{sc}(t, x) = \int \int g(t - \tau, x - z) \int v(\tau - t', z) \epsilon^{tot}(t', z) dt' d\tau dz \quad (3.10)$$

Because of its mathematical advantages, it is important to look at the *Lippmann-Schwinger integral equation* in the frequency domain. In this domain, the electric field and reflectivity function become:

$$E(\omega, x) = \int e^{i\omega t} \epsilon(t, x) dt \quad (3.11)$$

and

$$V(\omega, z) = \int e^{i\omega t} v(t, z) dt \quad (3.12)$$

and equation (3.10) is:

$$E^{sc}(\omega, x) = - \int G(\omega, x - z) V(\omega, z) E^{tot}(\omega, z) dz \quad (3.13)$$

The reflectivity function  $V(\omega, x)$  can be sensitively dependant on  $\omega$  [37][42][43]. In the case where the target is small in size, compared to the wavelength of the incident field,  $V$  becomes proportional to  $\omega^2$ . This behavior is called Rayleigh scattering. By the use of shorter wavelengths (higher frequencies), the dependence on  $\omega$  is typically smaller.  $V(\omega, x)$  is often approximated as independent of  $\omega$  in the 'optical region' [44]. The optical approximation is often used to get rid of the  $\omega$  dependence. This corresponds to  $v(t, z) = \delta(t) V(z)$  from the time domain where the delta function makes it possible to carry out the  $t'$  integration in equation (3.10) [16]

When dealing with Radar imaging,  $\epsilon^{sc}$  is measured at the antenna, and from there  $V$  is determined. However, both  $V$  and  $\epsilon^{sc}$  in the neighborhood of the target are unknown, and in equation (3.10) these two are multiplied together. This is a non-linearity that makes it difficult and mathematically complicated to solve for  $V$ . As a consequence, almost all work on Radar imaging makes use of the *Born approximation*, also known as the *weak-scattering* or *single-scattering* approximation [45][41]. The Born approximation replaces  $\epsilon^{tot}$  on the right-hand side of equation (3.10) by  $\epsilon^{in}$  which is known. This gives us the following expression for  $\epsilon^{sc}$  in terms of  $V$ :

$$\epsilon^{sc}(t, x) \approx \epsilon_B := \int \int g(t - \tau, x - z) V(z) \epsilon^{in}(\tau, z) d\tau dz \quad (3.14)$$

This gives the Born approximation in the frequency domain as:

$$E_B^{sc}(\omega, x) = - \int \frac{e^{ik|x-z|}}{4\pi|x-z|} V(z) E^{in}(\omega, z) dz \quad (3.15)$$

Which is the reason why the Born approximation is so valuable and useful. It makes the imaging problem linear. It is not however always a good approximation. It leaves out several physical effects, including not only multiple scattering and creeping waves, but also shadowing, obscuration and polarization changes. But without the Born approximation (or the Kirchhoff approximation, which is similar), the imaging problem is nonlinear [16].

## 3.2 The Pulse Compression Technique

Pulse compression is a signal processing technique commonly used by Radar, sonar and echography to increase the range resolution as well as the signal to noise ratio. This is achieved by modulating the transmitted pulse and then correlating the received signal with the transmitted pulse [46]. For example, for UWB SAR, one of the main criteria is the ability to transmit very short pulses. This enhances the receiver's ability to differ between two separate objects located close to each other. Though, to be able to get quality reception from short duration pulses, the pulses

have to be sent with large enough power. If not, the signal to noise ratio (SNR) will become very poor. The basic Radar equation [27]:

$$\rho_r = \frac{cT_p}{2} = \frac{c}{2B} \quad (3.16)$$

Where  $T_p$  is the pulse width,  $B$  is the bandwidth, and  $c$  is the speed of light. This equation shows us that two distinct objects have to be minimum half the pulse width separated from one another to be able to create two separate echoes. Objects located closer to one another than that distance will create one echo because the reflected echo from the latter object will catch up to the first one and merge into one signal.

One simple solution would seemingly be to transmit short pulses with high power. Though this is not a very good solution as it would require very sophisticated electronics because of the high power transmission. And since the hardware needs to be sophisticated and reliable enough, the cost goes up. There is, in fact, a solution that adds no extra costs, solely based on a mathematical maneuver/method called the *pulse compression technique*.

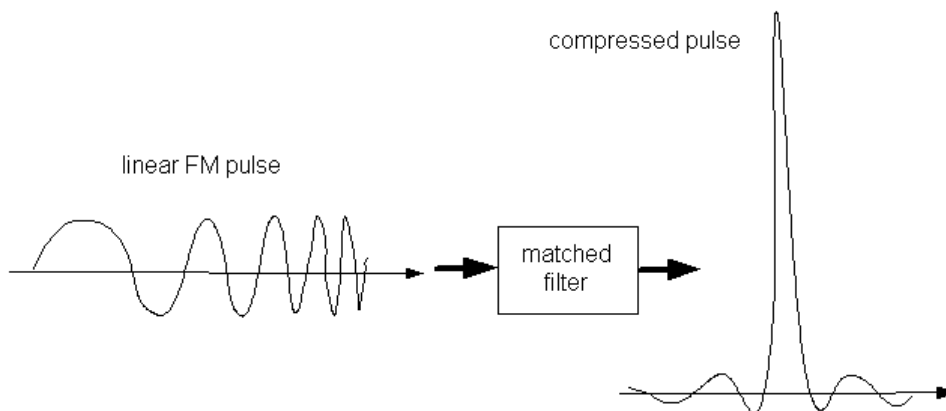


FIGURE 3.1: Illustration of the pulse compression technique

The illustration in figure(3.1) shows how a linear FM pulse is compressed via a matched filter to create a high peak short pulse. Every stage of this process will be explained in this chapter.

The pulse compression technique makes it possible for the transmitter to send long pulses. The pulse from the SAR must be modulated in such a manner that it gets compressed to a high peak valued pulse after passing through the matched filter [47]. The entire concept is rooted in the Fourier transform theorem. We know that Fourier transformation of a rectangular function gives a sinc function;  $\int_{-\infty}^{\infty} \text{rect}(t)e^{i2\pi Ft} dt = \text{sinc}(F)$ . Fourier transformation is simply the accumulation of the frequency components of a signal and plotting their magnitude. The pulse compression technique uses the same principle by sending an FM signal at first,

most commonly by the use of a rectangular window. Upon reception all the frequency elements are delayed and later added accordingly so that in the end they are jammed together to form a narrow high magnitude output. To be able to go through with the entire operation the transmitter has to send a proper FM signal. The applications on FM signals are common in radio broadcasting, though the advantage in Radar systems over radio broadcasting is that the Radar does not need to transmit any meaningful messages. The Radar system only sends a signal to get a reflection, therefore there is no need for complex manipulation of the frequency distribution within the signal itself. With Radar, a simple pulse containing numerous frequency components would suffice. One type of FM signal like that is a Compressed High Intensity Radar Pulse (CHIRP) signal. Basically, it is an FM signal in which case the frequency is either increased or decreased over time. A CHIRP signal is easy to generate and can either be generated in ascending order (up CHIRP) or descending order (down CHIRP). The frequency differences can be linear or exponential, though to keep it simple, Radar systems usually use a linear CHIRP signal (up CHIRP). The equation for the transmitted signal is;

$$s(\tau) = \text{rect}\left(\frac{\tau}{T_p}\right) e^{(i2\pi f_c \tau + i\pi K \tau^2)} \quad (3.17)$$

Where  $K$  is the ratio of the bandwidth and pulse width (CHIRP rate)  $B/T_p$  and  $f_c$  is the center frequency. Time goes along the horizontal axis and magnitude along the vertical axis, and for simplicity, the amplitude is set to 1.

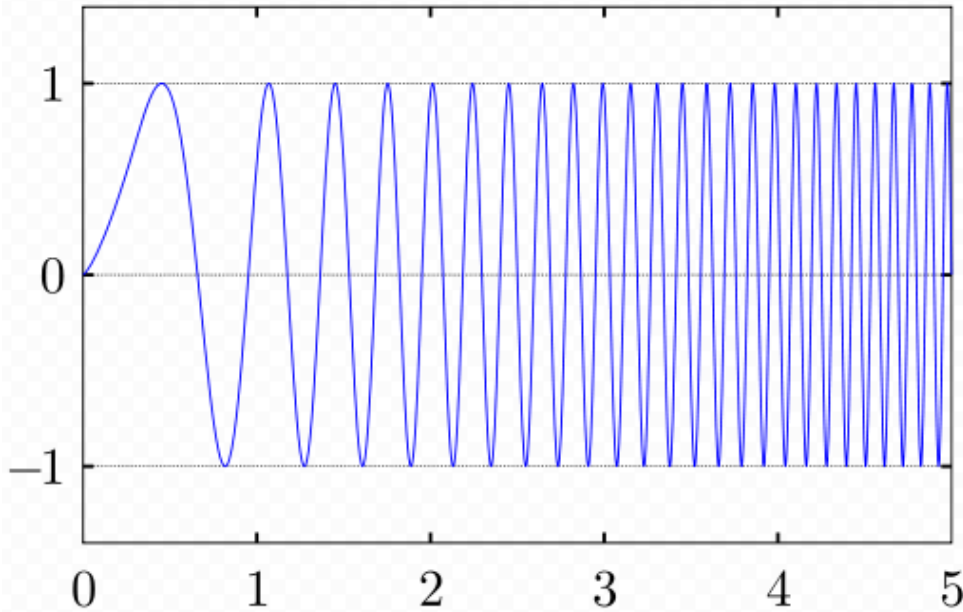


FIGURE 3.2: Linear FM CHIRP signal

### 3.2.1 Matched Filter

In signal processing, a matched filter is obtained by correlating a known signal, or template, with an unknown signal to detect the presence of the template in the unknown signal [48]. The matched filter is also the optimal linear filter regarding the SNR in the presence of additive stochastic/non-deterministic noise. When using SAR the matched filter is usually performed with the use of convolution. *Convolution* is a formal mathematical operation, just as multiplication, addition, and integration. Addition takes two numbers and produces a third number, while convolution takes two signals and produces a third signal. The general equation for convolution is:

$$y(\tau) = s(\tau) \otimes h(\tau) = \int_{-\infty}^{\infty} s(\tau)h(\tau - u)du \quad (3.18)$$

Where  $u$  stands as a dummy variable while  $h(\tau)$  is the matched filter signal and  $s(\tau)$  the transmitted signal. Before taking on the math of the matched filter it is important to understand the geometrical interpretation of convolution:

- Both signals are plotted on a predefined dummy variable.
- The target signal to be filtered is flipped  $h(-u)$ , and time-shifted  $h(\tau - u)$ . In SAR processing, the time shift is given by the signals round trip time delay.
- The target signal goes through the already defined boundary and as it passes through the other signal, the area as a result of the intersection is calculated. These areas are the similarities between the two signals.
- The final output  $y(\tau)$  equals the resulting plots of the areas (with respect to time)

With the signal from (3.17), SAR matched filtering can be derived as follows:

Ignoring the noise factor, the received signal should be an exact copy of the transmitted signal. Keeping in mind that the signal is complex and baseband, the center frequency  $f_c$  is zero. Where *baseband* refers to the original frequency of a transmission signal before its conversion, or modulation, to a different frequency range. This yields the received signal as:

$$s_r(\tau) = \text{rect}\left(\frac{\tau}{T_p}\right)e^{i\pi K\tau^2} \quad (3.19)$$

And the matched filter signal:

$$h(\tau) = \text{rect}\left(\frac{\tau}{T_p}\right)e^{-i\pi K\tau^2} \quad (3.20)$$

With equation (3.18) we acquire the matched filter output:

$$\begin{aligned}
s_{mf}(\tau) &= \int_{-\infty}^{\infty} s(u)h(\tau - u)du \\
&= \int_{-\infty}^{\infty} \text{rect}\left(\frac{u}{T_p}\right)\text{rect}\left(\frac{\tau - u}{T_p}\right)e^{i\pi K\tau u^2}e^{-i\pi K(\tau - u)^2}du \\
&= \int_{-\infty}^{\infty} \text{rect}\left(\frac{\tau - T_p}{T_p}\right)e^{-i\pi K\tau^2 + i2\pi K\tau u}du \\
&= e^{-i\pi K\tau^2} \int_{-\infty}^{\infty} \text{rect}\left(\frac{\tau - T_p}{T_p}\right)e^{i2\pi K\tau u}du
\end{aligned}$$

Then we have to set boundaries for the duration of the filter and split the integrals according to the rectangular function's position with respect to each other:

$$= e^{-i\pi K\tau^2} \left[ \int_{\tau - \frac{T_p}{2}}^{\frac{T_p}{2}} \text{rect}\left(\frac{\tau - T_p}{T_p}\right)e^{i2\pi K\tau u}du + \int_{-\frac{T_p}{2}}^{\tau + \frac{T_p}{2}} e^{i2\pi K\tau u}du \right] \text{rect}\left(\frac{\tau + T_p}{T_p} + \right)$$

And after simplifying:

$$\begin{aligned}
s_{mf}(\tau) &= (T_p + \tau)\text{rect}\left(\frac{\tau - T_p}{T_p}\right)\frac{\sin(\pi K\tau(T_p - \tau))}{\pi K\tau(T_p - \tau)} + (T_p - \tau)\text{rect}\left(\frac{\tau - T_p}{T_p}\right)\frac{\sin(\pi K\tau(T_p - \tau))}{\pi K\tau(T_p - \tau)} \\
&= (T_p - |\tau|)\text{rect}\left(\frac{\tau}{T_p}\right)\text{sinc}(K\tau(\tau + T_p))
\end{aligned}$$

The two first parts of the equation make a triangular function combined. It ends up weeding out the *sinc* function peaks ( $\tau = -T_p$  and  $\tau = T_p$  as its edge values are approximately zero [27]). As a result, we end up with one aggressive peak in the middle (at  $\tau = 0$ ) which is the final narrow pulse seen in figure 3.1, obtained from the long FM pulse  $s(\tau)$ .

### 3.3 Essential Tools for Frequency Domain Algorithms

Since signal history is in the time domain, frequency domain SAR signal processing uses two major techniques. FFT and interpolation. FFT has to be done as the RAW data has to be transformed into its frequency elements in at least one of its dimensions. Interpolation is a very versatile tool used in signal processing when maneuvering the frequency elements in order to cancel out image distortion. Interpolation also helps in smoothing the image by a technique called upsampling, which is a good method for improving range resolution.

### 3.3.1 Fast Fourier Transform

**Fast Fourier Transform (FFT)** is as mentioned earlier, a compact version of the Discrete Fourier Transform (DFT). Fourier analysis converts a signal from its original domain (often time or space) to a representation in the frequency domain and vice versa. While DFT requires  $O(N^2)$  computations, (where  $N$  is the number of samples and  $O$  is defining the upper bound) FFT produces the same result by  $O(N \log N)$  number of operations. Because of this distinct difference in computational time FFT is preferred in many applications. The first major breakthrough in the implementation of Fast Fourier transform algorithms was the Cooley-Tukey algorithm developed in the mid-1960s [49]. Further research resulted in many other algorithms such as the Fast Hartley Transform [50], the Split Radix algorithms [51], and many others. All these algorithms follow the standard decomposition or factorization of  $N$ . The same premise can be taken directly from complex number theory as a complex number can be decomposed into an imaginary part and a real part. Multiplying two complex numbers would essentially combine all four components to make the final output. In a similar fashion, the FFT breaks down a signal of  $N$  samples into  $N$  signals, each referring to a specific sample. By regarding a complex data sequence  $x_n$  and its discrete Fourier transform  $X_k$ , the transformation equation becomes:

$$X_k = \sum_{n=0}^{N-1} x_n e^{-ikn \frac{2\pi}{N}} \quad (3.21)$$

Where  $K$  ranges from 0 to  $N - 1$ .

$e^{-i \frac{2\pi}{N}}$  has symmetry property ( $-e^{-ik \frac{2\pi}{N}} = e^{-i(k+\frac{N}{2}) \frac{2\pi}{N}}$ ) as well as periodicity property ( $e^{-ik \frac{2\pi}{N}} = e^{-i(k+N) \frac{2\pi}{N}}$ ). FFT uses these properties for efficient and rapid computation [52].

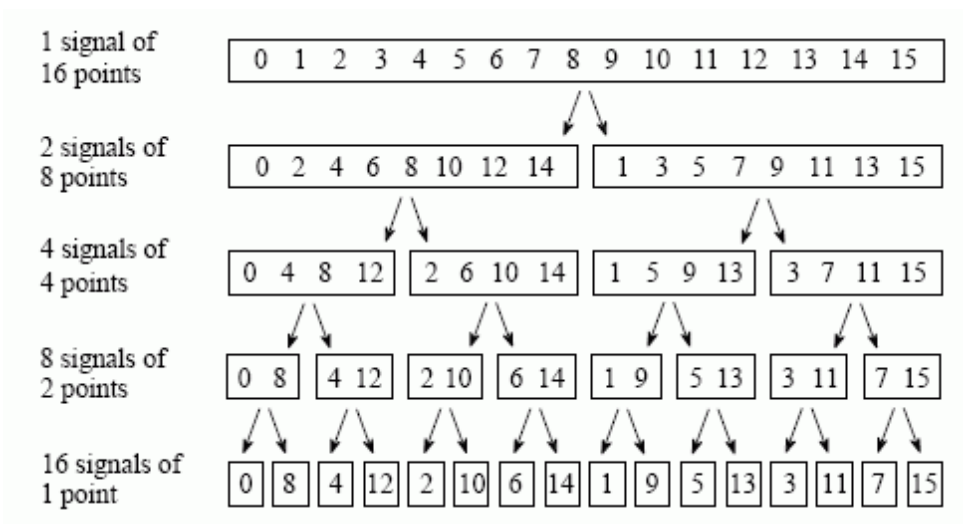


FIGURE 3.3: FFT process for a signal with  $N=16$  samples

It is easy to see from figure 3.3 the relationship between the number of stages with  $\log []$ .  $N = 16$  would require  $\log 16 = 4$  steps as 64 samples would require  $\log 64 = 6$  steps, and so on. The key thing to take away from FFT is that the FFT factorization is just rearranging the signal samples so that even numbered signals are on one side and odd numbered signals are on the other side.



FIGURE 3.4: Data distribution before (o) and after (•) interpolation

### 3.3.2 Interpolation

**Interpolation** is a concept with roots in numerical analysis theory. In mathematical and numerical analysis, interpolation is a method of constructing new data points within a range of a known set of discrete data points, see figure 3.4. When talking about a number of data points (samples) it is often required to interpolate (i.e., estimate) the value of that function for an intermediate value of the independent variable. Interpolation is an essential and powerful tool regarding curve fitting and/or curve smoothing. There have been developed many different methods of interpolating a function, ranging from simple methods such as *linear interpolation* and *nearest neighbor interpolation* to more advanced methods such as *spline interpolation*.

Linear interpolation uses linear polynomials to construct new data points within the range of a discrete set of already known data points. Let us say the two points are given by the following coordinates  $(x_0, y_0)$  and  $(x_1, y_1)$ , the linear interpolant  $y$

is defined as the straight line between the two points. For a value  $x$  in the interval  $(x_0, x_1)$  the interpolant  $y$  is given as:

$$y = y_0 + (x - x_0) \frac{y_1 - y_0}{x_1 - x_0} \quad (3.22)$$

which is essentially the formula for linear interpolation in the interval  $(x_0, x_1)$ .

Nearest neighbor interpolation, also known as proximal interpolation, or in some contexts, point sampling, is a simple method of multivariate interpolation in one or several dimensions. It is a very straightforward and efficient method for simple image processing. For any given point in a data set where the value is not known, a search is done to find its neighbors and the value of the nearest neighbor point is assigned to that unknown point. For simple images, this is an efficient and sufficient method, but for other signals with high-frequency components (i.e., greater changes in a short amount of time), this method becomes insufficient.

Spline interpolation is, on the other hand, a more advanced method. It is usually used when handling complicated functions and/or dealing with a system where a high level of accuracy is required. The interpolant is a special type of piece-wise polynomial called Spline. The type of spline is decided by the degree of the polynomial. For example, a spline interpolation with  $N$  data points, it will create  $N - 1$  additional points. These additional data points give spline interpolation a great advantage when upsampling. We could thereby say that spline interpolation is similar to linear interpolation. A spline polynomial function that comes from an arbitrary data set with variable  $x$  and containing  $N + 1$  sample points will be defined as:

$$S(x) = \{S_0(x) \quad x \in [x_0, x_1], S_1(x) \quad x \in [x_1, x_2], \dots, S_{n-1}(x) \quad x \in [x_{n-1}, x_n]\} \quad (3.23)$$

## 3.4 SAR Algorithms & Image formation

### 3.4.1 Migration Algorithms

Migration of seismic data involves re-positioning the measured data to determine accurately the topology of the subsurface reflectors. Migration is an inverse process in which the recorded waves are propagated back to their source by systematically solving the wave equation for each successive layer [53].

The *scalar wave equation* is seen as the basis for common migration algorithms and it is basically a linear hyperbolic partial differential equation (of different orders) used to describe waves, such as sound waves, light waves, and even water waves. Because of this, it is an important equation that arises in different field, such as acoustics, electromagnetics, and fluid dynamics.

There have been considerable amount of studies on different migration techniques, and they can all be linked to the early developed seismic migration

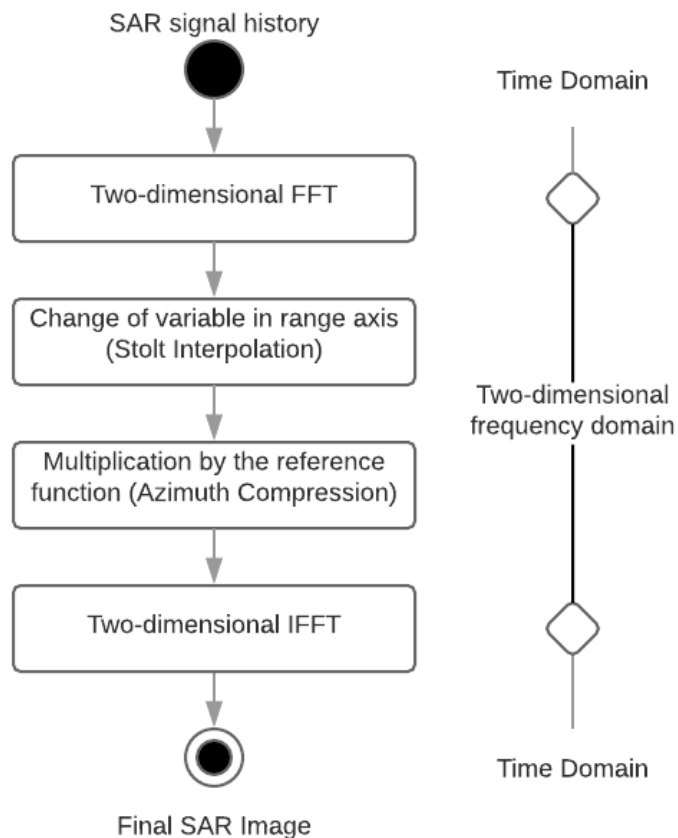


FIGURE 3.5: Block diagram illustrating the main steps of an RMA algorithm

algorithms used in seismic signal processing. Differences usually focusing around computational load, spatial resolution, differential resolution (image quality) and SNR.

### 3.4.2 Range Migration (FK-migration)

If there is an algorithm of this type worth mentioning, it is the Range Migration Algorithm (RMA), often referred to as the FK-algorithm. The RMA has its roots in seismic signal processing [47]. Processing seismic data can very easily be related to SAR processing as mentioned. For seismic data processing, a certain amount of geophones are put on a straight line on the ground, and then a charge is detonated along that same straight line. Collectively all the geophones use their received sound echo and combine the results to analyze the specific ground characteristics. The geophone placement along the straight line can be related to a specific SAR platform (in our case a multicopter) position at any given instance. The seismic signal processing also produces a hyperbolic phase function, exactly like SAR

phase data [28].

RMA is a frequency domain algorithm where both azimuth and range axis are frequency converted (two-dimensional FFT). The algorithm is based on back-propagation of the scalar wave equation and is derived using the exploding reflector model (ERM) which assumes that the wave field starts from the target at time zero with half the actual propagation speed. At every sample in azimuth, received signals are *downward continued* and afterwards reemerged. By doing this we end up eradicating the intrinsic Doppler effect of the SAR which is achieved by reconstructing the signal memory with respect to the ground range. The Range Migration Algorithm's key mechanism is the change of variable in the range axis. This is a method originally developed by Stolt and is a variable swap method in the frequency domain which is usually referred to as *Stolt Interpolation* [54]. The Stolt Interpolation method was implemented as to come up with a solution for the wave equation for seismic data processing [27], thereby the association between RMA and seismic migration. Figure 3.5 illustrates the main steps of an RMA and what domain it operates in at which step of the process.

### 3.4.3 Kirchhoff Migration

Kirchhoff Migration as opposed to RMA is a time domain algorithm which means that it does not require any form of Fourier transformation. Using an integral solution to the scalar wave equation, the idea of Kirchhoff Migration is to propagate the scalar wavefront which is measured in the data acquisition plane, to the object plane at time zero. Kirchhoff Migration on electromagnetic waves is feasible because the vector wave equations reduce to scalar wave equations in a homogeneous, isotropic medium. Based on the ERM explained earlier the migrated wave field is obtained from the following equation:

$$u(\mathbf{r}', t) = \frac{1}{2\pi} \int_{S_0} \frac{\cos \phi}{vR} \frac{\partial}{\partial t} u\left(\mathbf{r}, t + \frac{2R}{v}\right) dS_0 \Big|_{t=0} \quad (3.24)$$

$\phi$  is the angle between the range axis and the joining the migrated point  $\mathbf{r}'$  and data acquisition point  $\mathbf{r}$ . Use of the ERM limits Kirchhoff Migration to array-based configurations where the transmit antenna and receive antenna are not in the same place.

### 3.4.4 Diffraction Stack Migration

In a medium where you assume constant velocity, the unfocused data of a reflecting object, preferably a point like reflector is characterized by a so-called diffraction hyperbola. The diffraction hyperbola is shown in figure 3.6. Every time the Radar receives a reflected signal it constructs a part of the diffraction hyperbola by the use of the distance of that specific reflected signal. All these signals are then summed up and the result of the summation is taken as the value of the pixel. This value is in turn placed in the object plane at that exact point, usually at the top of the diffraction hyperbola.

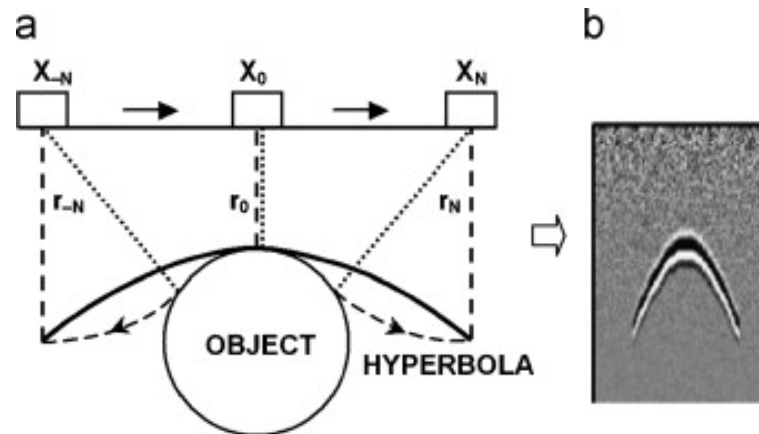


FIGURE 3.6: Generation of hyperbolic reflection [55]

### 3.4.5 Simple Summation Algorithm

Cambridge Dictionary defines an algorithm as follows: "a set of mathematical instructions or rules that, especially if given to a computer, will help to calculate an answer to a problem".

In the following section, a simple SAR algorithm solely based on the magnitude of incoming RF waves from a predefined UAV trajectory will be explained. The idea of the algorithm is not new, but it is almost as simple as a SAR algorithm can get. It will from now on be called, the Simple Summation Algorithm.

Every reflected RF wave taken in by the receiver contains both information about its phase and the magnitude of the wave. A real and an imaginary part. The magnitude tells us how strong the reflected signal is, and the phase can tell us from where the signal is coming. The distance to the reflecting target is measured by the time it takes for the signal to return to the antenna, by the use of a UWB Radar. Considering all this, combined with the UAVs position data it is possible to create a simple SAR image. Using the position of the UAV, the magnitude of the reflected signal and the distance to the reflecting target, the algorithm will sum up all reflected signals and interpolate them onto a two-dimensional matrix that will represent the SAR image. Each reflected signal has a value and a distance from the UAV, and if the UAV passes by the target at the same distance several times it is possible to obtain useful SAR imagery of different types of targets, as will be shown in Chapter 5. The step by step process of implementing this algorithm will be presented in Chapter 4.

## 3.5 Comparison regarding UWB Short-Range Imaging

This section will be entirely based on the results from the article "Comparison of Different Migration Techniques for UWB Short-Range Imaging" [12], referenced to several times in this project. Both Kirchhoff and the RMA are wave-equation-based

successors to the diffraction summation technique, and are originated in the field of geophysics. They belong to the category, wave-equation based algorithms, while diffraction stack migration goes into the base category synthetic aperture processing. [12].

RMA performs the image reconstruction in spatial Fourier domain and takes advantage of computing these transforms by means of a fast Fourier transformation [12]. This is an advantage when it comes to computational efficiency as opposed to the other time-domain integral approaches, such as Kirchhoff migration. Though on the other side, it would require a grid of evenly spaced data which can be challenging when talking about practical applications. By using the Kirchhoff integral theorem which expresses the value of the wave field at an arbitrary point, Kirchhoff migration is able to attain significantly higher image quality and lower sidelobe level than the diffraction stack technique. Since RMA is derived using the scalar wave equation it has the potential of producing high-quality images.

A test on performance for the three algorithms for point-like targets is presented in the article "Comparison of Different Migration Techniques for UWB Short-Range Imaging". They assume a 1m linear array operating in the frequency band from 3 to 8 GHz. In this test the transmitter and receiver are placed 10 cm apart and the point-like scatterer shown in figure 3.7 is at a range of 0.5m from the center of the aperture.

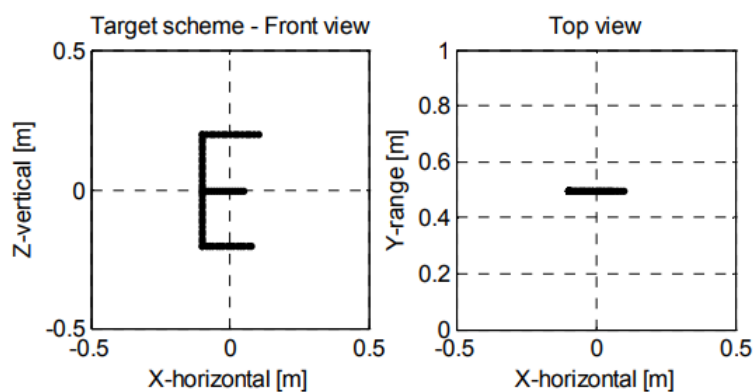


FIGURE 3.7: Scheme: Point-like target [12]

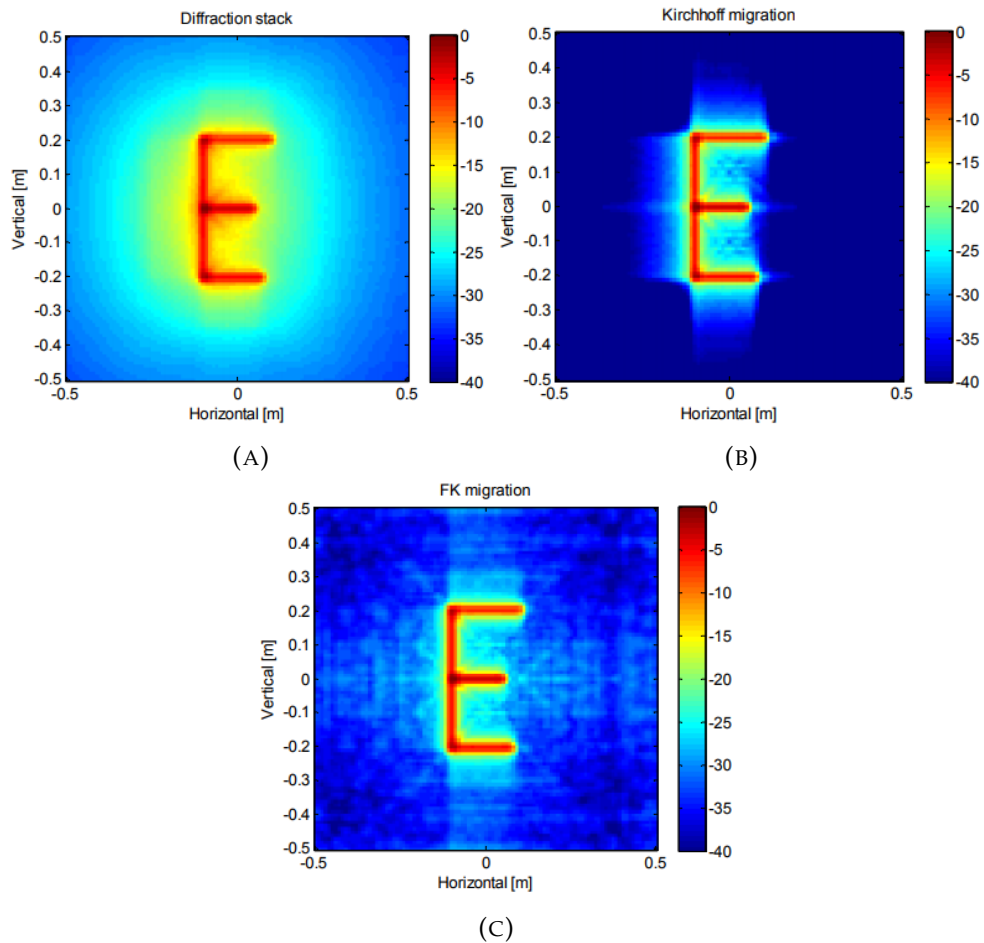


FIGURE 3.8: Performance for point-like target: Figure 3.7 [12]

And as we can see from the imaging results from a distributed target shown in figure 3.7 Kirchhoff migration shown in figure (3.8b), is able to produce a finer reconstruction of the shape of the target than both RMA and Diffraction stack migration. Diffraction stack migration ends up with a significantly higher sidelobe level close to the target in comparison to the RMA and Kirchhoff, while Kirchhoff migration focuses the energy onto a smaller area than the two other algorithms [12]. The article also compares another near-field SAR measurement test for further verification and concludes that among these algorithms, Kirchhoff migration provides the best image quality while RMA is computationally more efficient than the two other algorithms.

### 3.6 Discussion

Generating a high-quality SAR image depends on many different factors. Many of these, such as scattering of electromagnetic waves, are mathematically complex concepts and hard to fully comprehend. Limitations on size and power consumption on Radars mounted on small sized platforms require techniques such

as pulse compression to generate a signal powerful enough to be received by the Radar antenna without blending in with noise. In other words, maintaining a high SNR.

Many SAR algorithms are so-called frequency domain algorithms. By the use of FFT the raw Radar data is shifted to the frequency domain. This is done because of the many mathematical advantages of frequency domain analysis. Corrective measurement for noise disturbance generated in the system and parameter variation can easily be determined using frequency analysis. And as time domain response just gives you a function of amplitude changing over time, we know that all real-world signals consist of numerous signals of different types and frequencies, which are available in the frequency domain.

When considering what algorithms to use when dealing with SAR signal processing there are several things to consider. The main factor taken into account in this thesis was how much time had to be spent on applying our UAV test data on an already existing algorithm. Among them was a Python implementation of an RMA algorithm [56]. Integrating the UAV data in an orderly manner turned out to be a time demanding task that at first was postponed, but later dropped completely. It is worth mentioning that there are very few implementations of SAR algorithms available online. The implementation of the simple summation algorithm was prioritized to be able to test environments containing objects of different shapes, sizes, thus different scattering coefficients.

The summation algorithm, hence its simplicity has the ability to run in real-time and update the SAR image as new data comes in. While as earlier explained the migration algorithms need complete data sets to be able to process an entire image. Depending on the processing capabilities one could definitely discuss the possibility of running the summation algorithm parallel to a more complex and accurate migration algorithm and compare the images generated for extra redundancy. Though to do this, a more detailed review of available processing power would have to be done.

A study, comparing UWB short-range imaging by the use of the RMA, Kirchhoff and Diffraction Stack Migration algorithms shows the different results and concludes that the Kirchhoff Migration algorithm provides the best image quality, while the RMA is computationally more efficient than the two other algorithms.

### 3.7 Summary

In the domain of Radar signal processing, it is important to note the basis of which all Radar imaging systems are built upon, the start-stop approximation. It presumes that both the sensor and the scattering object (target) are stationary during the time interval in which the Radar pulse hits the target. Most imaging systems also consider the region between the Radar sensor and the target to consist

of a homogeneous, loss-less, non-dispersive atmosphere.

When talking about SAR and Radar imaging it is important to have some knowledge about scalar waves both scientifically and mathematically. When dealing mathematically with scattering of electromagnetic waves, equations are often transformed from the time domain to the frequency domain in order to facilitate for easier mathematical manipulation. Because of the behavior of scattered electromagnetic waves, there will always be non-linearities, which make the mathematical modeling much more complicated. The technique known as the Born approximation helps by making the imaging problem linear, though it is not always a good approximation.

There are many other techniques that enable for higher quality imaging with SAR. The Pulse Compression technique is an important one. For UWB SAR, it is crucial to be able to transmit very short pulses as to distinguish two separate objects located close to each other. Though, acquiring quality reception from very short duration pulses requires the pulses to be transmitted with high enough power. A more powerful pulse will ensure a better SNR. Thus, it would require a lot of power and sophisticated electronics from a UWB SAR to send out high power short duration pulses. The Pulse Compression technique, by the use of a matched filter, compresses a linear FM pulse to create a high peak short pulse. Since a Radar system only sends a signal to get a reflection, there is no need for complex frequency distribution manipulation within the signal. A simple pulse containing numerous frequency components would suffice. A Compressed High Intensity Radar Pulse (CHIRP) is such a signal. The matched filter is an operation in which a known signal, or template, is correlated with an unknown signal to detect the presence of the template in the unknown signal. The matched filter is an optimal filter in regards to SNR in the presence of additive stochastic/non-deterministic noise. Considering SAR, the matched filter is normally performed by the use of convolution - using two signals to produce a third signal.

Considering the fact that signal history is represented in the time domain, frequency domain SAR signal processing uses two major techniques. FFT and interpolation. FFT is a compact version of the DFT and is in short terms a mathematical maneuver that converts a signal from its original domain (often time or space) to a representation in the frequency domain and vice versa. FFT is computationally more efficient than the DFT. Interpolation is a method of constructing new data points within a range of a known set of discrete data points. It is an essential and powerful tool when it comes to curve fitting and/or curve smoothing.

Synthetic Aperture Radar Migration Algorithms are based on the scalar wave equation, a linear hyperbolic partial differential equation of different orders. The scalar wave equation is used to describe almost all types of waves. Among the many different migration techniques they often differentiate when it comes to computational load, spatial resolution, differential resolution (image quality), and

SNR. The Range Migration Algorithm (RMA), often referred to as FK-migration is a frequency domain algorithm where both azimuth (cross-range) and range axis are frequency converted by the use of two-dimensional FFT, which makes it somewhat computationally efficient. The RMA's key mechanism is a variable swap method in the frequency domain on the range axis, and is called Stolt Interpolation. Kirchhoff Migration is a different algorithm which does all its work in the time domain, thus no need for any Fourier transformation. It uses an integral solution to the scalar wave and is based on the ERM which assumes that the wave field starts from the target at time zero with half the actual propagation speed. A simpler algorithm is the Diffraction Stack Migration algorithm where constant velocity is assumed. The unfocused data of a reflecting object is characterized by a diffraction hyperbola, by summing up all reflected signals the image is constructed.

The algorithm to be tested in this thesis, which I have chosen to call the Simple Summation Algorithm does not require constant velocity as the Diffraction Stack Migration algorithm, but to work efficiently it needs stable positioning data from the platform as well as a good measure on the distance to the reflecting objects. All incoming reflected signals are summed up and interpolated over an empty two-dimensional matrix (SAR image) of a specified size.



## Chapter 4

# Software & Hardware

### 4.1 Software

In this thesis it was decided that coding in Python would be beneficial as the code database for extraction of UAV data was originally written in Python. PyCharm was then chosen as the Integrated Development Environment (IDE) without much further consideration. PyCharm is an IDE used in computer programming, specifically for Python. It was developed by JetBrains, a Czech company [57]. PyCharm provides tools for code analysis, graphical debugging, an integrated unit tester, integration with version control systems (VCSes), and support web development as well. It is a cross-platform and even though it has a Professional Edition released under a proprietary license with extra features, all work in this thesis is done in the Community Edition released under the Apache License [58].

To facilitate for simple and structured package management and deployment, *Anaconda* was used. Anaconda is a free and open source [59] distribution of the Python and R programming languages for data science, large-scale data processing, predictive analytics, scientific computing, etc. Anaconda uses the system called *conda*, to simplify package management and deployment [60] [61].

Understanding the functions of the libraries named *imcdatabase* and *radar\_frame\_parser* was important. These libraries were written by Kristian Klausen and Morten Fyhn Amundsen and contain specific code for extraction and structuring Radar data from the multirotor UAV used in this master thesis.

Furthermore, the need of libraries for plotting and scientific computing led to the use of *NumPy* and *Matplotlib*. NumPy is the fundamental package for scientific computing with Python. It contains among other things: a powerful N-dimensional array object; sophisticated (broadcasting) functions; tools for integrating C/C++ and Fortran code; useful linear algebra, Fourier transform, and random number capabilities [62]. Matplotlib is a Python 2D plotting library which produces publication quality figures in a variety of hardcopy formats and interactive environments across platforms. Matplotlib can be used in Python scripts, the Python and IPython shells, the Jupyter notebook, web application servers, and several graphical user interface toolkits [63]. When coding in Python there are several options to choose from concerning libraries for plotting and for scientific

computing. NumPy was mainly chosen as it was already integrated with the Radar data functions. Matplotlib, on the other hand is a visualization tool that has nearly no limitations regarding complexity. Given that I was not completely sure how complex the visualization of Radar data would get in this thesis I chose a tool with which I was certain would be sufficient.

Before creating a project in PyCharm, an open-source web application called Jupyter Notebook was used to test the functions from the `imcdatabase` and `Radar_frame_parser`. Jupyter Notebook is a web application that allows creating documents containing live code, equations, visualizations, and narrative text. When testing specific lines of code or specific functions Jupyter Notebook is of great value. Having an application like this, facilitated for much more efficient coding when implementing the algorithm, explained in section 4.3.

## 4.2 Hardware

Most of this section is based upon [64] and [65], as well as specifications given by researchers at the Department.

The UAV platform used is a small-sized (9.5 inch/241mm diagonal) quadrotor at 2000 grams with a battery capable of sustaining a flight time of approximately 17 minutes. It has an onboard computer (beaglebone black) for high-level processing, combined with an ardupilot for low-level auto piloting. Figure 4.1 shows a picture of the UAV used in this thesis.



FIGURE 4.1: UAV used during tests

The UAV uses the XeThru X4M05 Radar sensor with antennas for X4 UWB System on Chip (SoC) Radar. The X4M05 is targeted for those who want to do data processing on external MCUs. The X4M05 offers a Serial Peripheral Interface (SPI) interface to host [64]. Novelda's XeThru X4 is a UWB impulse Radar chip. The basic components of the X4 SoC are a transmitter, a receiver, and related control circuits. The system is controlled by the System Controller and is configurable through a 4(6)-wire Serial Peripheral Interface (SPI). It provides product developers

Parameters	Value
Weight (Battery & Propellers included)	2000g
Diagonal Length	Approximately 241mm
Flight Time	17mins
Center Frequency	7.29 GHz/8.748 GHz
Radar Detection Range	25m
Radar Azimuth Angle	65°

TABLE 4.1: NTNU research UAV with XeThru X4 UWB System on Chip Radar

with sub-mm movement sensing accuracy at distances from 0 to 25 meters depending on target size, which is good for the purposes of collision avoidance in indoor environments. Operating at sub 10GHz frequencies, the X4 UWB Radar enables sensors to see through obstacles and detect even the smallest movements, its performance being optimized for occupancy sensing and respiration monitoring. The X4 is the smallest available Radar SoC solution in its class and offers ease-of-use and BOM cost advantages [65]:

- Single-chip ultra wide band impulse Radar transceiver
- Human Presence simultaneous tracking range up to 10m
- Low power consumption, typically < 120 mW
- Industrial operating temperature range, -40/+85 °C
- Advanced power management enabling low power duty cycle controlled operation
- Bi-phase coding of transmitted pulses for spectrum spreading
- Is able to see through obstacles, sub 10GHz
- Ultra-high spatial resolution for simultaneous multi-object tracking
- Master/Slave Serial Peripheral Interface (SPI)
- Compact WLCSP, 0.4 mm pitch, 48 pin package

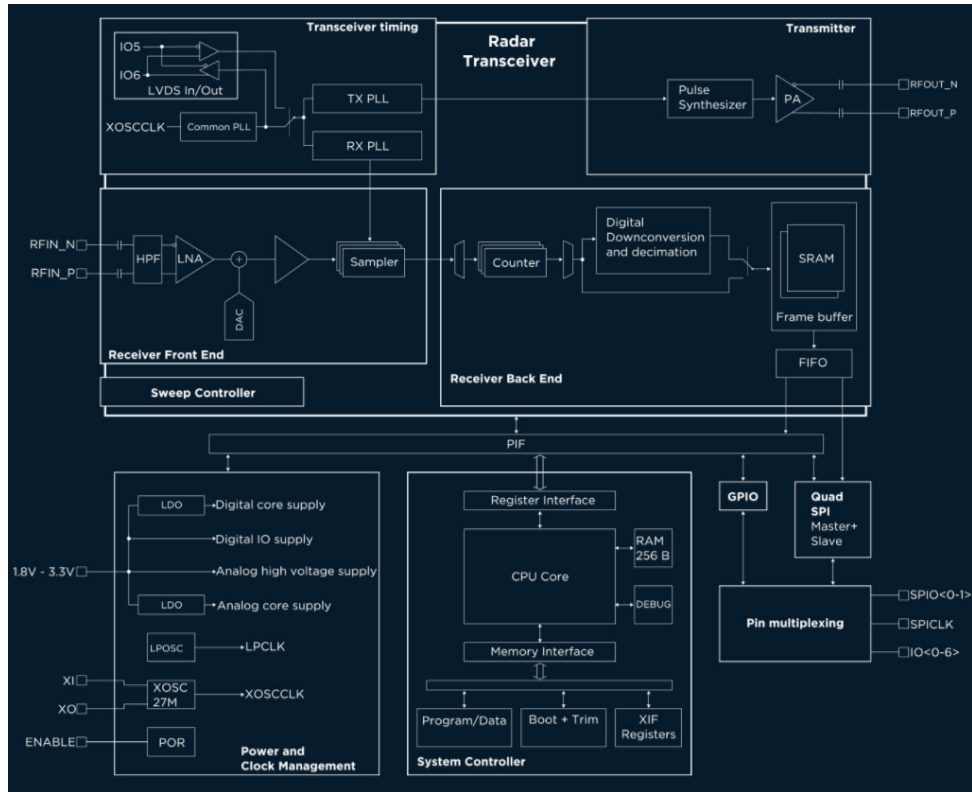


FIGURE 4.2: Novelda XeThru X4 Circuit Overview [65]

The basic components of the X4 SoC are a transmitter, a receiver, and related control circuits. The system is controlled by the System Controller and is configurable through a 4(6)-wire Serial Peripheral Interface (SPI). The X4 receive path (RX) consists of a Low Noise Amplifier (LNA), a Digital-to-Analog Converter (DAC), 1536 parallel digital integrators as well as an output memory buffer, accessible through the SPI. The X4 transmit path (TX) consists of a pulse generator capable of generating pulses at a rate of up to 60.75 MHz. The output frequency and bandwidth are designed to fit worldwide regulatory requirements.

The Radar transceiver operates autonomously and can be programmed to capture data at predefined intervals and then alert or wake up a host MCU or DSP through dedicated interrupt pins. The Power Management Unit is in control of the on-chip voltage regulators and enables low-power applications to use efficient duty cycling by powering down parts of the circuit when they are not needed. The system can be configured to consume less than 1mW in idle mode when all analog front end components are turned off [65]. Figure 4.2 shows the X4's circuit overview. The Radar module mounted on the UAV is shown in figure 4.3. From figure 4.1 it can be seen that the UAV is mounted with several Radar modules, though this thesis will only investigate the use of one.

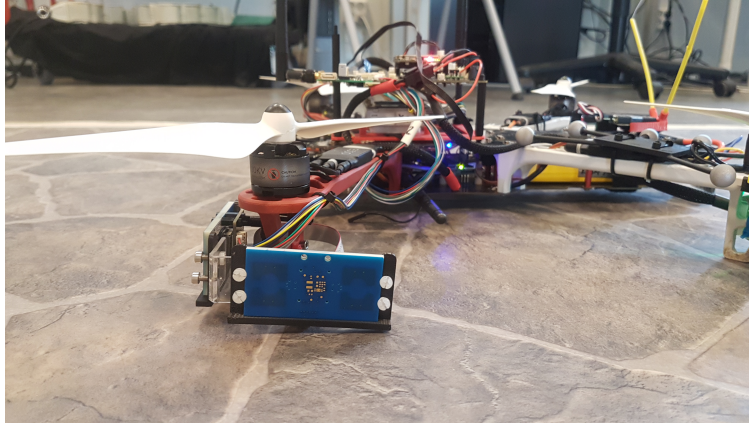


FIGURE 4.3: The Radar module mounted on the UAV

Choosing a suitable Radar sensor for the UAV has not been a part of this thesis, though it is noted that the Radar sensor described above suits its purpose considering the Radar frequency range, see table 4.2.

Band Designation	Frequency Range	Usage
HF	3-30 MHz	OTH surveillance
VHF	30-300 MHz	Very long-range surveillance
UHF	300-1000 MHz	Very long-range surveillance
L	1-2 GHz	Long-range surveillance - en route traffic control
S	2-4 GHz	Moderate-range surveillance - Long-range weather
C	4-8 GHz	Long-range tracking - airborne weather detection
<b>X</b>	<b>8-12 GHz</b>	<b>Short-range tracking</b>
$K_u$	12-18 GHz	High-resolution mapping
K	18-27 GHz	Little use (water vapor)
$K_a$	27-40 GHz	Very high-resolution mapping - airport surveillance
millimeter	40-100+ GHz	Experimental

TABLE 4.2: Radar Bands and Usage (similar to table 1.1 in [7])

### 4.3 Implementation Steps

During the course of this thesis, the implementation of the summation algorithm has been done in partial cooperation with a co-student, David Billdal. Mr. Billdal's thesis concerns testing of the summation algorithm on a multirotor UAV in a simulated environment with simulated Radar data collected in real time. While this thesis differs by taking the same algorithm and applying it on Radar data sets

generated from real-world testing in different environments.

The implementation of the simple summation algorithm explained in Chapter 3 is decently straightforward. Since the algorithm only depends on UAV position data with relevant time-stamps as well as the magnitude of the incoming reflected signals and distance to the target, there is not much mathematical manipulation or calculation needed. When implementing the algorithm at first, a simplification of the UAVs movement was made. Since the multirotor UAV was meant to fly in a straight line following the same x-position, this was assumed and the slightly varying x-position was not corrected for. In the second run, there was implemented a correction to create a better focus on the SAR-image. The implementation steps went as follows:

1. Load all Radar data from a specific log file
2. Loop through all Radar data in the log file
3. Extract and organize relevant data such as distance (using NumPy), magnitude, time-stamp, drone position
4. Filter all low-range noise (described in the section above)
5. Create an empty SAR image as a two-dimensional array
6. Interpolate the UAV position and distance to target values as to fit the SAR image
7. Map all values onto the empty SAR image
8. Generate SAR image with Matplotlib

When creating the empty SAR image, the resolution is chosen. In this thesis, the resolution was experimented with in regard to how much Radar data was available from the specific data set. One thing to point out is that this implementation of the algorithm can only be used on already generated Radar data sets. Though it would not be very difficult to re-write the code such that the SAR image could be continuously updated as the UAV was flying.

## 4.4 Discussion

The programming language chosen for this thesis was Python due to the writer's former knowledge of the language combined with the fact that already existing libraries for Radar data extraction were written in Python.

Considering the relatively straightforward programming task presented in this thesis, there was no need for a lengthy contemplation on what software to use. The already written libraries for extraction of data from the UWB Radars on the multirotor UAV were sufficient and no changes were applied to them.

As the development and choices concerning the UAV platform and what Radars to use is not within the scope of this thesis, there will be no discussion regarding other hardware components than those mentioned. Though comparing the UAV platform and Radar used in this thesis to the UAV platform and Radar used in the study presented in chapter 2.6, there are some things worth mentioning.

Parameters	Value
Weight (Battery & Propellers included)	1000g
Diagonal Length	350mm
Flight Time	25mins
Center Frequency	4.3 GHz
Radar Detection Range	40m (typically), 80m (optimized)
Radar Azimuth Angle	N/A

TABLE 4.3: DJI Phantom with PulsON 410 UWB Smart Sensor [66]  
[67]

Looking at the tables 4.3 and 4.1 there are no great differences regarding the UAV platforms. Considering that the PulsON 410 UWB Smart Sensor mounted on the DJI Phantom is an older version of the PulsON 440 one can expect the XeThru X4 UWB System on Chip to perform slightly better when it comes to operating conditions and power consumption. Combining this information with the results of the study presented in chapter 2.6 it is fair to say that one could expect similar SAR imaging results if the two UAVs would be tested side by side.

Implementation of the Simple Summation Algorithm was a straightforward operation on extraction and utilization of the Radar data needed. Generation of the SAR image was done experimentally considering resolution (size of the two-dimensional matrix). Here it would be possible to make the algorithm interpret the amount of Radar data available, and then go on to choose an appropriate resolution on the SAR image. Due to the small amount of testing in different environments this was not prioritized.

## 4.5 Summary

All programming in this thesis was done using the Python programming language and the IDE PyCharm Community Edition. Package management and deployment was handled by the open source distribution Anaconda. Using libraries developed by Kristian Klausen and Morten Fyhn Amundsen from NTNU, along with libraries for plotting and scientific computing everything was set for implementation of the Simple Summation Algorithm.

Using a light-weight 2000 gram UAV platform mounted with a UWB System on Chip Radar, the UAV can easily be characterized as state of the art, having a Radar detection range of 25m and a flight time of 17 minutes.

Implementation of the algorithm is based on the libraries for extraction of Radar data where the algorithm is initiated by loading the already captured Radar data from a specific log file, and by the use of summation and position data, generates a SAR image.

## Chapter 5

# Testing & Results

### 5.1 Test Setup

Since the Simple Summation Algorithm tested in this thesis is restricted to simple UAV movements in a straight line the test setup is rigged in its advantage. The test room is the so-called Motion Capture Lab (the old Snake Robot Lab) at NTNU. The room has decently low reflective concrete and plaster walls and the UAV described in chapter 4 is equipped with accurate positioning equipment. As can be noticed in the pictures from figure 5.1 is that the room is not completely sterile and contains several items that may interfere with the Radar while testing. Remembering that the Radar mounted on the UAV has an azimuth angle of  $65^\circ$  it is natural to assume that other objects in the room may interfere in some manner. The UAV will be operated manually with the intention to fly in a straight line at constant speed passing by the test object pointing towards them with the front-facing Radar. With the current Radar configuration the SAR imaging will be done in stripmap.

Figure 5.1 shows four pictures of the UAV flying past one of the objects (the circular metallic pole). The UAV was flown manually by a researcher at the Department with the intention of flying it in a straight line with constant heading past the object.

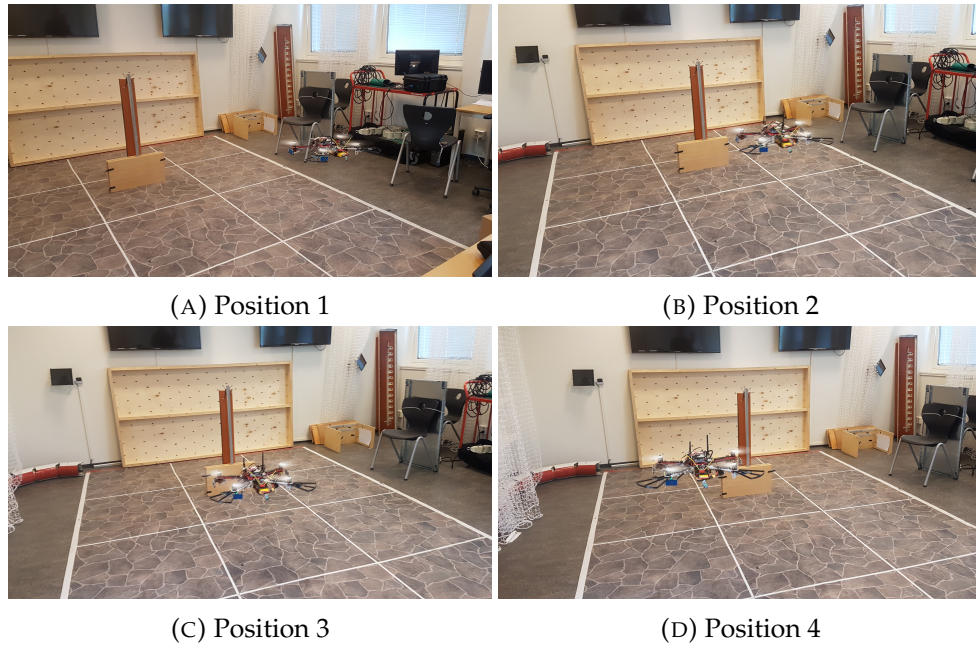


FIGURE 5.1: UAV flight

The five different objects that were imaged in this chapter is shown in figure 5.2 at their test setup. The objects were chosen because they represent different shapes of different materials and are similar to what can be found in many indoor environments. Behind all of them (except the plate) is a plastic half-pipe shaped structure mainly for the purpose of stabilizing the objects, so that they would not fall from the wind force projected upon them when the flying UAV. There was conducted no tests on the half-pipe structure. It was merely assumed that it would not cause enough back-scatter to affect the tests in any significant way. This assumption will be reflected upon in the discussion later in this chapter.

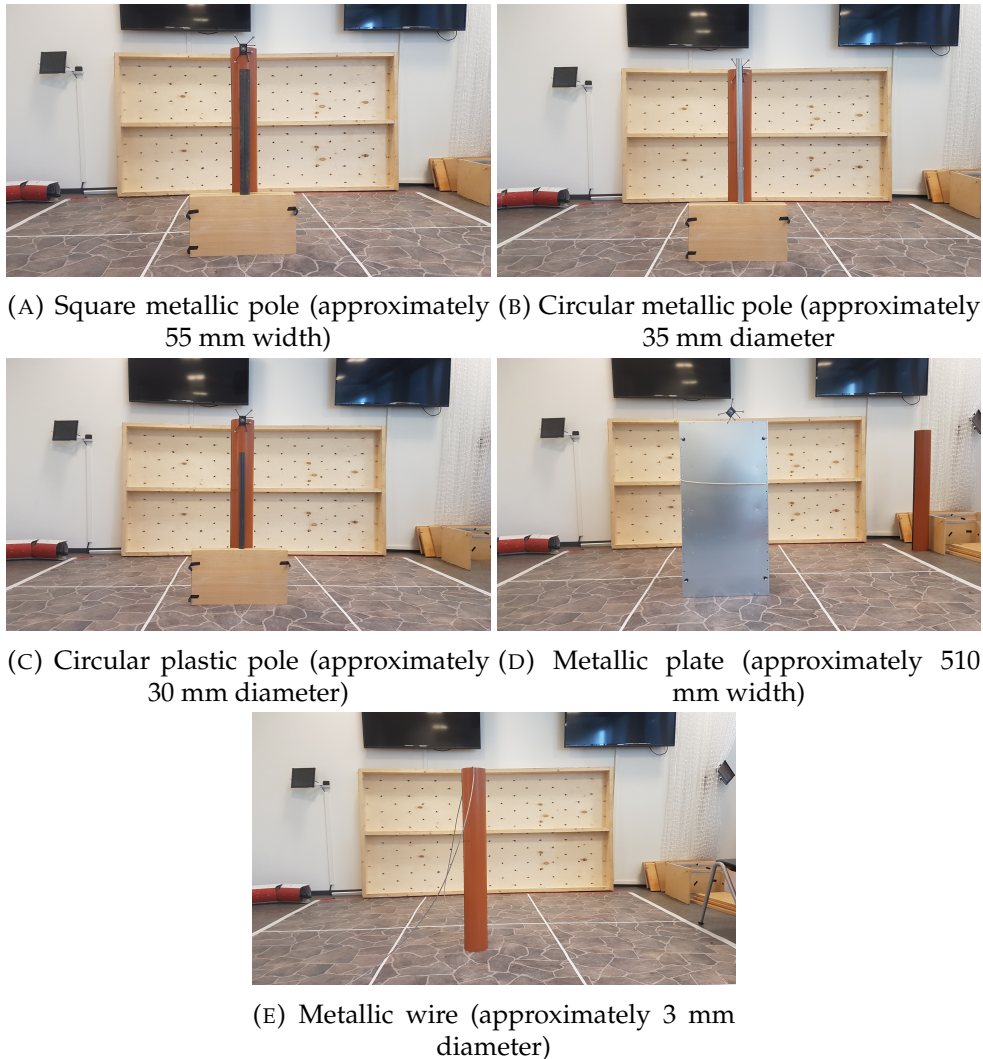


FIGURE 5.2: Test objects from the UAV's position

For all objects, 5 tests were completed. From those 5 tests, the one presented in the following section was the one with the most ideal flight path, and with the least amount of unwanted interference.

## 5.2 Test Results for Simple Summation Algorithm

The Radar used on the UAV experiences a type of noise which is mixed in with all incoming signals closer than approximately 1 meter in the range direction. This is, of course, an issue that has been worked on. It is caused by the Radar system internally and poses a great disadvantage when imaging objects closer than approximately 1 meter to the Radar. The final solution was simply to use a filter that removes all constant noise coming from the Radar. It is not necessarily a permanent solution, but in these tests it gave better results than with a strict low

pass filter.

Furthermore, it is important to mention the logic behind the azimuth axis in all SAR images considering that the UAV is flown manually and therefore not in a perfectly straight line. The Simple Summation Algorithm takes the first registered position of the UAV and makes it the UAV reference position in range direction while moving in the azimuth/horizontal (cross-range) direction. All measurements will therefore be adjusted for in range by the deviation of the UAV position relative to the reference position. Thus for all SAR images the UAV movement is projected on to the azimuth axis as if it had flown in a perfectly straight line.

Because of the issue regarding a straight UAV flight pattern it was considered to test the UAV using some sort of rail, or by placing it on, for example, a trolley and pushing it back and forth in a straight line. A test that was done earlier by the method of carrying the UAV back and forth was done while trying to capture the plate. Though the image generated by flying the UAV did not show any significant difference, so it was decided that it would be more interesting to see the results from a flying UAV test. This decision is evaluated in the discussion at the end of this chapter.

The simplicity of the Simple Summation Algorithm places a fairly low expectation on whether it will be possible to generate images where all tested objects can be seen. Considering that the test room, the NTNU Motion Capture Lab, contains other objects that may interfere with the tests it was interesting to see if the hard-to-see objects such as the wire and the circular poles could be seen in either the amplitude graph or the generated SAR image.

### 5.2.1 SAR test: Metallic Plate

SAR imaging results using the Simple Summation Algorithm is shown in figure 5.3. Summing up all amplitudes by what distance they were captured at makes the plot in figure 5.4. The metallic plate has a width of approximately 510 mm and was placed parallel to the desired straight flight path of the UAV. The UAV was, as mentioned earlier manually operated, thus causing some deviation from the desired straight line. The UAV flight path in this test can be seen in figure 5.5 along with the position of the object (red circle), and as one can notice, the UAV could need functionality concerning predefined flight patterns.

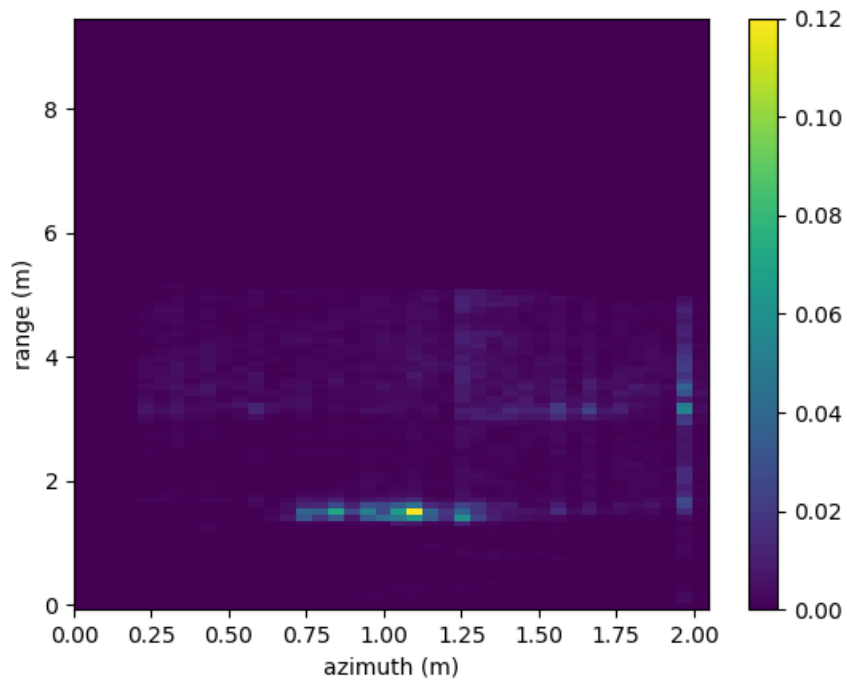


FIGURE 5.3: Generated SAR image of the metallic plate

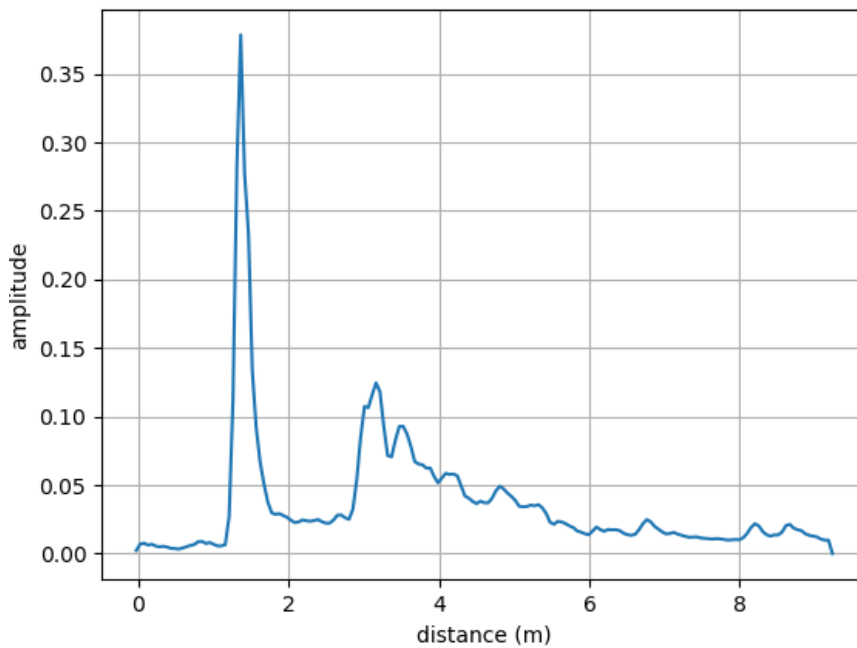


FIGURE 5.4: Magnitudes for the metallic plate summed up at all distances

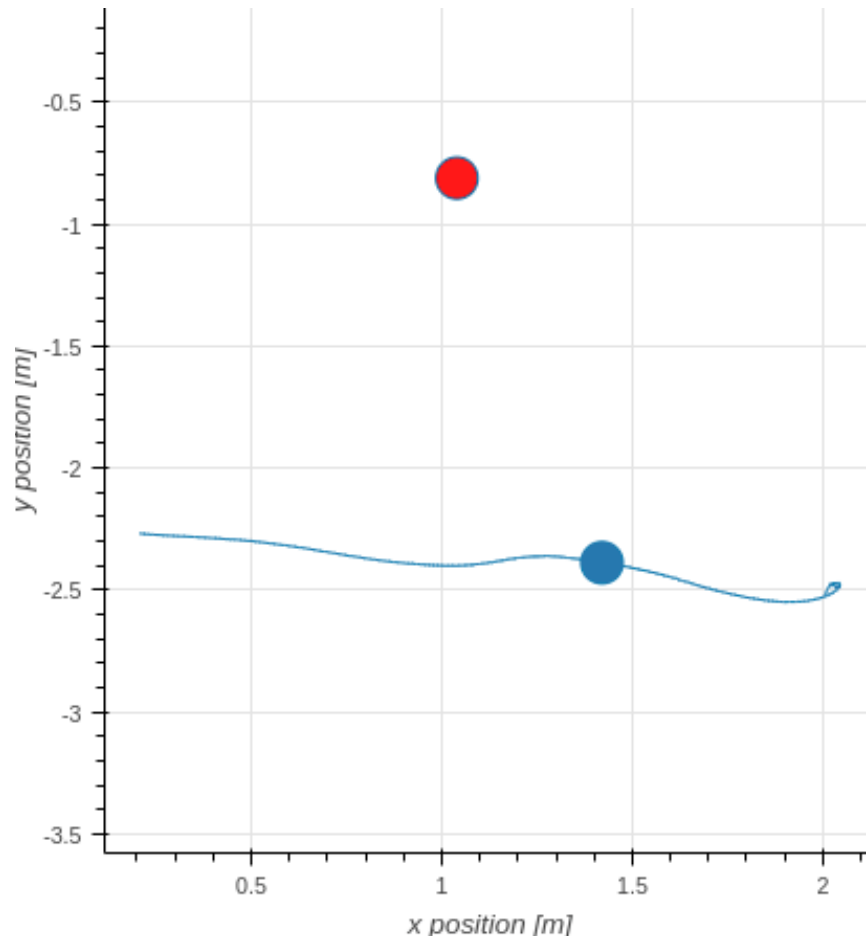


FIGURE 5.5: Manually flown UAV path for the metallic plate (Metallic plate center in red)

Figure 5.3 shows that the plate (which is approximately 1.6 meters from the UAV reference position) is clearly standing out as opposed to its surroundings. The graph, representing all amplitudes summed up at different ranges also shows a clear signature on where the plate is located. The SAR imaging of the plate should have been shaped more like a hyperbola, though it is not noticeable in figure 5.3. This is believed to be the results of inconsistent heading and a nonlinear flight path.

### 5.2.2 SAR test: Metallic Plate 45 degrees

The 45-degree test on the same metallic plate is done because it clearly shows the big difference in Radar imaging of an object when not all signals are reflected straight back to the receiver. Turning the plate 45 degrees away from the desired straight flight path makes it harder to see the entire plate from the perspective of the UAV, see figure 5.6.

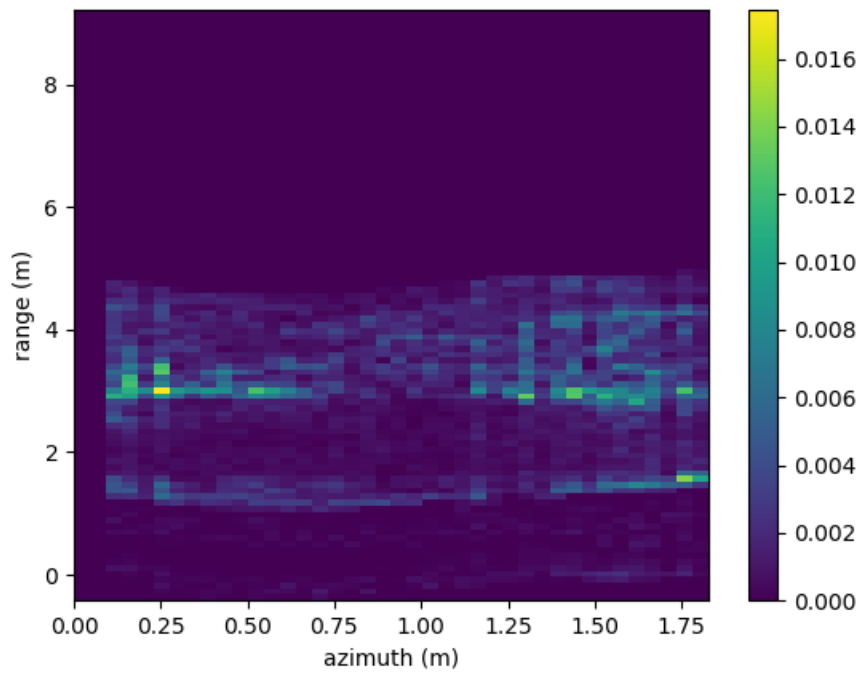


FIGURE 5.6: Generated SAR image of the metallic plate at 45 degrees

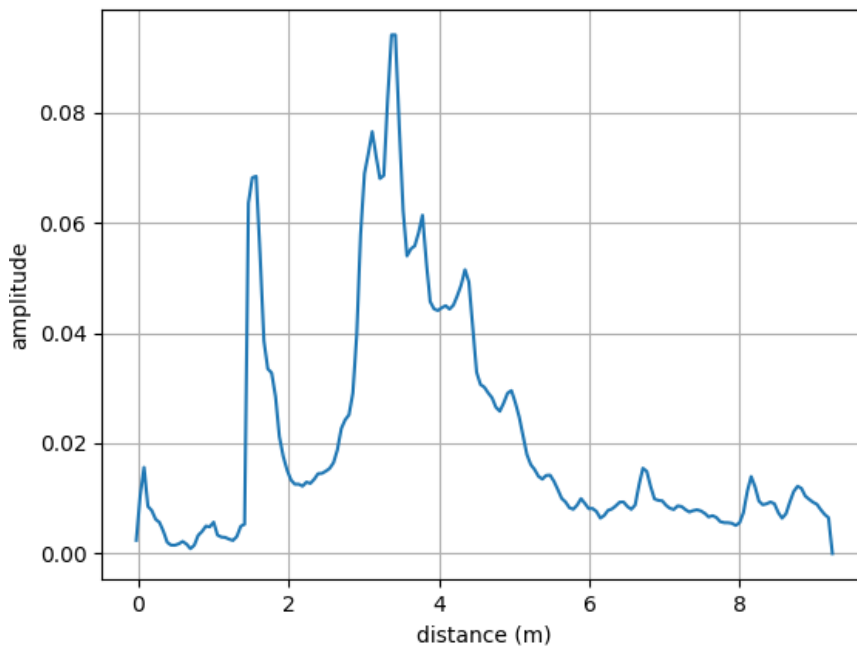


FIGURE 5.7: Amplitudes for the metallic plate at 45 degrees summed up at all distances

Since the UAV is flown manually, the flight path and flight time of the test differ from the  $0^\circ$  plate test. Therefore, the results are not perfectly comparable, see figure

5.8. Looking at the summation graph in figure 5.7 one can argue that the plate is captured at a distance of approximately 1.7 meters from the UAV reference position, though it blends in with the signature of the wall behind it. The results of the test show certain amounts of ambiguity. Mostly because of the widespread of amplitudes shown in the generated SAR image, which may have been caused by ground clutter and other interfering objects, but also considering the nonlinear flight path of the UAV. The vertical "strings" showing no radar signature at all come from lack of data caused by the UAV flying to fast for data to be captured by the radar.

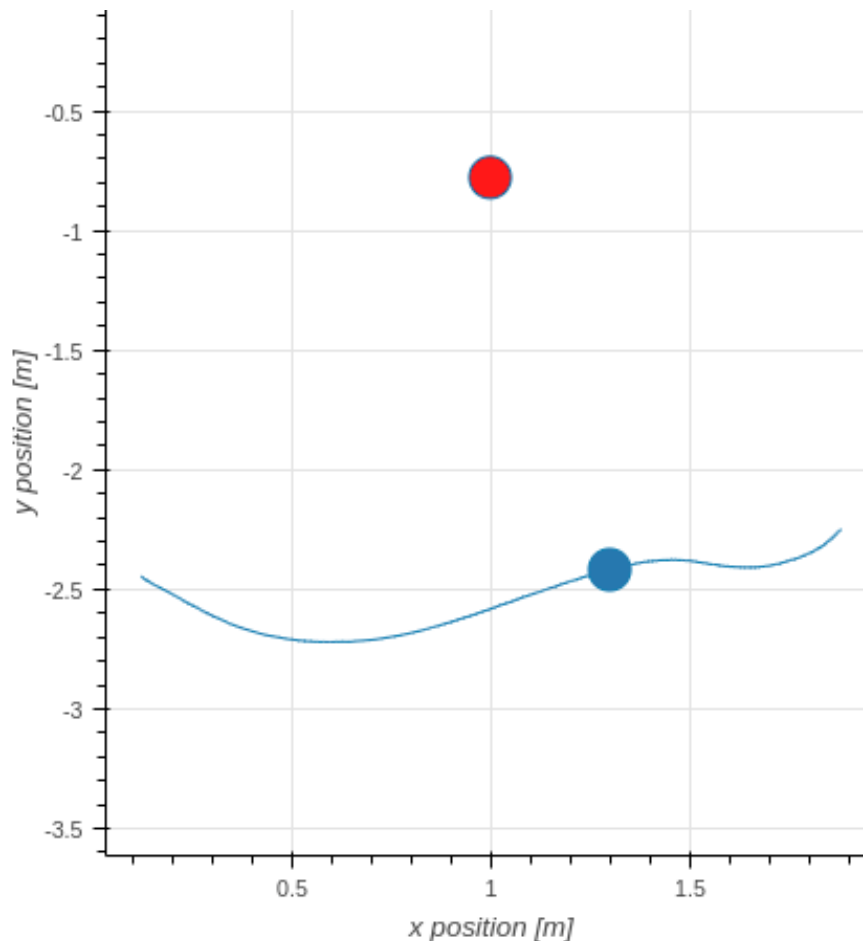


FIGURE 5.8: Manually flown UAV path for the metallic plate (red circle) at 45 degrees

### 5.2.3 SAR test: Metallic Square Pole

Looking at the graph in figure 5.10 the Radar clearly obtained a signature at a distance of approximately 1.6-1.8 meters. From the generated SAR image (see figure 5.9) it can be argued that it blends in with the wall behind, thereby creating an unclear image. The flight path (blue line) shown in figure 5.12 is slightly nonlinear which could argue for some ambiguity in the results. The vertical "strings" showing no radar signature at all come from lack of data caused by the

UAV flying too fast for data to be captured by the radar. The expectations to this test was that the radar should be able to see the pole, and looking at figure 5.11 which is a snapshot of the amplitudes recorded when the UAV passes by the square pole one can argue that it in fact is able to see the object.

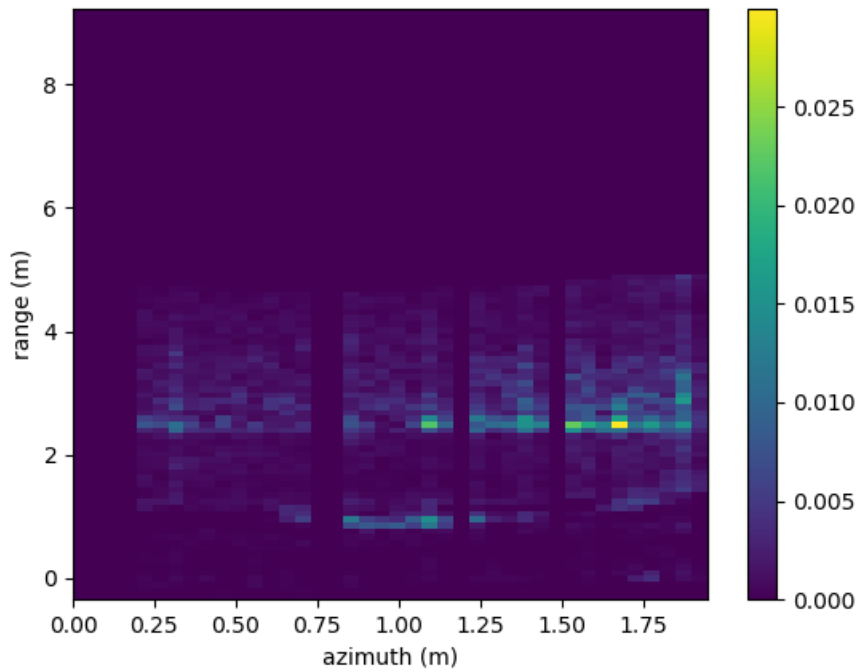


FIGURE 5.9: Generated SAR image of the metallic square pole

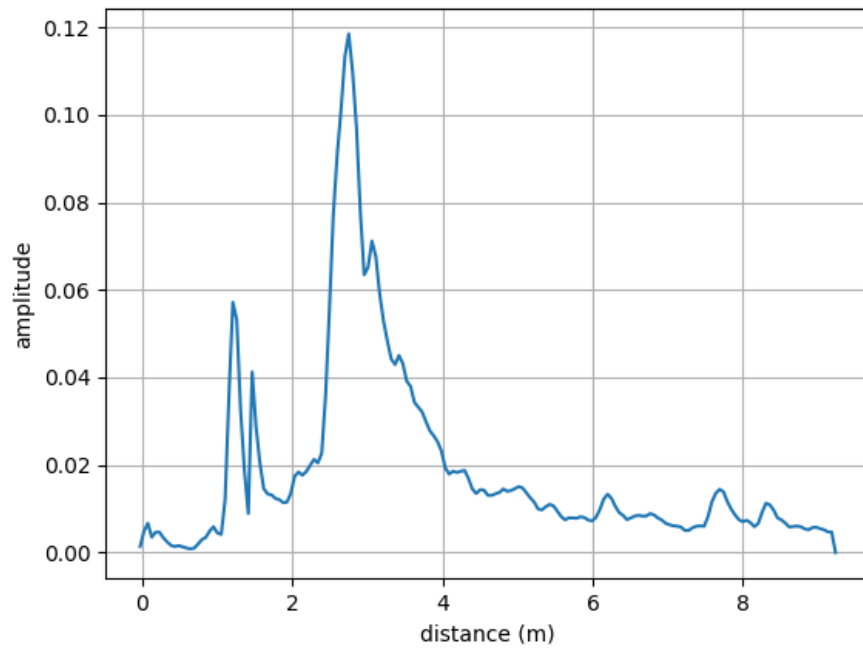


FIGURE 5.10: Amplitudes for the metallic square pole summed up at all distances

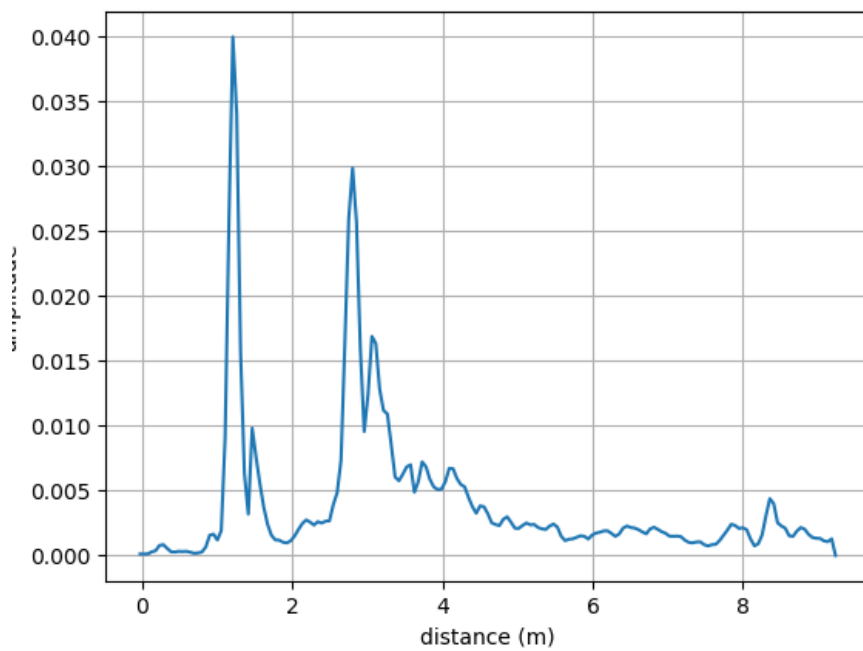


FIGURE 5.11: 1 second snapshot of the amplitudes summed up for when the UAV flies in front of the metallic square pole

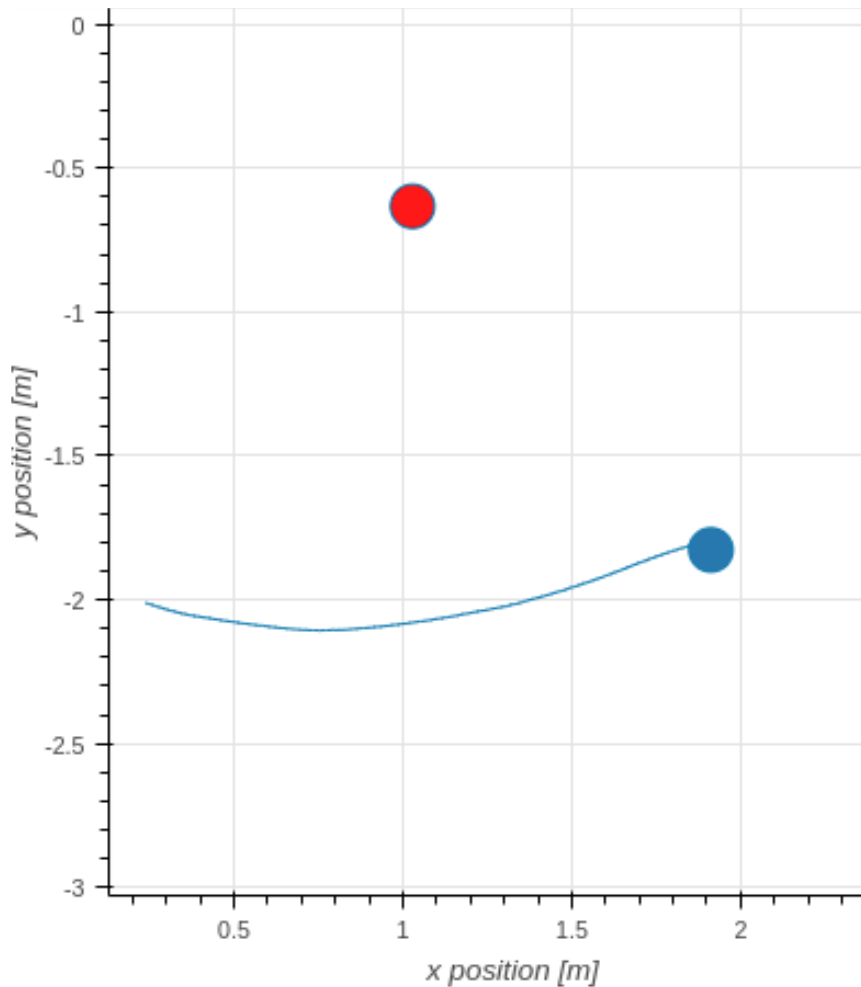


FIGURE 5.12: Manually flown UAV path for the metallic square pole shown as a red circle

#### 5.2.4 SAR test: Metallic Square Pole 45 degrees

What is meant by placing a square pole at 45 degrees can be seen in figure 5.13. Looking at the graph in figure 5.15 there is something at approximately 1.8 meters from the ideal UAV straight line path, though some of it is most likely ground clutter. As its summed up amplitude is fairly equal to what is being reflected from the wall, one can not see the object's signature on the image in figure 5.14. Even though flight path shown in figure 5.16 is fairly linear there is one particular thing that stands out in this test. The fact that the SAR image shows a clear signature on the right (not the position of the object). Thus making the result ambiguous to whether the Radar actually was able to detect the pole as clearly as the graph may show. In this test there also some places that lack radar data in azimuth caused by UAV velocity. The object position relative to the motion of the UAV is shown as the red circle in figure 5.16.



FIGURE 5.13: Metallic square pole at 45 degrees

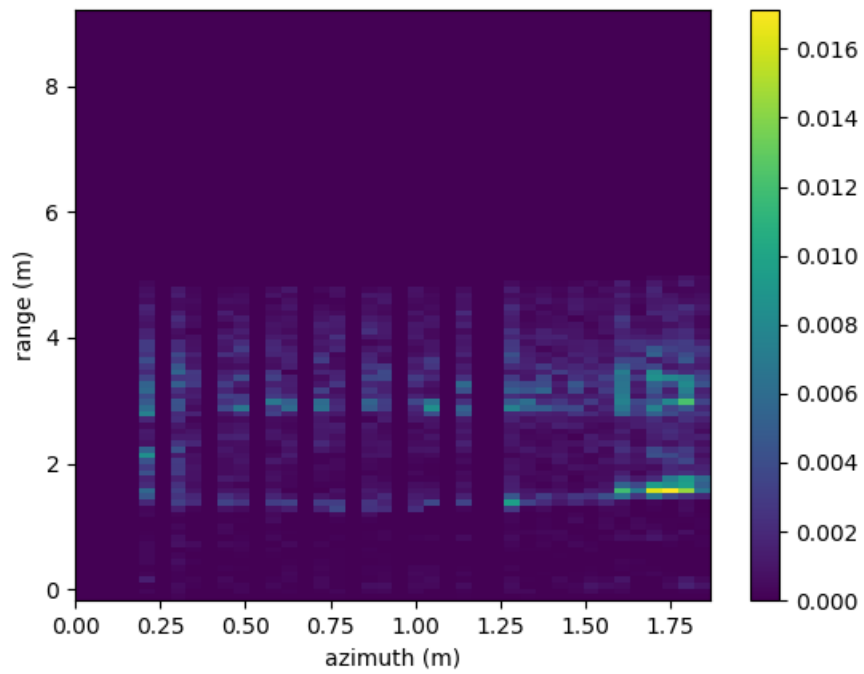


FIGURE 5.14: Generated SAR image of the metallic square pole at 45 degrees

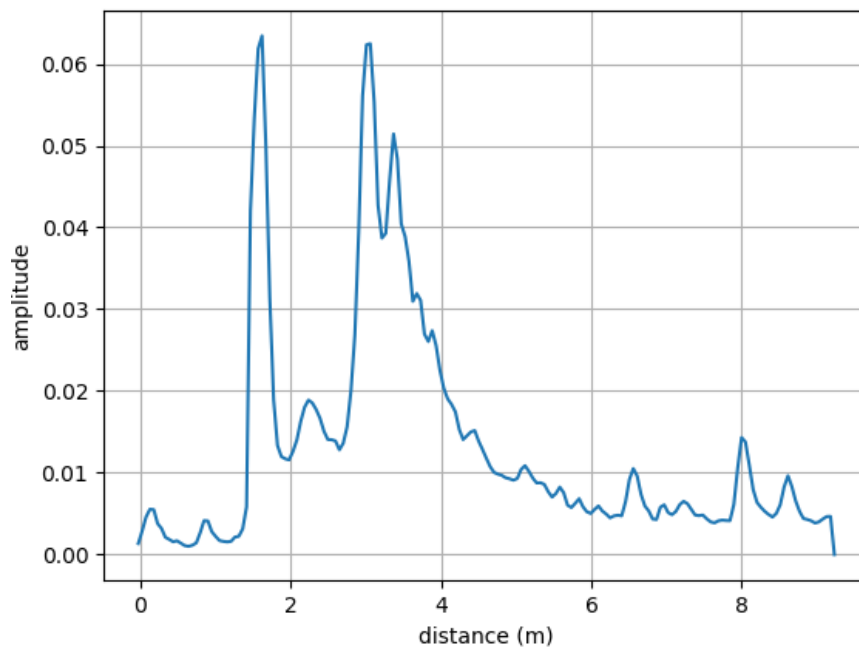


FIGURE 5.15: Amplitudes for the metallic square pole at 45 degrees summed up at all distances

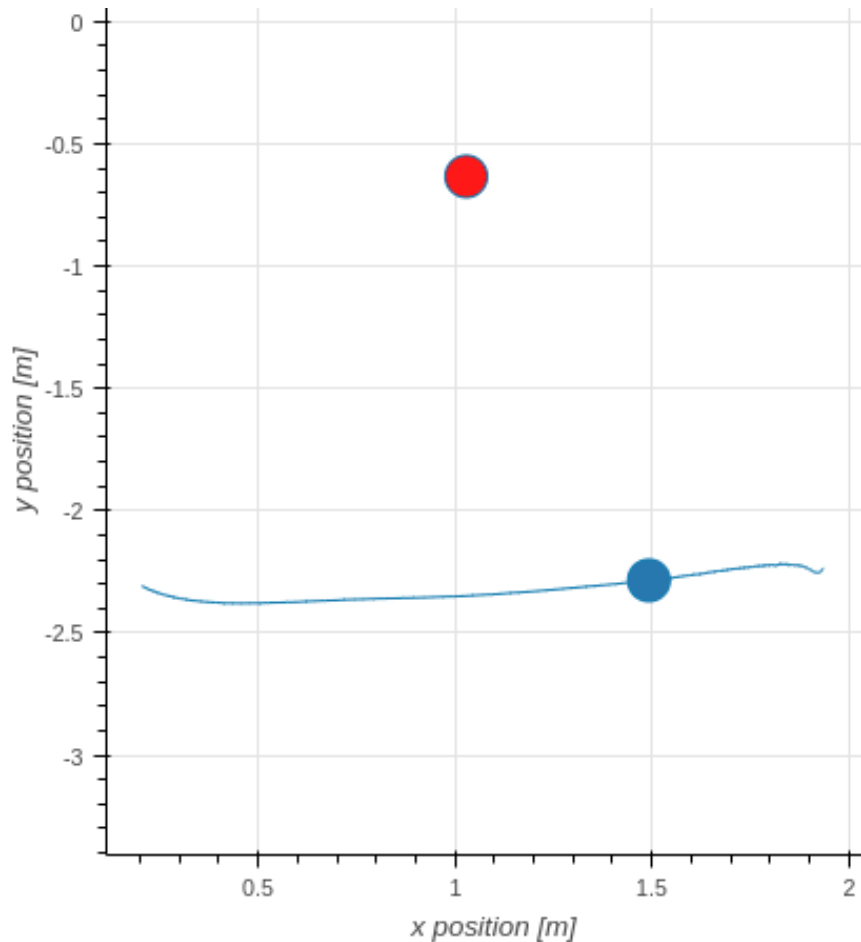


FIGURE 5.16: Manually flown UAV path for the metallic square pole (red circle) at 45 degrees

### 5.2.5 SAR test: Circular Metallic Pole

Figure 5.17 shows the least cluttered image taken during the five tests done on the circular metallic pole. The path is decently linear, see figure 5.19 and the amplitude signature seen in figure 5.18 at approximately 1.8 meters shows that the Radar registers that there is something there. Though, as mentioned for the other tests, it is not easy to say whether it is generated by ground clutter, interfering objects, the plastic half-pipe structure, or the circular metallic pole. This will be further assessed during the discussion of the test results. Vertical "strings" with no radar signature is caused by the radar not being able to collect enough data about the scene because of the UAV velocity.

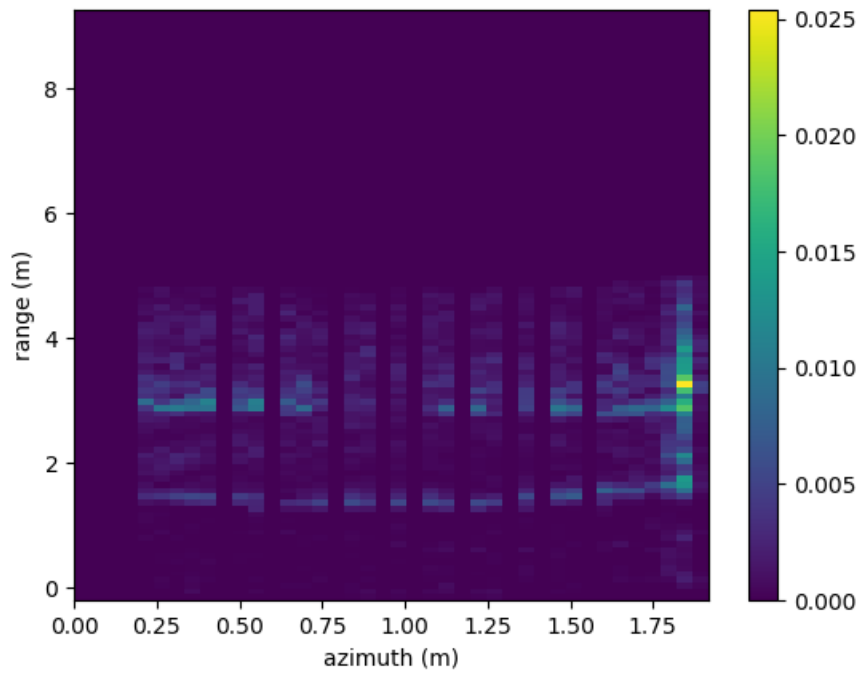


FIGURE 5.17: Generated SAR image of the circular metallic pole

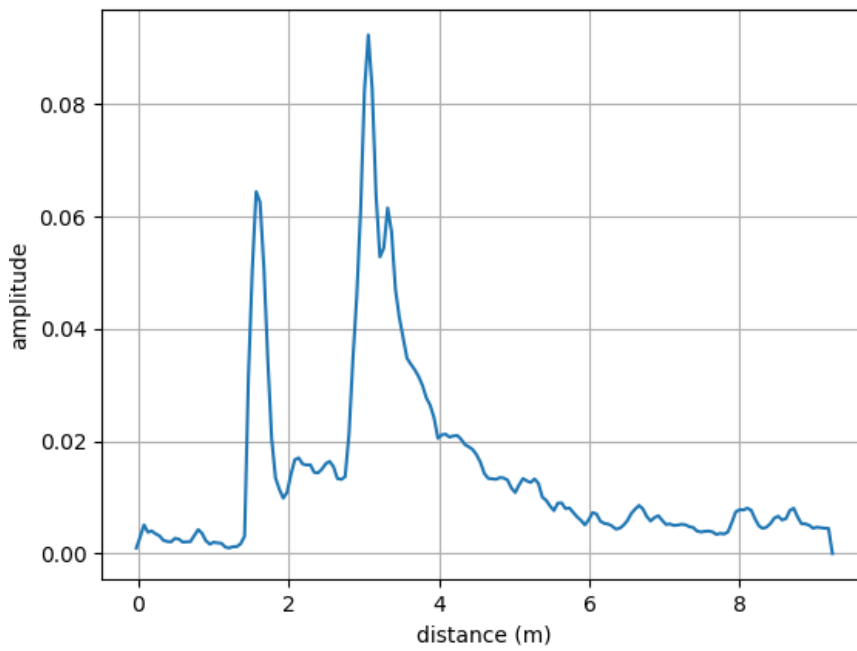


FIGURE 5.18: Magnitudes for the circular metallic pole summed up at all distances

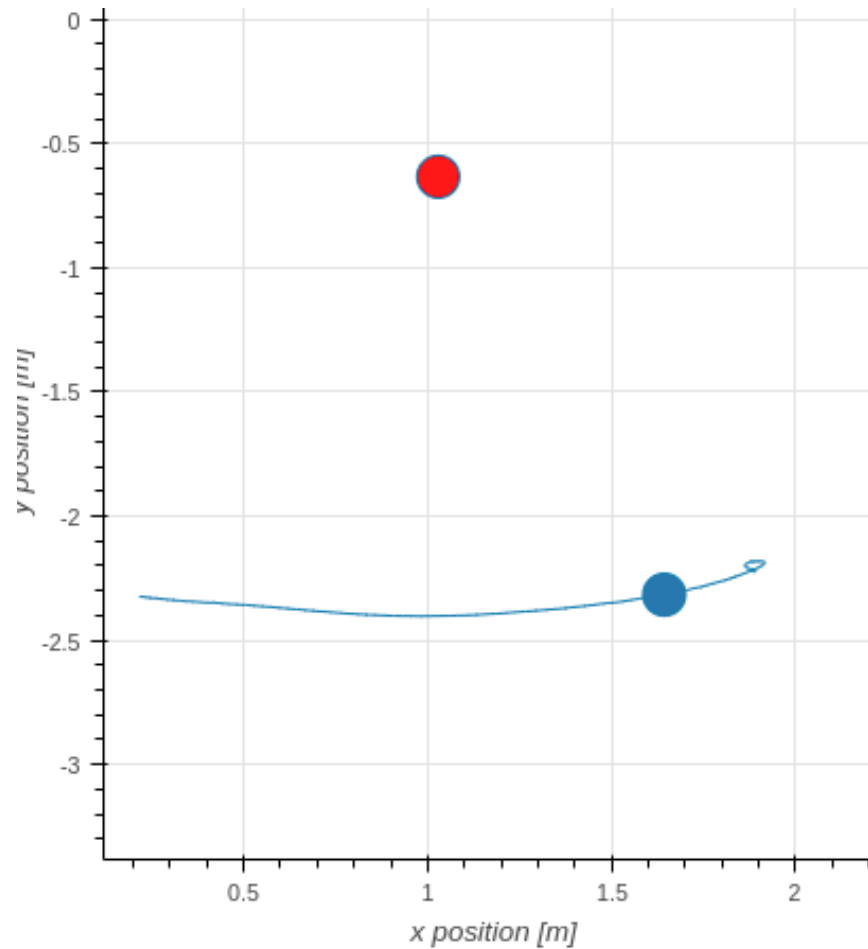


FIGURE 5.19: Manually flown UAV path for the circular metallic pole (red circle)

### 5.2.6 SAR test: Circular Plastic Pole

As with all the smaller objects, the wall behind stands out in the SAR image (figure 5.20). The flight path shown in figure 5.22 is not quite linear and the UAV heading is not kept stable during the entire flight. This causes for ambiguities when considering the spikes that show up on the graph in figure 5.21. Especially when trying to conclude whether the Radar actually sees the circular plastic pole or not. It is concluded that the plastic pole is not being imaged, and that the amplitudes registered at 1.7-1.8 meters mainly came from ground clutter.

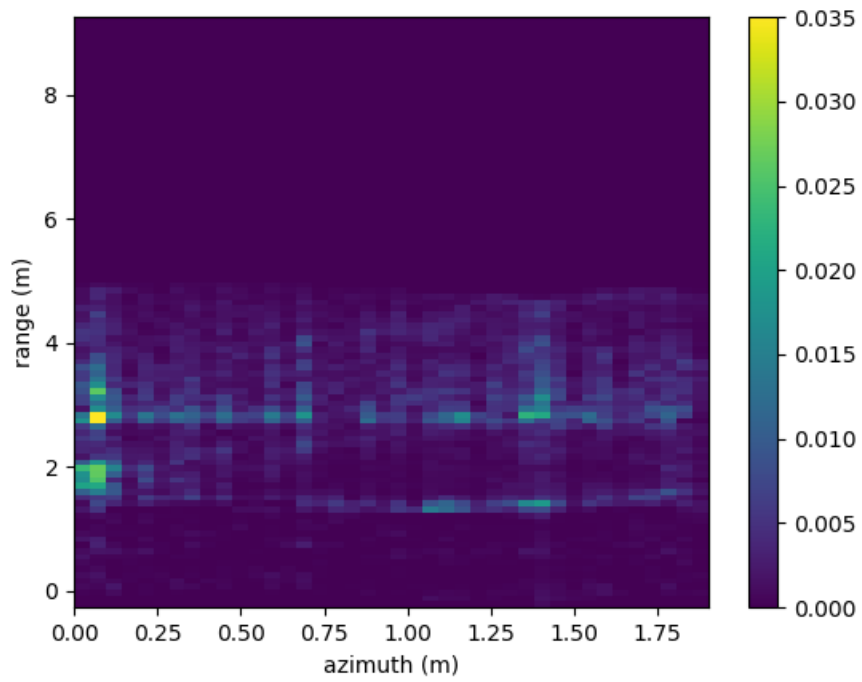


FIGURE 5.20: Generated SAR image of the circular plastic pole

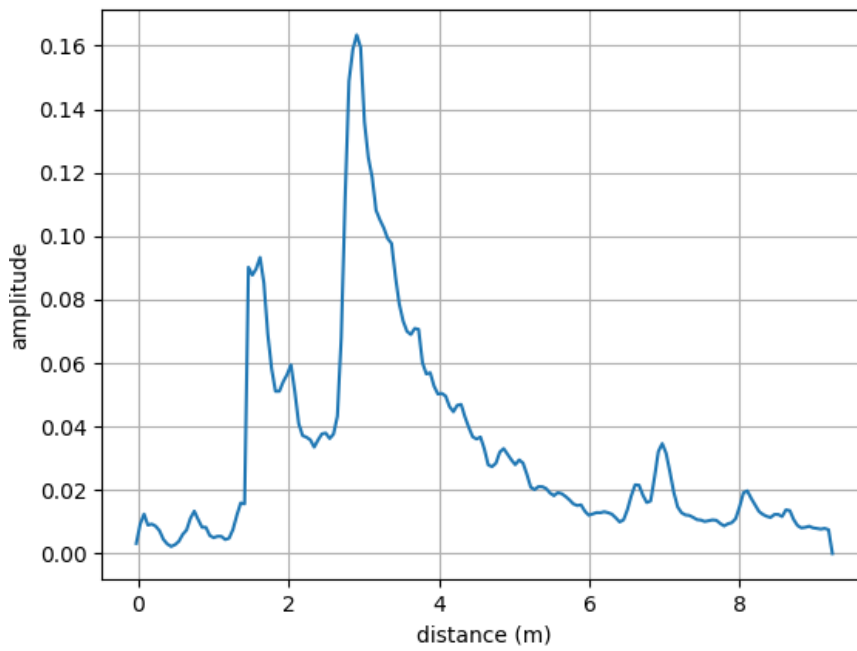


FIGURE 5.21: Amplitudes for the circular plastic pole summed up at all distances

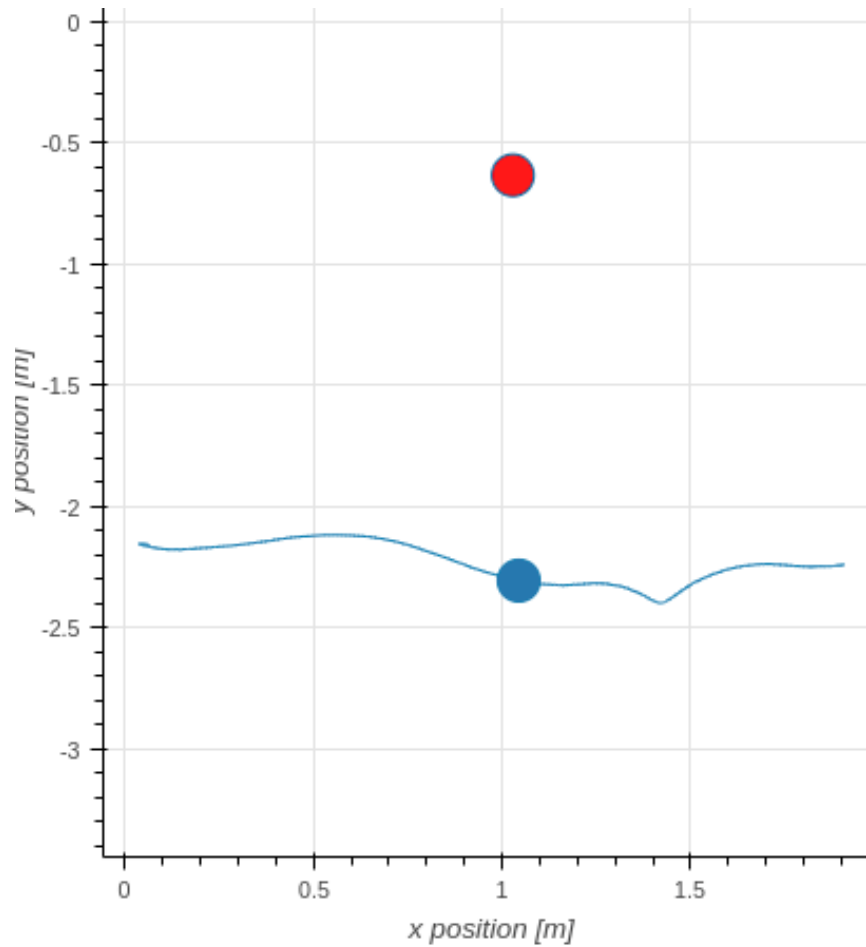


FIGURE 5.22: Manually flown UAV path for the circular plastic pole shown as a red circle

### 5.2.7 SAR test: Metallic Wire

The SAR imaging of the metallic wire (figure 5.23) is clearly cluttered and it can clearly be stated that the wire is not easily visible to the Radar. The graph (figure 5.24) shows a signature that can be interpreted as a mix of ground clutter, and the back-scatter from the plastic half-pipe used to hold the wire in its position. The UAV path shown in figure 5.25 was the best one done of all the tests done on the wire, and is not ideal, but acceptable compared to what was achieved in the other tests.

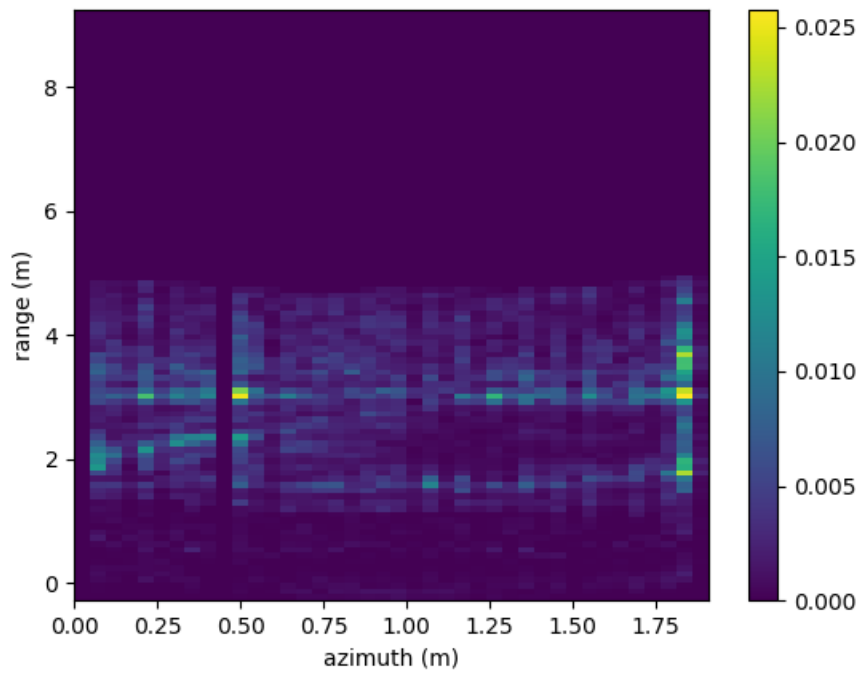


FIGURE 5.23: Generated SAR image of the metallic wire

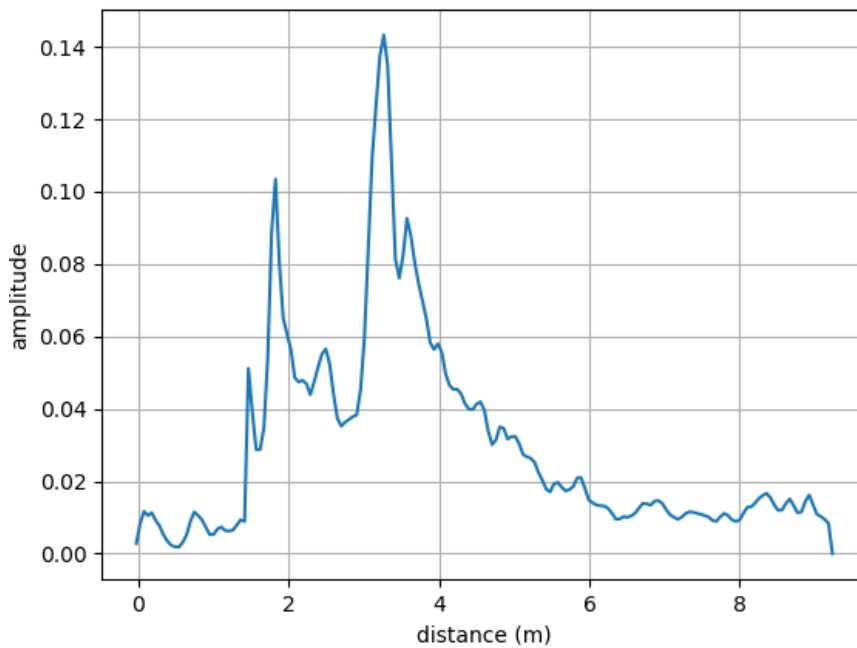


FIGURE 5.24: Amplitudes for the metallic wire summed up at all distances

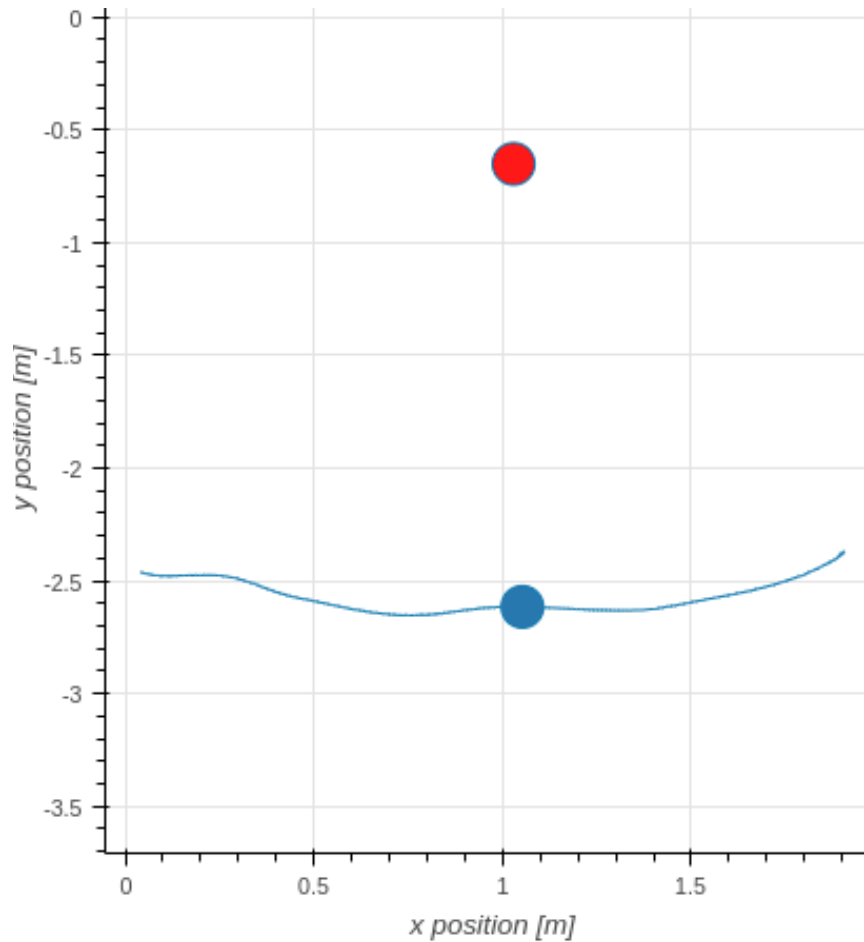


FIGURE 5.25: Manually flown UAV path for the metallic wire (approximately at the red circle)

### 5.3 Comparison with Results from Other Studies

When comparing the results of the testing done in this chapter to the research on SAR on a consumer drone [11] presented in chapter 2 - or the results from the comparison of UWB short-range imaging [12] from chapter 3, it is important to mention the difference in hardware and software. While the comparison study shows very precise imaging by the use of three different migration techniques presented in chapter 3 the complexity of the algorithm used in these tests is fairly small compared to the RMA and Kirchhoff migration techniques.

Looking at the generated SAR images in comparison to the ones in the consumer drone study one should note the absence of a wall in the consumer drone study. The difference between an indoor and an outdoor environment. Clearly, those tests were done in a slightly more professional fashion. Though one could assume that placing a wall 1 meter behind the same test objects would make them appear slightly more vague on the SAR images, even though the RCS of the objects

where higher than that of the objects tested in this thesis.

Comparing the results obtained from all tests conducted in this section it is clear that the object with the decidedly highest RCS, the plate, was the easiest one to image, and thus, the easiest to detect. The smaller objects showed some signatures, though with varying ambiguities concerning the results.

## 5.4 Discussion

The UAV possesses no predefined functionality that makes it able to fly a perfectly straight line from one position to another, which would have been an advantage during the tests conducted in this chapter. Furthermore, flying the UAV at constant speed to make sure that the Radar received the same amount of signals from all parts of the scenery would have been able to make the imaging less ambiguous. When operating the UAV manually it is not only difficult to fly a straight line at constant speed, but it is also hard to keep the UAV heading constant. This difficulty results in the fact that during testing, the Radar was not always pointing directly forwards, and since the Simple Summation Algorithm makes no correction on the viewing angle of the Radar, the signal processing will be sub-optimal. Concerning testing and test setup, there are several factors that should be reflected upon. The fact that the UAV is flown manually poses a disadvantage when it comes to the amplitude graph for all scenarios. When the UAV is flown manually, the flight time differs on every test, making it difficult to say whether summed up amplitudes on specific distances came from noise and clutter over time, or from other interfering objects. As some of the tests show, there is a lack of data caused by the UAV moving too fast across the scene, which could have been corrected by a velocity controller. Another challenge is regarding the unstable heading. While operating the UAV manually, it can be difficult to predict what the Radar will capture from other parts of the test room. Ideally the tests should also have been done by the use of a rail (to create a "perfectly" straight line) and with a strict timer in a room with nothing else. Those tests could then have been compared to the test results of a flying UAV. Accurate reference imaging of all objects to show their placement and position compared to the generated SAR images would also have been beneficial, and is something that should be improved in future work.

Furthermore, from the lack of unambiguous results there should have been conducted more tests, though with limited time as a contributing factor, it was decided that further tests can be conducted in future work. There was quite some time and effort put into an implementation of a more complex algorithm, but as the main priority was to actually be able to generate a SAR image the algorithm's complexity was scaled down - which led to the implementation of the Simple Summation Algorithm.

Considering the imaging results it is also clear that there should have been several other objects with good reflection capabilities, such as a dihedral and/or a trihedral, as most of the tests showed high ambiguity. All other tests than the  $0^\circ$

plate test showed no outgoing object signature on the SAR image compared to the wall behind. Sometimes it also seemed like interfering objects appeared at the edges of the SAR image, making it harder to see the object and the wall upon generation of the image. For further work, a test with an empty scenery should be conducted, making it possible to differentiate between the imaging results of an empty scenery and the hard-to-see elements. For future research, a test with only the plastic half-pipe structure should also be conducted to be able to see what Radar signature it would give. Several days of testing would absolutely have been beneficial. Testing in rooms with different types of surfaces could have illustrated how much ground clutter affected the Radar data and would also have made a better comparison for the tests.

One could have expected better imaging results with more complex algorithms and a more clean and operational test setup considering the points made in this section and the comparison section above.

## 5.5 Summary

All tests completed during the course of this thesis has been conducted in the Motion Capture Lab at NTNU in cooperation with researchers at the Department. The UAV position is accurately measured as it is manually operated to fly past several objects, collecting Radar data from all of them. The five objects tested was a metallic plate, a square metallic pole, a circular metallic pole, a circular plastic pole, and a metallic wire. All tests were done five times for each object with the intention of flying the UAV in a straight line at constant speed with constant heading. The best imaging result has been presented in this chapter. Comparing the results to other studies brought up in earlier chapters, these results show higher ambiguity even considering the fact that some of the objects were hard to see from a Radar's perspective.

Reviewing the results and the test setup there are many lessons to be learned. Drawing lines from the discussion could facilitate for better testing in future work. More tests with better UAV functionality should also be conducted in future work so that an even better test comparison could be achieved.

## Chapter 6

# Conclusion

Radar can detect, track, and generate images of targets with high accuracy at long range, in all weather conditions. Given these abilities, Radar has been widely used for military and civilian purposes, such as wide-area surveillance, air defense and weapon control, high-resolution Radar imaging, remote sensing of environment, weather observation, air traffic control, vehicle collision avoidance and cruise control, harbor and river traffic surveillance, and industry automation [68].

Radar systems are required to operate in increasingly complex spectral environments with a lot of potential interference, noise and clutter. Take for example an urban area where the airwaves may include lots of wide-band radio frequencies and microwave emitters, as well as wireless communication infrastructure, wireless networking systems and civilian Radar devices. The challenge with noise is persistent in Radar and SAR because the signal processing algorithms must be able to recognize the relevant information. When taking small Radar systems that can fit on a consumer drone into account there will always be a challenge with directivity, which measures the degree to which the emitted radiation is concentrated in a single direction. Small Radar systems therefore have a wider beam, see figure 2.2. Electromagnetic waves, in this case Radar signals, will interact with objects and the media in which they travel. When this happens, the Radar signals can be reflected several times before reaching the receiver. Especially in indoor environments where signals can bounce off walls and objects in every direction. This can be challenging for a SAR algorithm to detect as it would need intelligent mechanisms to be able to detect only the signals coming straight from an object, and filter out the irrelevant information (clutter, noise, etc).

### 6.1 Closing Discussion

This thesis has aimed to explain, in understandable terms, the fundamentals and concepts of Radar technology and SAR, while trying to investigate the applicability of using SAR for indoor visual inspection by the use of Unmanned Aerial Vehicles (UAVs). The main goal was to implement and test a SAR algorithm on real-world Radar data acquired from a small-sized multirotor UAV to see what results could be achieved. Critical to a collision avoidance system is its ability to detect and avoid obstacles such as wires, pipes, and walls. By the use of a light-weight Ultra-Wide

Band (UWB) Radar mounted on a multirotor UAV, a simple algorithm for classification of Radar data has been implemented and tested in different environments. Thus, the questions to be answered in this closing discussion will be the following. What did this thesis achieve compared to its purpose, and what needs to be done in future work?

Studies like the one on SAR imaging using a small consumer drone presented in chapter 2.6 [11] or the comparison study regarding UWB short-range imaging using migration algorithms [12] show that there has been conducted relevant research to what this thesis brings up - exploring the potential of SAR to aid UAV navigation when for example the Inertial Navigation System (INS) measurements are not accurate enough due to the GPS signal being absent or corrupted by either intentional or unintentional interferences. It is clear from these studies that the possibility of using SAR as part of a collision avoidance system on UAVs is feasible. There is yet no study showing the feasibility of a fully functional collision avoidance system for small-sized UAVs mainly reliant on SAR, and that was not set as a goal of this study either.

The results acquired presented in chapter 5 using the Simple Summation Algorithm shows limitations when it comes to hard-to-see objects such as wires, or thin objects with rather poor reflectivity. Whether it is mainly because of the simplicity of the algorithm, or because of the test setup can be discussed. In this case the ambiguity of the results was most likely caused by a mixture of all the points made in the chapter 5 discussion. In future work there should be conducted more tests with a wider range of objects and in different types of environments. As part of a collision avoidance system, SAR can definitely be used in combination with other imaging data acquired from for example a camera, a laser sensor (LIDAR) or seismic measurements. This could facilitate for a more robust collision avoidance system, given that the Radar data is reliable.

The conclusion to be drawn from this thesis is the fact that even with a simple SAR algorithm applied on data from a small relatively low-cost Radar mounted on a UAV - a UAV which was operated manually with both unstable heading and velocity, it was able to image a large object and the walls of an indoor environment. In comparison to more reactive collision avoidance systems based upon singular radar measurement samples, SAR can be used for mapping, and be making the collision avoidance able to operate by accessing the SAR "memory" generated - which in many cases pose as a great advantage. Radar technology and SAR are absolutely interesting research subjects with infinite branches of literature - the following section will look at some other areas where research could be conducted.

## 6.2 Further Research Prospects

Within the domain of Radar systems to aid in collision avoidance on small-sized multirotor UAVs, there are an enormous amount of questions and challenges that pose as great candidates for further research prospects. Here are some suggestions:

- Even though the study presented in chapter 2 section 6 confirmed the feasibility of mounting an entire SAR system on a small multirotor UAV and creating images of satisfying quality there should definitely be done more testing with such a system. Running tests in different environments, both indoor and outdoor, in urban areas, and industrial facilities. And if the UAV should be able fully to rely on SAR imaging to navigate its surroundings the UAV has to be able to look in all directions; sideways, downwards, and upwards.
- When it comes to signal processing and imaging we can consider the review of methods to describe and mathematically interpret Radar scattering in chapter 3 section one. It is clear that there is a need for the development of scattering models that include as much of the physics as possible without making the model too complex to be used in the inverse problem. An example of a simple model that includes the relevant physics can be found in [44].
- Since SAR is based on known relative motion between target and sensor, there is often a challenge in forming well-focused images because of the motion is not well enough known. More efficient and precise methods for finding the relative motion between target and sensor are also needed [69] [70]. To do this there is also a need for better algorithms for determining the antenna position from the Radar data itself. Methods like that often include auto-focus algorithms [35] [71], some of which require image contrast to focus the image. Even more challenging is when the target motion is complex (pitching, rolling and yawing). Fast, efficient and accurate methods to three-dimensional image are needed [70] and can a UAV be able to simultaneously track [72] moving objects while forming three-dimensional images of them? Fast and accurate imaging by the use of target classification/identification algorithms is also an interesting research prospect. Target identification is important when mapping a scene or differing between individual vehicles and is a problem that may be closely related to computer vision. Algorithms regarding classification and identification should ideally be able to run in real time.
- Combining these challenges with the idea of integrating all these skills on a small-sized multirotor UAV it can seem nearly impossible considering the limitations on payload, power consumption and processing power. On top of this it can definitely be an idea to investigate the possibility of using a SAR system as part of a collision avoidance system in combination with for example a camera or other sensory equipment. A camera can on one hand show clear contrast in images, though it struggles with depth. The SAR image could then be used to provide depth and thereby ensure better mapping of the UAVs local environment.

- In chapter (2) the Radar shadow is mentioned briefly. The idea of exploiting the information given in the Radar shadow is definitely interesting. In a lot of cases, it is much more simple to utilize the Radar shadow of an object than to process its direct-scattering image. A back-projection method used to reconstruct an object's three-dimensional shape from its Radar shadows captured at different viewing angles is proposed in [20].
- Earlier in this thesis, the automotive industry was mentioned as an example of where Radar is widely used. When talking about collision avoidance in the automotive industry the question of LIDAR vs Radar comes up. Light detection and ranging (Lidar), as opposed to radio detection and ranging (Radar). As light waves and radio waves have different capabilities the solution to a fully operational collision avoidance system seems to fall on a combination of the two technologies. Since Lidars usually have been bigger in size, not to mention more expensive, they have not been thoroughly tested in small-sized UAVs. However, there are being developed smaller laser range sensors, and their cost is also going down [73]. Therefore, it is fair to say that soon, small-sized UAVs will be mounted with both Radar and lidar systems.
- The list could go on. The key element is that Radar technology as a means to aid in UAV local navigation is a field that still needs a lot of testing. The use of low-cost portable drones for Radar imaging could open up other potential applications and research prospects in scientific, agricultural, and environmental monitoring. This is definitely an interesting area for research. Developing collision avoidance systems and systems for navigational aid is only getting more relevant as we move towards an autonomous future with UAVs embedded into more and more aspects of our lives. The possibilities are almost endless, and considering the ongoing advances in all fields of electronics and computer science, I assume it will not take long before UAVs of almost all sizes are able to navigate crowded environments.

## Appendix A

# Simple Summation Algorithm Python Code

### Running the code:

1. Acquire access to radar log-files from the Motion Capture Lab at NTNU and download logs referred to in the code
2. Set up an Anaconda environment by the use of the file "pylive.yml" from the py-imcdatabase (access granted from Scout Drone Inspection AS)
3. Activate the Anaconda environment
4. Install the file "pyimc.egg" from the py-imcdatabase
5. Set the Anaconda environment as python interpreter for the project
6. Remove the "#" from the log to be run (see line 42-61 in the code)
7. Run code

```
1 # The Simple Summation Algorithm
3 import sys
5 sys.path.append('..')
7 from imcdatabase import ImcDatabase, NoMessageFound
8 from radar_frame_parser import *
9
10 import numpy as np
11 import matplotlib.pyplot as plt
12 from scipy.interpolate import interp1d
13
14 # Number of elements within the radar magnitude list (99 for old test, 181
15     for new)
16 M_SIZE = 181
17
18 # Load up a log
19 db = ImcDatabase()
20
21 # All conducted tests
```

```

23 # Square pole
#db.load_log('../logs/20180528_mocap_radar_sar_proper/scout-disco
    -01/20180528/135417_square_pole_4/Data.lsf')

25 # Square pole 45
#db.load_log('../logs/20180528_mocap_radar_sar_proper/scout-disco
    -01/20180528/140038_square_pole_45/Data.lsf')

27

29 # Metallic pole
#db.load_log('../logs/20180528_mocap_radar_sar_proper/scout-disco
    -01/20180528/140323_metallic_pole/Data.lsf')

31 # Plastic pole
#db.load_log('../logs/20180528_mocap_radar_sar_proper/scout-disco
    -01/20180528/140639_plastic_pole/Data.lsf')

33

35 # Wire
#db.load_log('../logs/20180528_mocap_radar_sar_proper/scout-disco
    -01/20180528/141359_wire/Data.lsf')

37 # Plate
#db.load_log('../logs/20180528_mocap_radar_sar_proper/scout-disco
    -01/20180528/141927_plate/Data.lsf')

39

41 # Plate 45
#db.load_log('../logs/20180528_mocap_radar_sar_proper/scout-disco
    -01/20180528/142203_plate_45/Data.lsf')

43 # Front-facing radar ID: 0 - constant noise filter: dst_ent: 21
all_messages = db.get_messages('RadarFrame', filter_field={'id':0, '
    dst_ent':21})

45
sum_magnitude = [0]*M_SIZE
47 distance_list = [0]*M_SIZE

49 magnitude_list = []
drone_pos_list = []
51 drone_y_pos = []

53 count = 0

55 for radar_data in all_messages:
    distance = np.linspace(radar_data.area_start, radar_data.area_end,
        radar_data.num_bins)
57 magnitude = get_frame_magnitude(radar_data.data, radar_data.num_bins)
    time = radar_data.timestamp - db.get_start_time()
59 drone_pos_data = db.get_message_at_time('EstimatedState', radar_data.
        timestamp)

61     if count == 0:
        #set reference range position of the UAV
63         start_pos_y = drone_pos_data.y

65
        for i in range(0, len(magnitude)-1):
67             sum_magnitude[i] = sum_magnitude[i] + magnitude[i]

```

```

69     drone_y_pos.append(drone_pos_data.y-start_pos_y)
       drone_pos_list.append(drone_pos_data.x)
71
73     magnitude_list.append(magnitude)
       distance_list = distance
75
77     count = count + 1
79
81     #Find the distance range to be interpolated
82     max_range = 0
83     min_range = 0
84
85     for i in range(0,count):
86         for d in distance_list:
87             if d+drone_y_pos[i] < min_range:
88                 min_range = d+drone_y_pos[i]
89             if d+drone_y_pos[i] > max_range:
90                 max_range = d+drone_y_pos[i]
91
92     #Based on the movement of the UAV, find the maximum and minimum value in
93     azimuth (x-direction):
94     min_x = 0
95     max_x = 0
96
97     for i in range(0, count):
98         if drone_pos_list[i] < min_x:
99             min_x = drone_pos_list[i]
100         if drone_pos_list[i] > max_x:
101             max_x = drone_pos_list[i]
102
103     # creating the two-dimensional array that will represent the SAR image:
104     interp_x = interp1d([min_x, max_x], [0, 39])
105     interp_y = interp1d([min_range, max_range], [0, 99])
106     SAR_image = np.zeros((100, 40))
107
108     # iterate through all data:
109     for i in range (0, count):
110         # find out which index in SAR_image this mapping belongs to based on
111         # what position the drone is at
112         if drone_pos_list[i] < min_x:
113             drone_pos_list[i] = min_x
114         if drone_pos_list[i] > max_x:
115             drone_pos_list[i] = max_x
116         cross_range = int(interp_x(drone_pos_list[i]))
117
118         # go through all distances and sum up magnitudes at the specific cross
119         # -range
120         for j in range (0, 98):
121             if distance_list[j] > max_range:
122                 distance_list[j] = max_range
123             if distance_list[j] < min_range:
124                 distance_list[j] = min_range
125             SAR_image[int(interp_y(distance_list[j]+drone_y_pos[i]))][
126                 cross_range] += magnitude_list[i][j]
127
128     f = np.array(SAR_image)

```

```
123 # SAR Image plotting (range/azimuth)
plt.imshow(SAR_image, interpolation="nearest", origin="lower", extent=[
    min_x,max_x,min_range,max_range], aspect="auto")
125 plt.xlabel('azimuth (m)')
plt.ylabel('range (m)')
127 plt.colorbar()
plt.show()
129
# Summed up magnitudes graph
131 fig, ax = plt.subplots()
ax.plot(distance_list, sum_magnitude)
133 ax.set(xlabel='distance (m)', ylabel='amplitude')
ax.grid()
135 plt.show()
```

# Publications

- [1] Snorre Jablonski. "Feasibility of using Synthetic Aperture Radar as navigational aid on multicopter UAVs". In: (2017).
- [2] Renee Knight. "The Future of Autonomy". In: (2017). URL: <http://insideunmannedsystems.com/future-autonomy>.
- [3] Jane Wakefield. "Dubai tests drone taxi service". In: (2017). URL: <http://www.bbc.com/news/technology-41399406>.
- [4] Allistair A. Moses. "RADAR Based Collision Avoidance for Unmanned Aircraft Systems". In: *Electronic Theses and Dissertations* (2013). URL: <https://digitalcommons.du.edu/etd/455>.
- [5] Peter Tait. "Introduction to Radar Target Recognition". In: (2006).
- [6] ETHW. "Synthetic Aperture Radar". In: (2015). URL: [http://ethw.org/Synthetic\\_Aperture\\_Radar](http://ethw.org/Synthetic_Aperture_Radar).
- [7] Merrill I. Skolnik. *Radar Handbook*. Third edition. McGraw-Hill Education, 2008, p. 1328.
- [8] University of Michigan. "Emmett Leith - Inventor of Practical Holography". In: (). URL: <http://ece.umich.edu/bicentennial/stories/emmett-leith.html>.
- [9] Rolando L. Jordan. "The Seasat-A synthetic aperture radar system". In: *IEEE Journal of Oceanic Engineering* 5.2 (1980).
- [10] H. Cantalloube; P. Dubois-Fernandez. "Airborne X-band SAR imaging with 10 cm resolution: technical challenge and preliminary results". In: *IEEE Proceedings - Radar, Sonar and Navigation* 153.2 (2006).
- [11] Chenchen J. Li\* and Hao Ling. "Synthetic Aperture Radar Imaging Using a Small Consumer Drone". In: (2015).
- [12] X. Zhuge; T.G. Savelyev; A.G. Yarovoy; L.P Ligthart; B. Levitas. "Comparison of Different Migration Techniques for UWB Short-Range Imaging". In: (2009).
- [13] Constantine A. Balanis. *Antenna Theory: Analysis and Design*. Fourth edition. John Wiley & Sons, 2016, p. 1072.
- [14] Naval Air Warfare Center Weapons Dvn Scott O'Neill. *Electronic Warfare and Radar Systems Engineering Handbook*. US Government department of the Navy, 2012, p. 398.
- [15] ESA. *Radar Course 2.18 Shadow* [Accessed (12.05.2018)]. URL: [https://earth.esa.int/web/guest/missions/esa-operational-eo-missions/ers/instruments/sar/applications/radar-courses/content-2/-/asset\\_publisher/qIBc6NYRXfnG/content/radar-course-2-shadow](https://earth.esa.int/web/guest/missions/esa-operational-eo-missions/ers/instruments/sar/applications/radar-courses/content-2/-/asset_publisher/qIBc6NYRXfnG/content/radar-course-2-shadow).

- [16] Cheney. Margaret. "Problems in Synthetic-Aperture Radar Imaging". In: *Inverse Problems* 25 (2009).
- [17] William A. Holm Mark A. Richards James A. Scheer. *Principles of Modern Radar: basic principles, chapter 10*. The Institution of Engineering and Technology, 2010.
- [18] Merrill I. Skolnik. *Introduction to Radar Systems*. Second edition. McGraw-Hill Education, 1981, p. 590.
- [19] Christian Wolff. *Synthetic Aperture Radar Modes*. URL: <http://www.radartutorial.eu/20.airborne/ab08.en.html>.
- [20] Martin Schneider. "Automotive Radar Status and Trends". In: (2005).
- [21] V.V. Viikari; T. Varpula; and M. Kantanen. "Road-condition recognition using 24-ghz automotive radar". In: (2009).
- [22] A. Bartsch; F. Fitzek; R.H. Rasshofer. "Pedestrian recognition using automotive radar sensors". In: (2012).
- [23] W. Menzel and A. Moebius. "Antenna concepts for millimeter-wave automotive radar sensors". In: (2012).
- [24] Andrew Viquerat; Lachlan Blackhall; Alistair Reid; Salah Sukkarieh; Graham Brooker. "Reactive collision avoidance for unmanned aerial vehicles using doppler radar". In: (2007).
- [25] McCandless S.W. *Space Based Radar Handbook - The theory, design, engineering and application of a space-based SAR system*. Artech House, 1989, p. 472.
- [26] Robert O. Harger. *Synthetic Aperture Radar Systems: Theory and Design*. Academic Press, 1979, p. 240.
- [27] Frank Hay-chee Wong Ian G. Cumming. *Digital Processing of Synthetic Aperture Radar Data*. Artech House Remote Sensing Library. Artech House Print on Demand, 2005, p. 660.
- [28] Samiur Rahman. "Focusing Moving Targets Using Range Migration Algorithm in Ultra Wideband Low Frequency Synthetic Aperture Radar". In: (2010). URL: <https://www.diva-portal.org/smash/get/diva2:830729/FULLTEXT01.pdf>.
- [29] Amit Rastogi. *Synthetic Aperture Radar*. URL: <https://www.slideshare.net/AmitRastogi11/synthetic-aperture-radar>.
- [30] Donald R. Wehner. *High resolution radar*. Artech House, 1987, p. 472.
- [31] J. Wellman; R. Silvius. "Doppler signature measurements of an mi24 hind d helicopter at 92ghz". In: (1998).
- [32] "An/zpy-1 starlite small tactical radar". In: (2013).
- [33] K. Tomiyasu. "Tutorial review of synthetic aperture radar with applications to the imaging of the ocean surface". In: 66.5 (1978).
- [34] F.M. Henderson and A.J. Lewis. "Principles and applications of imaging radar. Manual of remote sensing: Volume 2". In: Third edition (1998).

- [35] Charles V. Jakowatz Jr.; Daniel E. Wahl; Paul H. Eichel; Dennis C. Ghiglia; Paul A. Thompson. *Spotlight-Mode Synthetic Aperture Radar: A Signal Processing Approach*. Sandia National Laboratories Albuquerque, New Mexico. Springer, 1996, p. 420.
- [36] Giorgio Franceschetti; Riccardo Lanari. *Synthetic Aperture Radar Processing*. CRC Press, 1999, p. 324.
- [37] John David Jackson. *Classical Electrodynamics*. John Wiles & Sons, 1999.
- [38] Treves Francois. *Basic Linear Partial Differential Equations*. Academic Press Inc, 1975.
- [39] F. G. Friedlander; M. Joshi. *Introduction to the Theory of Distributions*. Cambridge University Press, 1982.
- [40] Ivar Stakgold; Michael J. Holst. *Green's Functions and Boundary Value Problems*. Wiley-Interscience, 1997.
- [41] Roger G. Newton. *Scattering Theory of Waves and Particles*. Mineola: Dover Publications, 2002.
- [42] A. Ishimaru. *Wave Propagation and Scattering in Random Media*. IEEE, 1997.
- [43] Kurt E. Oughstun; G.C. Sherman. *Electromagnetic Pulse Propagation in Casual Dielectrics*. Springer, 1997.
- [44] L.C. Potter; R.L. Moses. "Attributed Scattering Centers for SAR ATR". In: *IEEE Transactions on Image Processing* 6.79-91 (1 1997).
- [45] K.J. Langenberg; M. Brandfass; K. Mayer; T. Kreutter; A. Brüll; P. Fellingner; D. Huo. "Principles of Microwave Imaging and Inverse Scattering". In: *EARSel Adv. Remote Sens* 2.163-86 (1993).
- [46] S. Darlington J. R. Klauder A. C Price and W. J. Albersheim. "The Theory and Design of Chirp Radars". In: *Bell System Technical Journal* 39.745 (1960).
- [47] C. Cafforio C. Prati and F. Rocca. "SAR data focusing using seismic migration techniques". In: *IEEE Transactions on Aerospace and Electronic Systems* 27.2 (1991). URL: <http://ieeexplore.ieee.org/document/78293>.
- [48] P. M. Woodward. *Probability and Information Theory, with Applications to Radar*. McGraw-Hill, 1953, p. 128.
- [49] James W. Cooley; John W. Tukey. "An Algorithm for the Machine Calculation of Complex Fourier Series". In: *Mathematics of Computation* 19.90 (1965).
- [50] H.S Hou. "The Fast Hartley Transform Algorithm". In: *IEEE Transactions on Computers* (1987), pp. 147-155.
- [51] P. Duhamel; H. Holloman. "Split Radix FFT Algorithm". In: (1984).
- [52] John G. Proakis; Dimitris K. Manolakis. *Digital Signal Processing*. 4th edition. Pearson, 2006, p. 1004.
- [53] Vijay K. Madisetti. "Seismic Migration Algorithms on Parallel Computers". In: (1991).
- [54] R. H. Stolt. "Migration by fourier transform". In: *Geophysics* 43.23-48 (1978).

- [55] A.V. Ristic; D. Petrovacki; M. Govedarica. "A new method to simultaneously estimate the radius of a cylindrical object and the wave propagation velocity from GPR data". In: *Comput. Geosci.* (2009).
- [56] Kevin Secretan. *RMA Algorithm* [Accessed (21.02.2018)]. URL: [https://github.com/Jach/radar\\_sar\\_rma](https://github.com/Jach/radar_sar_rma).
- [57] Darryl K. Taft. *JetBrains Strikes Python Developers with PyCharm 1.0 IDE* [Accessed (25.04.2018)]. 2010. URL: <http://www.eweek.com/development/jetbrains-strikes-python-developers-with-pycharm-1.0-ide>.
- [58] Dmitry Jemerov. *PyCharm 3.0 Community Edition source code now available* [Accessed (25.04.2018)]. 2013. URL: <https://blog.jetbrains.com/pycharm/2013/10/pycharm-3-0-community-edition-source-code-now-available/>.
- [59] Girish Modgil. *Anaconda Distribution* [Accessed (27.04.2018)]. URL: <https://www.anaconda.com/what-is-anaconda/>.
- [60] Team Anaconda. *Anaconda for R users: SparkR and rBokeh* [Accessed (27.04.2018)]. 2016. URL: <https://www.anaconda.com/blog/developer-blog/anaconda-r-users-sparkr-and-rbokeh/>.
- [61] Team Anaconda. *Conda Documentation* [Accessed (27.04.2018)]. 2016. URL: <https://conda.io/docs/>.
- [62] Unknown Author. *NumPy* [Accessed (12.04.2018)]. URL: <http://www.numpy.org/>.
- [63] Unknown Author. *Matplotlib* [Accessed (12.04.2018)]. URL: <https://matplotlib.org/>.
- [64] Unknown Author. *X4M05 radar sensor* [Accessed (13.04.2018)]. URL: <https://www.xethru.com/shop/x4m05-radar-sensor.html>.
- [65] Unknown Author. *Xethru X4* [Accessed (13.04.2018)]. URL: <https://www.xethru.com/x4-radar-chip.html/>.
- [66] DJI. *Phantom 2 Specs* [Accessed (05.05.2018)]. URL: <https://www.dji.com/phantom-2>.
- [67] Time Domain. *Ultra Wide Band Radar Module PulsON 410* [Accessed (05.05.2018)]. URL: [http://www.uwbtechnology.com/datasheets/TD\\_DS\\_P410\\_MRM\\_FA.pdf](http://www.uwbtechnology.com/datasheets/TD_DS_P410_MRM_FA.pdf).
- [68] Victor C. Chen; Marco Martorella. *Inverse synthetic aperture radar imaging : principles, algorithms, and applications*. SciTech Publishing, 2014.
- [69] Brett Borden. "Mathematical problems in radar inverse scattering". In: (2001).
- [70] Mark A. Stuff; Pedro Sanchez; Martin Biancalana. "Extraction of Three-Dimensional Motion and Geometric Invariants from Range Dependent Signals". In: 14.1-3 (2003).
- [71] Forest Lee-Elkin. "Autofocus for 3D imaging". In: (2008).
- [72] Ramachandra K. V. "Filtering Techniques for Radar Tracking". In: (2000).

- [73] Katsumi Kimoto; Norihiro Asada; Toshihiro Mori. "Development of small size 3D LIDAR". In: (2014).